POLITECNICO DI TORINO

Corso di Laurea Magistrale
in INGEGNERIA MECCANICA

Tesi di Laurea Magistrale

Calculation of the Coupling Loss Factors for a Hybrid FEM/SEA Line Junction

Relatore
Prof. Aurelio Somà

Candidato
Francesco Marcella

Luglio 2018

Abstract

In the present thesis a hybrid theory [Shorter and Langley 2005b] for calculation of Coupling Loss Factors (CLFs) in hybrid Finite Element Method (FEM) / Statistical Energy Analysis (SEA) modelling is applied to a hybrid line junction, with the aim of providing a derivation example. The case study is chosen to be a hybrid line junction composed by a rigid beam modelled with FEM, which couples two incident SEA plates coincident to the beam along one of their edges. The theory allows to obtain the Coupling Loss Factors from the Stiffness Matrix of the deterministic subsystems and the Direct Field Dynamic Stiffness Matrix of the statistical subsystems. Most of this work is focused on the derivation of the plate's Direct Field Dynamic Stiffness under the assumption of semi-infinite plate, explaining in detail the reason why such a hypothesis can be reliable when computing the CLFs, and its resulting benefits. Three possible methods for the derivation of the direct field stiffness in modal coordinates are proposed using Green's Functions, wavenumber modal transformation and defining complex-valued shape functions in the wavenumber domain for a Galerkin method, which has consequences on the symmetry of the stiffness. Results for the CLFs are shown and compared between the different derivations of the direct field stiffness.

Keywords:

- Hybrid FEM / SEA method
- Hybrid Coupling Loss Factors - Transmission Loss
- Hybrid line junction
- Direct Field Radiation Dynamic Stiffness Matrix
- Semi - Infinite Plate

Declaration

Acknowledgements

I am grateful to Dr. Alexander Peiffer, head of Team Vibroacoustics and Dynamics - Airbus Defence and Space, for giving me the opportunity to work on this topic for which I really got interested, and being patience in confronting ideas with me. I also want to thank Prof. Gerhard Müller and Christoph Winter M.Sc. from the Chair of Structural Mechanics at the Technische Universität München for taking care of my thesis and helping me with my stay at TUM. From my home university, Politecnico di Torino, I honestly thank Prof. Giovanni Belingardi for taking responsibility for my abroad period, and Prof. Aurelio Somà for the supervision of my thesis.

I would like to acknowledge Italdesign Giugiaro and the Erasmus Plus Programme for giving me financial support and the opportunity to move from Torino to München.

Grazie ai miei genitori per avere riposto fiducia nel mio lavoro e per aver dato priorità al mio percorso da studente, sostenendomi economicamente e consentendomi di dedicarmi unicamente allo studio. Grazie a tutti gli amici, per le esperienze vissute insieme che ci hanno cresciuto, aspettando di accumulare nuovi ricordi.

Y gracias a ti Paula por todas las risas, todos los viajes y la felicidad que me has dado durante mi trabajo.

Declaration of Originality

I hereby declare that I have prepared the present work independently and without the help of others. The literature and other aids used are fully cited and mentioned in the bibliography.

Torino, June 16, 2018

Francesco Marcella

Contents

Abstract III

Declaration IV

Listings VII

List of Symbols VIII

1 Introduction 1

2 Numerical Methods in Vibroacoustics 2
- 2.1 Deterministic Numerical Methods: FEM, BEM . . . 3
- 2.2 Limits of Deterministic Methods in High Frequency Problems . . . 5
- 2.3 Statistical Energy Analysis and Coupling Loss Factor . . . 6
  - 2.3.1 SEA Procedure and Assumptions . . . 7
  - 2.3.2 Damping Loss Factor . . . 11
  - 2.3.3 Modal Density . . . 13
  - 2.3.4 Coupling Loss Factor's . . . 15
- 2.4 Hybrid Methods: Motivations and Applications . . . 21

3 Hybrid FEM/SEA Method 24
- 3.1 Subsystems, Boundaries and Hybrid Junctions . . . 25
- 3.2 Diffuse Field Reciprocity Relationship . . . 28
  - 3.2.1 Free Field Radiation Stiffness of Statistical Subsystems . . . 29
  - 3.2.2 Natural Coordinates for Direct and Reverberant Fields . . . 31
  - 3.2.3 Maximum Entropy at Random Boundary: the Diffuse Field . . . 34
  - 3.2.4 Cross Spectrum of the Blocked Reverberant Force . . . 36
- 3.3 Hybrid Equations and Coupling Loss Factors . . . 38

4 Hybrid Line Junction 47
- 4.1 Plate - Beam - Plate System . . . 47
- 4.2 Assumptions . . . 48
- 4.3 Direct Field Dynamic Stiffness Matrix . . . 51
  - 4.3.1 Governing equations for the Direct Field . . . 51
  - 4.3.2 Green's Function Method . . . 52
  - 4.3.3 Wavenumber Direct Modal Transformation Method . . . 54
  - 4.3.4 Wavenumber Cardinal Sine Method . . . 61
- 4.4 Procedure for the Coupling Loss Factors and Power Balance . . . 66

5 Results **68**
5.1 Wavenumbers and Mode Shapes 68
5.2 Wavenumber Domain Direct Field Stiffness 71
5.3 Power Transmission Coefficients and Coupling Loss Factors 72

6 Conclusions **77**

A Derivations **79**
A.1 Blocked Reverberant Force 79
A.2 Green's Function derivation for the deflection of plates 80
A.3 Wavenumber Domain Free Field Dynamic Stiffness Matrix 82

B Model Data **85**

C Software **86**

D MATLAB® Code examples **87**
D.1 Fast Fourier Transform 87
D.2 Wavenumber Direct Modal Transformation Method 88
D.3 Wavenumber Cardinal Sine Method 89

Bibliography **91**

Listings

D.1 Example of Fast Fourier Transform of the mode shapes 87
D.2 Example of computation for $\mathbf{D}_{dir}$ with the wavenumber modal transformation 88
D.3 Example of computation for $\mathbf{D}_{dir}$ with the sinc shape functions method . . . 89

List of Symbols

Greek Sybols

α		Amplitude of modes
Γ		Constant
ε	J	Modal Energy
ζ		Damping Ratio
η_i		Damping Loss Factor
η_{ij}		Coupling Loss Factor
θ_i	m	i Component of Rotation
κ	m	Radius of Gyration
λ	m	Wavelength
λ		Eigenvalue
ν		Poisson Coefficient
μ	$\frac{\text{rad}}{\text{m}}$	y Wavenumber
ρ	$\frac{\text{kg}}{\text{m}^3}$	Mass Density per Unit Volume
σ		Radiation Efficiency
τ_{ij}		Transmission Coefficient
$\Phi(x)$		Mass-Normalized Mode Shapes in Space Domain
$\Phi(k)$		Mass-Normalized Mode Shapes in Wavenumber Domain
$\varphi(x)$		Shape Functions in Space Domain
$\varphi(k)$		Shape Functions in Wavenumber Domain
ω	$\frac{\text{rad}}{\text{s}}$	Time Angular Frequency
ω_n	$\frac{\text{rad}}{\text{s}}$	Natural Frequency

Latin Symbols

A	m^2	Area
a	m	Characteristic Linear Dimension
c	$\frac{\mathrm{m}}{\mathrm{s}}$	Wave Speed
D_{dir}		Direct Field Dynamic Stiffness Matrix
D_{dir}^{wn}		Wavenumber Direct Field Dynamic Stiffness Matrix
$D_{dir,q}$		Direct Field Stiffness in Generalized Coordinates
D_d		Deterministic Dynamic Stiffness Matrix
D_{tot}		Total Dynamic Stiffness Matrix
E	J	Energy
E	Pa	Young's Modulus
f_s	$\frac{1}{\mathrm{m}}$	Sampling Space Frequency
f	N	Force
F		Force Wavenumber Transform
G	Pa	Shear Modulus
G		Green's Function
h	m	Thickness
h_{ij}		Power Transmission Coefficients
I_p	m^4	Area Polar Inertia
J	$\mathrm{kg\,m}^2$	Torsional Inertia
k	$\frac{\mathrm{rad}}{\mathrm{m}}$	Wavenumber
k	$\frac{\mathrm{N}}{\mathrm{m}}$	Stiffness
K	Pa	Bulk Modulus
L	m	Space Length
M		Number of Modes, Modal Overlap Factor
n		Modal Density
P	$\frac{\mathrm{J}}{\mathrm{s}}$	Power
P	m	Perimeter
q		Generalized Coordinates
S	m^2	Area
$\langle S_{...} \rangle$		Ensemble Average Cross-Spectral Matrix
T		Scattering Matrix
t	t	Time
u	m	x Component of Displacement
U^{wn}		Displacements and Rotations Wavenumber Transform
v	m	y Component of Displacement

v	$\frac{\mathrm{m}}{\mathrm{s}}$	Generic Velocity
V	m^3	Volume
w	m	z Component of Displacement
Y	$\frac{\mathrm{m}}{\mathrm{Ns}}$	Mobility
z		Number of Wavelengths
Z	$\frac{\mathrm{Ns}}{\mathrm{m}}$	Impedance

Other Symbols

$\mathscr{B}$	Constant
$\mathcal{M}$	Constant
$\mathcal{Q}$	Differential Operator

1 Introduction

In chapter 2 the thesis begins with a quick review of the most used numerical methods in vibroacoustics, explaining their features at different frequency ranges and values. Deterministic FEM and BEM methods are summarised and compared, SEA method and its governing parameters are introduced, paying particular attention to the Damping Loss Factor, Modal Density and Coupling Loss Factors formulation. The need of hybrid methods is introduced from the inadequacies of deterministic and statistical methods.

In chapter 3 the Hybrid FEM/SEA method used in this implementation is reviewed defining the configuration of the model organised in deterministic and statistical subsystems. The diffuse field reciprocity relationship is derived in detail, as well as the procedure for the calculation of the Hybrid Coupling Loss Factors and the Hybrid Reverberant Power Balance, writing the system of linear equations used for computing the energy response.

In chapter 4 the hybrid theory is applied to a model containing the hybrid line junction plate-beam-plate. The properties and geometry of the model are described. A detailed discussion on the assumptions made for the model and the derivation of the direct field dynamic stiffness matrix is exposed. A detailed analytic explanation of three possible methods for the derivation of the direct field stiffness of a semi-infinite plate is reported, developing the stiffness defined in wavenumber domain using Green's Functions, Modal Transformation and a Galerkin Method.

In chapter 5 results for wavenumbers, modes and coupling loss factors are presented. The CLFs are compared with the two derivations of the direct fields stiffness adopted, by using two different lengths of the line junction and by changing the damping loss factor.

The thesis ends with the conclusions in chapter 6. The proposed methods are summarised and discussed underlining pros and cons.

2 Numerical Methods in Vibroacoustics

Considering a certain component excited by the direct transmission of vibration in the mechanical coupling with other components or by the interaction with a surrounding fluid, its vibroacoustic behaviour is the relation between its dynamic displacement and the consequent acoustic pressure led by waves propagating through the medium until reaching the observation point. When studying the vibroacoustc behaviour of a system, one of the most important aims is the estimation of the noise produced by the vibrations, which has negative effects on the comfort of the users interacting with the system. In order to perform a vibration control and noise reduction in advance of the production of a prototype, numerical simulations are used to predict the vibroacoustic response.

With the aim of solving motion's differential equations, several computational methods have been using and developing since the end of the 1930s, and the evidence of their usefulness came up in the early 1960s with the coming of digital computers. The most traditional and important among these methods for vibroacoustics can be mainly sorted by time as Finite Element Method (FEM), Boundary Element Method (BEM), Statistical Energy Analysis (SEA).

In order to face problems deriving from the defects of these classical procedures, starting from the 1990s new methods have been developing to fill the gap of the traditional vibroacoustic analyses. These methods can be listed as follows: Energy FE Analysis, Wave-Based Structural Analysis, Hybrid FEM/SEA Method, Hybrid FEM/TPA Method. [Hambric et al 2016].

In the following sections, an overview of the evolution from classical methods to hybrid methods is proposed distinguishing FEM, BEM and SEA as deterministic or statistical approaches.

2.1 Deterministic Numerical Methods: FEM, BEM

Deterministic methods such as FEM and BEM aim to find an approximate solution of partial differential equations in the integral form on a domain that must be finite in the case of FEM, and can be infinite in the case of BEM. The solution obtained with these methods is affected by an overall error produced because of different causes: discretization through nodes and shape functions, residual energy due to the loss of stiffness of the model compared to the reality, irregular shape of the finite elements, numerical integration and numerical approximation.

The FEM approach consists in writing the system of governing equation in integral form over a finite domain, and applying a discretization of the continuum introducing shape functions. Substituting the vectorial form of the shape functions in the governing integral an algebraic system of equations is obtained, and the problem is transformed in a matrix equation. The discretization is performed using a finite number of nodes to define a finite number of elements with which one attempt to fit the real geometry. For a given component of the solution vector, the number of degrees of freedom corresponds to the number of unconstrained nodes, or to the number of considered mode shapes if a modal superposition is adopted. The resulting matrices are typically banded if the shape functions are appropriately selected so that they can be stored as sparse matrices [Somà 2016].

Concerning the BEM approach, it can be noticed that the partial differential equation does not need to be solved through the integration all over the domain, but it is sufficient to apply the divergence theorem and transform the domain integral in the correspondent boundary integral, provided that the Green's Function of the problem is known. Once the boundary integral is written, the solution at any point of the domain can be calculated using a discretization only over the boundary along lines or surfaces and substituting the coordinates of interest in the resulting function which is analytical. The BEM has many simulation advantages compared to the FEM, such as a greater precision when the same discretization is used, a fewer number of degrees of freedom since only the boundary of the domain is discretized, that means smaller dimension of the matrices and shorter computational time, and a great time saving in the preparation of the model since only the boundary must be modelled. Also a higher resolution of the response over the domain is ensured since the solution is continuous, and the Green's Function can be defined also for semi-infinite and infinite spaces which cannot be modelled with FEM. On the other hand, the boundary element method also presents disadvantages and limits with respect to the FEM, such as the inability to consider an eventual heterogeneous materials which require to be modelled in

all their volume other than over the boundaries, and the inability to model the non-linear behaviour. Besides, although the BEM matrices are smaller in dimension, they are fully populated [Banerjee 1994].
Concerning vibroacoustics, the main advantages of the BEM matches the most of the application cases of waves propagating in closed or open environments, and represents a powerful tool for predicting the system's behaviour in the early phase of the design since the changes in geometry are easy to perform since the only boundary has to be discretized.

To choose which method suits better the simulation of a given problem can depend on many factors, for example if the problem is linear or non-linear. One method can be well-suited for solving a problem and preferred to other methods depending on the type of application and on the geometrical discretization of the structural-acoustic system, on how important is considered to model geometrical details with high precision and on the relative size of the whole system compared to these small details. For example it is possible to divide noise studies in two different cases: interior and exterior sound. When an interior sound problem is given, it is possible, for example, to model the system using the finite element method, with a 1, 2 or 3-dimensional geometrical discretization of the closed environment within which the waves propagate, or with a boundary element method discretizing only the contour lines or surfaces, reducing the number of degrees of freedom involved and so reducing the computational time, but also generating asymmetric and fully populated matrices. On the contrary, for exterior sound problems, it is not possible to model the radiation of waves to infinity by using finite elements, and the variation 'Infinite finite elements method' can be applied, as well as the boundary element method since it implicitly includes the infinite environment with a considerable reduction of degrees of freedom [Hambric et al 2016], [von Estorff 2007].
A simple confront of two different systems for which the sound pressure is computed using different methods is shown in Figure 2.1. While in the finite element model of the car all the volume is discretized, in the aircraft section only the boundaries of the cavity are computed and the results can be evaluated over any domain within the system.

The common aspect of these two methods is the philosophy used to describe the relation between excitation and response, that is obtained with a numerical solution of the analytical governing equation, and the certainty with which the properties of the system are considered. Neglecting the source of errors listed at the beginning of the section, to a certain domain distribution of the excitation corresponds an unique domain distribution of the response variables which satisfy the equation. This is the reason why they are called "deterministic methods". These methods provide the most accurate procedure to obtain the solution of

partial differential equations, but only when the number of nodes used for the discretization is big enough to properly represent these results.

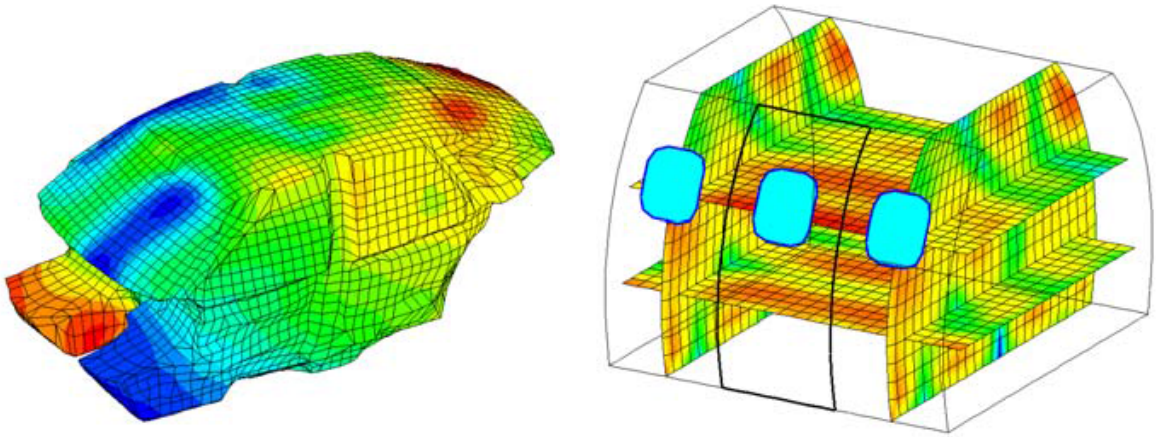

(a) Sound pressure displayed on a FEM model of a car

(b) Sound pressure displayed on a BEM model of an aircraft section

Figure 2.1: FEM and BEM models (figure of [von Estorff 2007])

2.2 Limits of Deterministic Methods in High Frequency Problems

Whilst using a huge number of nodes in the discretization increases the model accuracy in fitting the reality, on the other hand it implies a greater computational effort which results in an increased computation time and bigger numerical error, so that the number of nodes cannot be easily chosen as big as necessary without negative consequences.

The choice of the number of nodes can be mainly motivated by two reasons: the level of detail desired to properly fit the real geometry and resolution of the response required to analyse all the relevant amplitudes of wave components. The resolution is not arbitrary when talking about vibroacoustics, but it is governed by the minimum wavelength it is intended to capture in the results in order to represent all the harmonic components of the vibrations. In the particular case of the noise prediction, the fundamental wavelength of the noise vibrations are the shortest among all the relevant components, and they get even shorter as the frequency values of the simulation increase, requiring a huge density of nodes on order to be approximated even with simplest shapes of wave.

This last consideration implies that the reliability of a vibracoustic numerical method mainly depends on the frequency range of the response. Indeed, the efficiency of one method depends on the frequency values around which the system vibrates, and the previous example of comparison between FEM and BEM makes sense only when the frequency range of the simulations floats around low values, the so called Low Frequency Problem (LF), in which the number of nodes required for representing the minimum relevant wavelength does not compromise the numerical procedure in terms of time consumption and storage request.

Wanting to classify the need of a huge number of nodes to represent the response at a certain frequency, it is possible to define a parameter that keeps track of the frequency and the size of the system. Considering a component or an acoustic region with a characteristic dimension L along a certain direction, vibrating with a wavenumber k along that same direction, it is possible to define how many wavelengths occur within L through the non-dimensional parameter $z = kL/2\pi$ [Hambric et al 2016].
If the solution frequencies are large enough to correspond to space wavelengths which are small with respect to the characteristic space dimension of the domain, also z will be large and a huge number of nodes would be required to represent the mode shapes participating in the response, and if the frequency range is wide, also a huge number of modes must be taken in account. This condition typically occurs when one structure is very big with respect to the wavelength of its vibration, like aircraft components, and the consequence is an unsustainable computational time if the problem is solved with a deterministic method.
An example of how the wavenumber increases when the frequency values are large can be seen in Figure 5.1a together with the decreasing of the wavelength in Figure 5.1b .

The computational inadequacy of FEM and BEM when z is big is one of the reasons why the Statistical Energy Analysis has taken hold in high frequencies vibroacoustic simulations.

2.3 Statistical Energy Analysis and Coupling Loss Factor

In this section, any information regarding SEA method is referred to [Lyon and DeJong 1995].

When the frequencies of a problem reach high values, two main consequences can be deduced. One phenomenon consist in the relevant participation of the high frequency resonant modes to the response of the system, which are characterised by high wavenumbers getting back to the problem of the huge number of nodes required to correctly represent the results, as explained in section 2.2. Another consequence is the high sensitivity of the results to the

minimum details of a system, in terms of geometrical features and mechanical properties. Indeed, when high frequencies are used in the excitation, a non-negligible variance of the response is caused by the small variance of mechanical properties due to the manufacturing process which it not predictable, and the non complete repeatability in applying the load and impose boundary conditions. Because of the first phenomenon, deterministic methods fail in high frequency simulations in terms of numerical error and time consumption due to the high number of degrees of freedom required, whereas the variance of the response would require a large number of different models on the same system, varying properties and geometry, so that they cannot be taken in account with a deterministic approach.

These failure problems of deterministic methods can be circumvented by using a statistical approach, developed in the Statistical Energy Analysis [Lyon and DeJong 1995]. Starting from the analysis of complex structures excited by random loads in 1959, Richard Lyon and Preston Smith carried out the two fundamentals facts on which the SEA is based on. It has been proven that in a given system with lightly coupled components, energy flows from the high energy vibrating system to the low energy one, and the flow is proportional to the difference between the energy level of the two components. This oscillation energy flow can be compared to the thermal and electric energy flow in the presence of electric potential difference or temperature difference.

2.3.1 SEA Procedure and Assumptions

Based on the results of Lyon and Smith, SEA method is developed in such a way that:

- the degrees of freedom are constituted by subsystems (components and modes) in which the system is subdivided
- the input of the model is given in the form of powers, the output is a set of averaged energies
- the unknown variables to be computed are the energies, instead of the displacements, flowing through the degrees of freedom
- the flow of energy is governed by three fundamental parameters that have to be known in advance of the statistical analysis: modal densities, damping loss factors, coupling loss factors
- the energy result of the method is then converted into the physical quantity of interest like velocity or acoustic pressure, in the form of root mean square (RMS)

The system is subdivided into many subsystems as it is necessary to subdivide its modal behaviour. This means that two subsystems may differ because they represent different components like beams and plates, but also because representing different wave types of one same component (for example out of plane and in plane modes of a thin plate can be modelled as two different subsystems). The energy is modelled as a quantity flowing through these subsystems, and the flow depends on three fundamental parameters: Coupling Loss Factor, Modal Density and Damping Loss Factor. The last two are taken as an average over the subsystem.
A very quick derivation of the SEA equations can be summarised as follow.

Considering a system subdivided in N subsystems as schematically shown in Figure 2.2a the time average input power can be defined through the boundary impedance Z or mobility Y and the exciting mean square velocity or force or pressure.
Being

$$f = Zv \qquad\qquad v = Yf \tag{2.1}$$

In the simple case of a point excitation with harmonic functions (and so complex vectors with absolute values $|f| = F$ and $|v| = V$), the input power is

$$P_{in,i} = \langle vf \rangle_t = \frac{1}{2}\,\mathrm{Re}(v^* f) = \frac{1}{2}F^2\,\mathrm{Re}(Y^*) = \frac{1}{2}V^2\,\mathrm{Re}(Z) \tag{2.2}$$

For line or surface excitation the input power is computed averaging the physical quantities over the excitation area and using line or surface impedances, which involve more complicated formulas. Some examples can be found in [Lyon and DeJong 1995, chapter 11].

A generic subsystem i excited with a power input $P_{in,i}$ over a frequency range $\Delta\omega$ vibrates with a certain energy E_i at steady state with the participation of M_i modes, in an equilibrium given by the energy flowing to all the other j communicating subsystems P_{ij} and the dissipated power in its damping behaviour $P_{d,i}$.

$$P_{in,i} = P_{d,i} + \sum_j P_{ij} \tag{2.3}$$

Given a Damping Loss Factor $\eta_{d,i}$ [see subsection 2.3.2], the dissipated power of the i-th subsystem can be expressed as

$$P_{d,i} = \omega \eta_{d,i} E_i \tag{2.4}$$

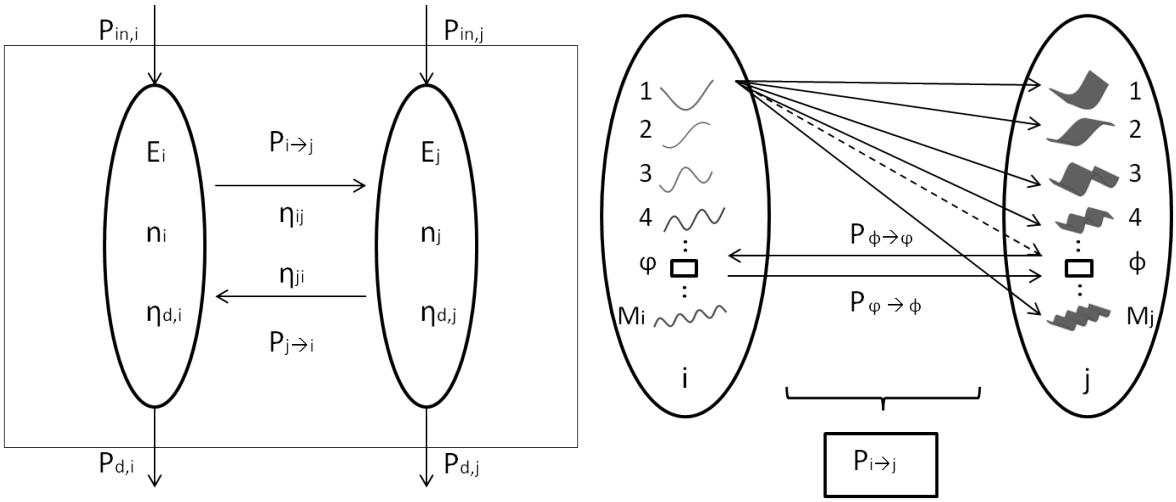

(a) Power balance between two generic subsystems i and j

(b) Power flow between modes φ and ϕ of the subsystems i and j

Figure 2.2: SEA subsystems

The net power flow P_{ij} which transfers energy from the subsystem i to the subsystem j is the subtraction of the two single power flows

$$P_{ij} = P_{i\to j} - P_{j\to i} = -P_{ji} \tag{2.5}$$

The single power flows are the summations of the energy exchange between all the communicating modes of the two subsystems. The direction of the net power flow between modes is from the higher to the lower modal energy $\mathcal{E}_i$, proportionally to the difference in modal energy value with a constant $\mathscr{B}$. As it is shown in Figure 2.2b the energy exchange between a mode φ of subsystem i and a mode ϕ of subsystem j is

$$P_{\varphi_i\to\phi_j} = \mathscr{B}(\mathcal{E}_{i,\varphi} - \mathcal{E}_{j,\phi}) \tag{2.6}$$

The modal energy $\mathcal{E}_i$ is define through the number of modes M_i participating over the frequency range $\Delta\omega$. The number of participating modes is given by the modal density [see subsection 2.3.3], and under the assumption that the total energy is equally distributed in each of the M_i modes:

$$\mathcal{E}_{i,\varphi} = \mathcal{E}_i = E_i/M_i \tag{2.7}$$

Considering all the modal energy exchanges in Equation 2.6, and using Equation 2.7:

$$P_{ij} = M_iM_j\mathscr{B}(\mathcal{E}_i - \mathcal{E}_j) = \mathscr{B}(E_iM_j - E_jM_i) \tag{2.8}$$

Defining the Coupling Loss Factor η_{ij} [subsection 2.3.4] the power flow can be written as

$$\eta_{ij} = \frac{\mathscr{B} M_j}{\omega} \tag{2.9}$$

$$P_{ij} = \omega(\eta_{ij} E_i - \eta_{ji} E_j) \tag{2.10}$$

Substituting Equation 2.10 in the power flow balance Equation 2.3, the final balance for the i-th subsystem can be obtained depending on the total energies E or the modal energies $\mathcal{E}$

$$P_{in,i} = \omega(\eta_{d,i} E_i + \sum_{j \neq i}^{N} \eta_{ij} E_i - \sum_{j \neq i}^{N} \eta_{ji} E_j) \tag{2.11}$$

$$P_{in,i} = \omega[(\eta_{d,i} + \sum_{j \neq i}^{N} \eta_{ij}) M_i \mathcal{E}_i - \sum_{j \neq i}^{N} \eta_{ji} M_j \mathcal{E}_j] \tag{2.12}$$

Considering all the N subsystems of a system behaving like in Figure 2.2a, the power balance can be extended and written in a matrix form

$$\begin{pmatrix} P_{in,1} \\ P_{in,2} \\ \vdots \\ P_{in,i} \\ \vdots \\ P_{in,N} \end{pmatrix} = \omega \begin{bmatrix} \eta_{d,1} + \sum\limits_{j \neq 1}^{N} \eta_{1j} & -\eta_{21} & \dots & -\eta_{j1} & \dots & -\eta_{N1} \\ -\eta_{12} & \eta_{d,2} + \sum\limits_{j \neq 2}^{N} \eta_{2j} & \vdots & -\eta_{j2} & \vdots & -\eta_{N2} \\ \vdots & \vdots & \ddots & & & \vdots \\ -\eta_{1i} & -\eta_{2i} & & \eta_{d,i} + \sum\limits_{j \neq i}^{N} \eta_{ij} & & -\eta_{N1} \\ \vdots & \vdots & & & \ddots & \vdots \\ -\eta_{1N} & -\eta_{2N} & \dots & -\eta_{jN} & \dots & \eta_{d,N} + \sum\limits_{j \neq N}^{N} \eta_{Nj} \end{bmatrix} \begin{pmatrix} E_1 \\ E_2 \\ \vdots \\ E_i \\ \vdots \\ E_N \end{pmatrix} \tag{2.13}$$

If the relation is expressed considering the modal energies as the unknown variables, the matrix of the system becomes symmetric

$$\begin{pmatrix} P_{in,1} \\ P_{in,2} \\ \vdots \\ P_{in,i} \\ \vdots \\ P_{in,N} \end{pmatrix} = \omega \begin{bmatrix} (\eta_{d,1} + \sum\limits_{j \neq 1}^{N} \eta_{1j}) M_1 & \dots & -\eta_{j1} M_j & \dots & -\eta_{N1} M_N \\ & \ddots & \vdots & \vdots & \vdots \\ & & (\eta_{d,i} + \sum\limits_{j \neq i}^{N} \eta_{ij}) M_i & \dots & -\eta_{Ni} M_N \\ symm. & & & \ddots & \vdots \\ & & & & (\eta_{d,N} + \sum\limits_{j \neq N}^{N} \eta_{Nj}) M_N \end{bmatrix} \begin{pmatrix} \mathcal{E}_1 \\ \mathcal{E}_2 \\ \vdots \\ \mathcal{E}_i \\ \vdots \\ \mathcal{E}_N \end{pmatrix}$$

(2.14)

This symmetry can be proven by multiplying Equation 2.9 by M_i, obtaining the reciprocity relation

$$\eta_{ij} M_i = \eta_{ji} M_j \tag{2.15}$$

which guarantees the equality of the off-diagonal terms and justify the preference to use this matrix because of the convenience in the storage.

Once the energies are computed, the mean square velocity or pressure can be derived from the subsystems properties as follow

$$E = \rho V \langle v^2 \rangle_t = \frac{V \langle p^2 \rangle_t}{\rho c^2} \tag{2.16}$$

These linear equations make sense only if some assumptions are taken in account, like the uncorrelation between the exciting sources necessary for the linearity, the proportionality between the power flow and the difference in modal energy (Equation 2.6) and the modal energy uniformly distributed over all the participating modes (Equation 2.7). Also, the dissipated power in a subsystem is proportional to its energy (Equation 2.4), the negligibility of power loss in the coupling through subsystems (Equation 2.9), and the coupling must be considered weak, that means it must not be strong enough to generate such a power flow to produce an energy of the excited subsystem of a different order of magnitude compared to the uncoupled condition.
With this short resume of the SEA method, the vibroacoustic problem is reduced to a simple linear algebraic system of power balance and the matrix of the problem is composed of three different parameters: damping and coupling loss factors, and the number of relevant participating modes.

2.3.2 Damping Loss Factor

The Damping Loss Factor $\boldsymbol{\eta}_d$ is one way to represent the capability of a system to reduce the amplitude of vibration dissipating energy. To create a reliable mathematical formulation for damping is very complicated for many materials because of different phenomena occurring in the dissipation. An easy way to model the damping behaviour for small displacements and linear parameters is under the assumption of hysteretic damping, adopted in this implementation, in which the dissipation is due only to viscous forces. This formulation is supported

by fast experimental methods for the direct evaluation from the response, such as Logarithmic Decrement Method, Half-Power Point Method, Kennedy-Pancu Method [Fasana and Marchesiello 2006]. The formulation for the damping can be quickly derived considering a single degree of freedom system vibrating with harmonic displacement $x(t) = X\cos(\omega t)$, completing one oscillation cycle as a result of an external excitation of frequency ω which does a work per cycle equal to

$$W_c = \int_{cycle} c\dot{x}\mathrm{d}x = \int_T c\ddot{x}^2\mathrm{d}t = \pi\omega c X^2 \tag{2.17}$$

However many experimental results showed that for many materials, the dissipated energy is almost independent of the frequency. In order to obtain a simple model, the correspondence between the work per cycle in Equation 2.17 and the work done by viscous force in a viscous damper ($W_{damper} = aX^2$, which depends on a material constant a) is imposed: $W_c = W_{damper}$. This equality can be obtained writing the damping coefficient in an equivalent form as follow:

$$c_{eq} = \frac{a}{\pi\omega} \tag{2.18}$$

Using the exponential notation $x(t) = X\exp^{\mathrm{i}\omega t}$, the motion equation can be written as

$$m\ddot{x} + c_{eq}\dot{x} + kx = F\exp^{\mathrm{i}\omega t}$$

$$m\ddot{x} + k(1 + \mathrm{i}\eta_d)x = F\exp^{\mathrm{i}\omega t} \tag{2.19}$$

where η_d is the constant damping loss factor, it depends on the material mechanical hysteresis and can be written as $\eta_d = a/k\pi$. Considering Equation 2.18 the damping loss factor is related to the damping ratio:

$$\eta_d = 2\zeta\frac{\omega}{\omega_n} \tag{2.20}$$

In the resonant condition in which the damping loss factor is typically measured, the relation becomes

$$\eta_d = 2\zeta \tag{2.21}$$

Using the previous notation, the stiffness of the system $k(1+\mathrm{i}\eta_d)$ can be studied as a complex value where the real part is the elastic component and the imaginary part represents the damping [Fasana and Marchesiello 2016].

One advantage of using this notation is that in order to consider the damping it is sufficient to multiply the elastic constants by $(1 + \mathrm{i}\eta_d)$, as it is done in section 4.3

2.3.3 Modal Density

The modal density $\boldsymbol{n}$ is the quantity with which it is possible to find the number of modes M participating in the vibration of a subsystem over a certain frequency range $\Delta\omega$. When talking about modes, it is possible to discern between different types of shapes based on different motions, for example modes of a beam can be divided in bending, torsional and longitudinal, as well as for a thin plate with the addition of the shear waves. To evaluate the modal density experimentally requires many measures since it is necessary to excite a system in all the possible ways of the related application, otherwise there would be a risk of missing some shapes which would not manifest unless subjected to precise conditions. Analytic formulations of the modal density are derived from its definition through the wavenumber:

$$n(\omega) = \frac{\mathrm{d}M}{\mathrm{d}\omega} \tag{2.22}$$

$$n(\omega) = \frac{M}{\Delta\omega} \quad \text{, if } n \text{ is constant} \tag{2.23}$$

Referring to [Lyon and DeJong 1995, chapter 8], the angular frequency derivative of the number of modes can be simplified if transformed in a wavenumber derivative.

$$n(\omega) = \frac{\mathrm{d}M}{\mathrm{d}\omega} = \frac{\mathrm{d}M}{\mathrm{d}k}\frac{\mathrm{d}k}{\mathrm{d}\omega} \tag{2.24}$$

It follows that the modal density can be calculated once the relation between the wavenumber and the time frequency of the load is defined.
In a one-dimensional system of length L, the wavelength and the wavenumber can be derived as a function of the number of modes:

$$\lambda_M = \frac{2L}{M+\delta} \qquad\qquad k = (M+\delta)\frac{\pi}{L} \tag{2.25}$$

where δ is a constant depending on the boundary conditions, $\delta = 0$ for simply supported beams. Deriving the number of modes with respect to the wavenumber gives the modal density. In order to do it, it is possible to change the differentiation variable using wave group speed c_g and wave phase speed c_ϕ

$$c_g = \frac{\mathrm{d}\omega}{\mathrm{d}k} \qquad\qquad c_\phi = \frac{\omega}{k} \tag{2.26}$$

Being the number of modes

$$M(k)_{1D} = \frac{kL}{\pi} - \delta \tag{2.27}$$

The modal density in the 1D systems can be derived as

$$n(\omega)_{1D} = \frac{\mathrm{d}M(k)}{\mathrm{d}k}\frac{\mathrm{d}k}{\mathrm{d}\omega} = \frac{L}{\pi c_g} \tag{2.28}$$

Considering the different values of c_g and c_ϕ for different type of waves, the modal density of a 1D system can be obtained as reported in Table 2.1, where κ is the radius of gyration ($= h/\sqrt{12}$ for beams of thickness h, and $= r/\sqrt{2}$ for pipes of radius r), E is the Young's Modulus, G is the shear modulus, J the torsional inertia, I_p the polar inertial moment of the cross section, K the bulk modulus and c_L, c_T, c_B, c_0 respectively the longitudinal, torsional, bending and medium wave speed.

Considering 2-dimensional systems like flat plates, the same approach leads to the following wavenumber expression, where 1, 2 are the two coordinate directions and σ and τ are mode indices:

$$k_{\sigma,\tau} = \sqrt{\left[(\sigma - \delta_1)\frac{\pi}{L_1}\right]^2 + \left[(\tau - \delta_2)\frac{\pi}{L_2}\right]^2} \tag{2.29}$$

Defining A as the plate area, P as the plate perimeter, h the plate thickness, ν as the Poisson's ratio and $\kappa = h/\sqrt{12}$ the radius of gyration of the plate, the modal densities for the 2D system are reported in Table 2.1.
The number of modes results in:

$$M(k)_{2D} \sim \frac{Ak^2}{4\pi} + \Gamma P k \tag{2.30}$$

where Γ is the correspondent of δ for the 2-dimensional problem, and the modal density

$$n(\omega)_{2D} \sim \frac{A\omega}{2\pi c_\phi c_g} \tag{2.31}$$

Repeating the same procedure for a 3-dimensional system, the results are the following

(Table 2.1):

$$k_{\sigma,\tau,\theta} = \sqrt{\left[(\sigma - \delta_1)\,\frac{\pi}{L_1}\right]^2 + \left[(\tau - \delta_2)\,\frac{\pi}{L_2}\right]^2 + \left[(\theta - \delta_3)\,\frac{\pi}{L_3}\right]^2} \tag{2.32}$$

$$M(k)_{3D} \sim \frac{Vk^3}{6\pi^2} + \Gamma_1 Ak^2 + \Gamma_2 Pk \tag{2.33}$$

$$n(\omega)_{3D} \sim \frac{V\omega^2}{2\pi^2 c_\phi^2 c_g} \tag{2.34}$$

	Wave type	c_g, c_ϕ	$n(\omega)$
1D	Longitudinal	$c_g = c_\phi = c_L = \sqrt{E/\rho}$	$L/(\pi c_L)$
	Torsional	$c_g = c_\phi = c_T = \sqrt{GJ/\rho I_p}$	$L/(\pi c_T)$
	Bending	$c_g = 2c_\phi = 2c_B = 2\sqrt{\omega\kappa c_L}$	$L/(2\pi c_B)$
	In a pipe	$c_g = c_\phi = c_0 = \sqrt{K/\rho}$	$L/(\pi c_0)$
2D	Longitudinal	$c_g = c_\phi = c'_L = \sqrt{E/\rho}$	$\omega A/(2\pi {c'_L}^2)$
	Shear	$c_g = c_\phi = c_S = \sqrt{G/\rho}$	$\omega A/(2\pi {c_S}^2)$
	Bending	$c_g = 2c_\phi = 2c_B = 2\sqrt{\omega\kappa c'_L}$	$A/(4\pi\kappa c'_L)$
	Flat rigid cavity wall	$c_g = c_\phi = c_0 = \sqrt{K/\rho}$	$\omega A/(2\pi {c_0}^2) + \omega P/(2\pi c_0)$
3D	In elastic solid	c_L and c_S constants	$\frac{V\omega^2}{2\pi^2 c_L^3} + \frac{V\omega^2}{2\pi^2 c_S^3}$
	In 3D rigid acoustic chamber	$c_g = c_\phi = c_0$	$\frac{V\omega^2}{2\pi^2 c_0^3} + \frac{A\omega}{8\pi^2 c_0^2} + \frac{P}{16\pi c_0}$

Table 2.1: Modal Density for 1D, 2D, 3D subsystems.

2.3.4 Coupling Loss Factor's

The coupling loss factors $\boldsymbol{\eta_{ij}}$, $\boldsymbol{\eta_{ji}}$ are the ratio between the respective gross power flows $P_{i\to j}$ and $P_{j\to i}$ between two subsystems i and j, and the respective subsystems energies E_i and E_j as defined in Equation 2.9 and 2.10. It can be written generically as

$$\eta_{ij} = \frac{P_{i\to j}}{\omega E_i} \tag{2.35}$$

The coupling loss factors in the two directions are related to each other by the reciprocity relation (Equation 2.15), so that it is sufficient to compute one of them, and the second can

be calculated knowing the number of modes of the two subsystems:

$$\eta_{ij} = \eta_{ji}\frac{M_j}{M_i} = \eta_{ji}\frac{n_j}{n_i} \tag{2.36}$$

The CLFs are the most important parameters of SEA since they constitute the matrix of the algebraic system, and it is necessary to know their values in advance of the simulation. Experimentally, the CLFs can be evaluated using the Power Injection Method, which consists in exciting all the subsystems with a unit power and measuring the power output, building a matrix composed by the ratios between excitation and response. The resulting response matrix can be inverted and the CLFs evaluated. It is clear how the CLFs only depend on the geometry of the connection between two subsystems, the so called **Junction**. It will be explained in section 3.2 how, if the frequency values are high enough to induce strong uncertainty, the dependency of the CLFs is only related to the junction and to the modal densities of the subsystems. This fact allows to define the calculation of the CLFs only by dividing the different possible types of junctions through subsystems of the same or different space dimension:

- Point junctions: can be obtained by coupling a 1D subsystems in its extreme points to a 1D (beam-beam) or a 2D (beam-plate) subsystem, or also coupling two 2D subsystems (plate-plate) using only one common point on their boundaries.
- Line junctions:can be obtained by coupling 1D and 2D subsystem along a line (beam-plate or plate-plate).
- Surface junctions: can be obtained by coupling 2D and 3D subsystems (plate-cavity), or two 3D subsystems (cavity-cavity)

The approach to compute the CLFs between a source and a receiving subsystem, consists in writing the transmitted power $P_{i\to j}$ using the geometric features of the junction, that is the impedance of the subsystem's boundary. Then, neglecting the dissipation in the transmission and considering the CLFs independent of the whole subsystem's details (section 3.2), divide this power by the frequency value and the subsystem's energy. The transmitted power is usually defined though the transmission coefficient τ_{ij} that is the fraction of the input power in i transmitted to j

$$\tau_{ij} = \frac{P_{i\to j}}{P_{in,i}} \tag{2.37}$$

The transmission coefficient is also symmetric [Cremer et al 2010]. As an example of derivation of the CLFs, a 1D system can be considered in the transmission of power between two

adjacent collinear beams i, j in a point junction [Lyon and DeJong 1995]. The energy of a beam i is composed by its power input $P_{in,i}$ plus the reflected power at the point junction P_r:

$$E_i = \frac{L_i}{c_{g,i}}(P_{in,i} + P_r) \tag{2.38}$$

The reflected power is related to the transmission coefficient for the point junction between beams, which is defined through the point impedance of the semi infinite beam Z_∞

$$P_r = P_{in,i} - P_{i\to j} = P_{in,i}(1 - \tau_{ij,\infty}) \tag{2.39}$$

$$\tau_{ij,\infty} = \frac{4\,\mathrm{Re}\left[Z_{i,\infty}\right]\mathrm{Re}\left[Z_{j,\infty}\right]}{\left|Z_{i,\infty} + Z_{j,\infty}\right|^2} \tag{2.40}$$

where the impedance depends on the type of wave considered:

$$Z_\infty = (1 + \mathrm{i})\rho_l c_B \quad \text{, for bending waves} \tag{2.41}$$

$$Z_\infty = \rho_l c_L \quad \text{, for longitudinal waves} \tag{2.42}$$

Considering the fact that the reflected power is the same magnitude of the input power, the transmitted power is much smaller giving a τ_{ij} value much smaller than 1. The coupling loss factor can therefore be derived as

$$\eta_{ij} = \frac{c_{g,i}}{\omega L_i}\frac{\tau_{ij}}{2 - \tau_{ij}} \simeq \frac{c_{g,i}\tau_{ij}}{2\omega L_i} \tag{2.43}$$

With similar and different approaches, CLFs for other type of junctions have been derived.

Point Junctions can involve connection between two beams or between beam and plate. As shown in [Langley and Shorter 2003], referring to Figure 2.3a, a point junction between a certain number of beams and a plate of area A is studied.

Generically, the mean power associated to a certain wave is proportional to its square amplitude a and group velocity c_g

$$P = \alpha c_g \left|a\right|^2 \tag{2.44}$$

With α proportionality constant. Considering two subsystems i and j, the transmission coefficient of a certain wave incident to the junction is the ratio of the power transmitted away from the junction by the wave component α_{ij} to the power carried towards the junction

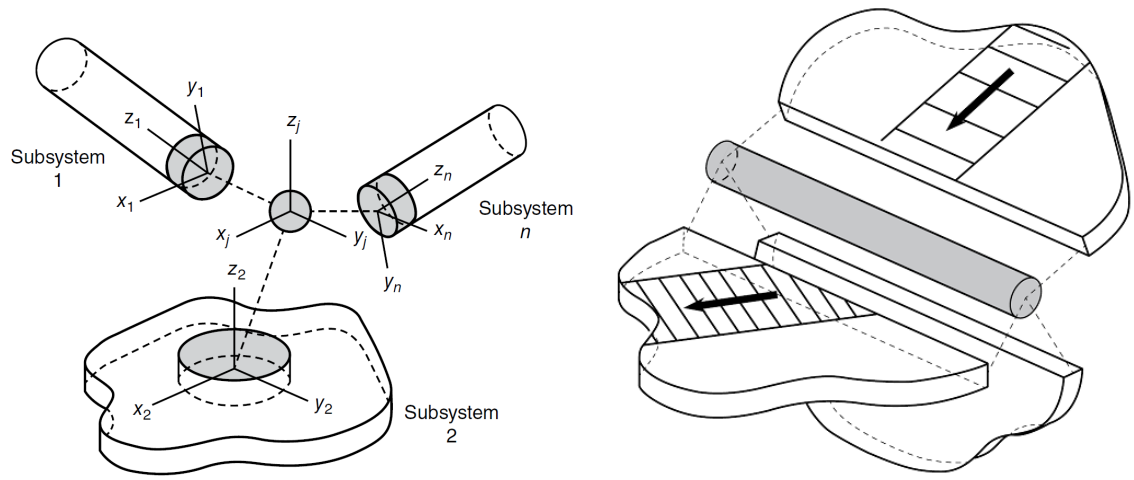

(a) Point junction between plate and beams **(b)** Line junction between beam and plates

Figure 2.3: Point and Line Junctions (figures of [Hambric et al 2016])

by an incident wave component a_{in}

$$\tau_{ij} = \frac{\alpha_j c_{g,j} \left|a_{ij}\right|^2}{\alpha_i c_{g,i} \left|a_{in,i}\right|^2} = \tau_{ji} \tag{2.45}$$

The power carried by one wave towards the junction in this system is:

$$P = \frac{E_i c_{g,i}}{2L} \quad \text{when carried by a 1D subsystem} \tag{2.46}$$

$$P = \frac{E_i c_{\phi,i} c_{g,i}}{\omega A} \quad \text{when carried by a 2D subsystem} \tag{2.47}$$

Considering the modal density formulation in Table 2.1 for 1D and 2D subsystems

$$n_{1D} = \frac{L}{\pi c_g} \qquad n_{2D} = \frac{\omega A}{2\pi c_g c_\phi} \tag{2.48}$$

and considering all the possible incident waves (R) at the junction with the plate, the transmitted power is

$$P_{i\to j} = \frac{E_i c_{g,i}}{2L} \sum_{r_j}^{R} \tau_{ir_j} \quad \text{when } i \text{ is 1D} \tag{2.49}$$

$$P_{i\to j} = \frac{E_i c_{\phi,i} c_{g,i}}{\omega A} \sum_{r_i}^{R} \tau_{r_i j} \quad \text{when } i \text{ is 2D} \tag{2.50}$$

The CLFs are calculated dividing the transmitted power by ωE_i:

$$\eta_{ij} = \frac{c_{g,i}}{2\omega L} \sum_{r_j}^{R} \tau_{ir_j} = \frac{1}{2\pi\omega n_i} \sum_{r_i}^{R_i} \tau_{r_i j} \quad \text{for 1D} \rightarrow \text{2D transmission} \tag{2.51}$$

$$\eta_{ij} = \frac{c_{\phi,i} c_{g,i}}{\omega^2 A} \sum_{r_i}^{R} \tau_{r_i j} = \frac{1}{2\pi\omega n_i} \sum_{r_i}^{R_i} \tau_{r_i j} \quad \text{for 2D} \rightarrow \text{1D transmission} \tag{2.52}$$

If both i and j are 2D subsystems with R incident waves at the junction in i and S incident waves at the junction in j, the resulting CLF is

$$\eta_{ij} = \frac{1}{2\pi\omega n_i} \sum_{r_i}^{R} \sum_{s_j}^{S} \tau_{r_i s_j} \tag{2.53}$$

Line Junctions can involve connection between two plates along one edge or between a beam and plates along the length of the beam and the edge of the plate. Referring to Figure 2.3b, a method to calculate CLF for line junctions was developed in [Langley and Heron 1990]. The method consists in averaging the coupling loss factor over all the possible angle θ of incidence of the waves with the junction:

$$\eta_{ij} = \frac{1}{\pi} \int_{-\frac{\pi}{2}}^{\frac{\pi}{2}} \eta_{ij}(\theta) \mathrm{d}\theta \tag{2.54}$$

Considering the energy carried by the vibrating plate of area A_i towards the junction of length L_{junc}

$$E_i = \frac{A_i (P_{in,i} + P_r)}{L_{junc} c_{g,i} \sin\theta} = \frac{A_i}{L_{junc} c_{g,i} \sin\theta} P_{in,i} (2 - \tau_{ij}(\theta)) \tag{2.55}$$

$\tau_{ij}(\theta)$ depends on the line impedance of the plate. The CLF of the line junction between two plates i and j where the plate i transmits power with a wave of type p in the plate j generating a wave of type r, can be written:

$$\eta_{ij}^{pr}(\theta) = \frac{P_{i \rightarrow j}}{\omega E_i} = \frac{L_{junc} c_{g,i} \sin\theta}{\omega A_i} \frac{\tau_{ij}^{pr}(\theta)}{2 - \tau_{ij}^{pr}(\theta)} \tag{2.56}$$

Since $\tau_{ij}^{pr}(\theta)$ is nearly zero, the integral becomes:

$$\eta_{ij^{pr}} \simeq \frac{2}{\pi} \int_0^{\frac{\pi}{2}} \frac{L_{junc} c_{g,i} \sin\theta}{\omega A_i} \frac{\tau_{ij}^{pr}(\theta)}{2} \mathrm{d}\theta = \frac{1}{\pi} \frac{L_{junc} c_{g,i}}{\omega A_i} \int_0^{\frac{\pi}{2}} \tau_{ij}^{pr}(\theta) \sin\theta \mathrm{d}\theta \tag{2.57}$$

Writing as τ_{ij}^{pr} the integral of the transmission coefficient, the CLF for the line junction

results in

$$\eta_{ij}^{pr} \simeq \frac{c_{g,i} L_{junc} \tau_{ij}^{pr}}{\pi \omega A_i} \tag{2.58}$$

which can be related to the modal density of the plate i in base of which types of wave are considered. An alternative method is proposed in [Skeen and Kessissoglou 2007], where a scattering matrix method is combined with an analytical waveguide model for the calculation of the transmission coefficients.

Surface Junctions can involve connection between a cavity and a plate over its surface or between two cavities over the surface that delimits the two volumes. Considering a plate of mass m_{plate} vibrating with a root mean square velocity $\langle v^2 \rangle$, its energy can be written as

$$E_{plate} = m_{plate} \langle v^2 \rangle \tag{2.59}$$

Considering now a cavity containing a fluid with volumetric mass density ρ_0 and wave speed c_0, excited from one of its surfaces S by the vibration of the plate, the radiated power in the cavity depends on the radiation efficiency σ_{rad} of the plate:

$$P_{rad} = \sigma_{rad} \rho_0 c_0 A \langle v^2 \rangle \tag{2.60}$$

The radiation efficiency can be calculated as shown in [Fahy 2000, Chapter 10.14.3]:

$$\begin{cases} \sigma_{rad} \simeq 1 & k \geq k_c \\ \sigma_{rad} \simeq \frac{2P}{\pi k_c A} \sqrt{\frac{k}{k_c}} & k \ll k_c \end{cases} \tag{2.61}$$

Where P and A are the perimeter and area of the plate, and k_c is the critical wavenumber of the plate, at which the acoustic and structural wavenumbers and phase speed are the same. The coupling loss factor of the power transmission from the plate to the cavity, assuming $A \geq S$ is:

$$\eta_{plate \to cavity} = \frac{P_{rad}}{\omega E_{plate}} = \frac{\rho_0 c_0 A \sigma_{rad}}{\omega \rho_S S} \tag{2.62}$$

Considering the power transmission in the direct coupling between two cavities, the coupling loss factor can be calculated using the same approach as the plate-plate coupling, defining the CLF as a function of the angle of incidence with which a wave reaches the junction and integrating over all the possible angles given by the geometry of the problem. Considering a

transmission surface S, and the cavity volume V:

$$\eta_{ij}(\theta) \simeq \frac{c_{0,i}S}{2\omega V_i}\tau_{ij}(\theta) \tag{2.63}$$

Performing the same integration of Equation 2.57 in two dimensions, the CLF is finally expressed as follow

$$\eta_{ij} \simeq \frac{c_0 A}{4\omega V_i}\langle\tau\rangle \tag{2.64}$$

In chapter 3, a more generic method to compute the CLFs is explained considering also the presence of deterministic components for hybrid theory.

2.4 Hybrid Methods: Motivations and Applications

In this chapter it was explained how deterministic methods are the best way to simulate the low-frequency problem, and how they fail in the high frequency range because of two reasons:

- great computational effort requested because of the huge amount of degrees of freedom needed to appropriately represent the response, which has consequences on the computational time and the numerical error
- the variability of the response due to minimal changes in the system properties cannot be predicted with deterministic variables, unless a large number of simulation is carried out

Statistical Energy Analysis is a valid alternative in the high-frequency range because it compensates the limits of deterministic methods since the result is related to the average energetic behaviour of the components, instead of being the exact deformed shape of displacements. Also, it treats the loading and the mechanical properties with a stochastic approach resulting in a certain variance of the response comparable with experimental data. On the other hand, it is exactly for these reasons that SEA is not suitable for low frequency values.

Since it is not possible to define a frequency value and a frequency range threshold to discriminate whether it is better to use a deterministic method (FEM, BEM) or a statistical method (SEA), and since in one system can be present subsystems of different wavelength of vibration in base of their modal behaviour, starting from the 1990s a new method has been studied: the Hybrid FEM/SEA method. This method is supposed to be used when

the frequency values related to the dimensions are neither small enough to justify a FEM approach, which would lead to a very dense mesh, nor high enough to justify a SEA approach, which would require a high frequency to produce reliable results. This kind of problem is the so called **'Mid-Frequency Problem'**.
A gross guide to choose the numerical method depending on the frequency range of the problem can be found in Table 2.2, in any case it is very challenging trying to give such a guide since the choice of the method can strongly depend on many features of the problem. For the sake of completeness, is worth mentioning that also Hybrid methods FEM/EFEM and FEM/TPA are used to perform simulation in the mid-frequency range, and EFEM in the high-frequency range [Hambric et al 2016].

Another possible criteria for choosing the method can be seen in [Peiffer 2016], where in a resume of acoustic methods for aircraft, several simulation strategies are classified in relation to their complexity and the frequency range as shown in Figure 2.4. The primary structures of an aircraft are typically very stiff and vibrate with a low wavenumber over a large frequency range. For this reason they can be modelled with deterministic methods until $\sim$ 400 Hz, where the panels wavenumber strongly increases favouring a hybrid method. The lining has less structural requirement than the fuselage, therefore it is composed by thinner panels which produce high wavenumber at lower frequency values. For these subsystems, the necessity to be modelled with a statistical approach occurs around 200 Hz. When big cavities containing fluid are considered the wavenumber of the vibration gets easily high, requiring ray-tracing techniques. Also very complex systems cannot be analytically modelled at high frequencies and energy flow method (EFM) must be adopted between detailed subcomponent finite element models.
Other typical applications of the hybrid method FEM/SEA are for example automotive or buildings, but the generic frequency threshold would shift with respect to the aircraft case

Frequency range	$z = kL/2\pi$	Methodology	Resolution
Low Frequency	$0 < z <\sim 10$	FEM, BEM	High
Mid Frequency	$\sim 5 < z <\sim 20$	Hybrid FEM/SEA Hybrid FEM/EFEM Hybrid FEM/TPA	
High Frequency	$\sim 10 < z$	SEA, EFEM	Low

Table 2.2: Approximate frequency range based classification of computational methods in vibroacoustics

because of the different application frequencies and because of the different typical thickness and area of components affecting the wavenumbers.
As it will be shown in section 3.1, *the frequency range is not the only reason why the hybrid modelling must be taken in account; a new procedure for the calculation of CLFs must be adopted if deterministic subsystems and boundary conditions to the statistical subsystems are present in the model. The reason is that SEA formulas* (subsection 2.3.4) *are not able to consider deterministic conditions, and are not able to model junctions with complex shapes, but can only represent a subsystem as it was totally statistical and junctions in the simplest form.*

The aim of this thesis is therefore to compute the CLFs for the plate-beam-plate line junction considering the beam as a deterministic component and the plates as statistical (random) components (section 4.1), so that the energies can be computed. Such a target cannot be satisfied with the method proposed in subsection 2.3.4 for the line junction, since it does not allow to impose deterministic conditions and compute deterministic results (loads or displacements) on the deterministic subsystem (beam).

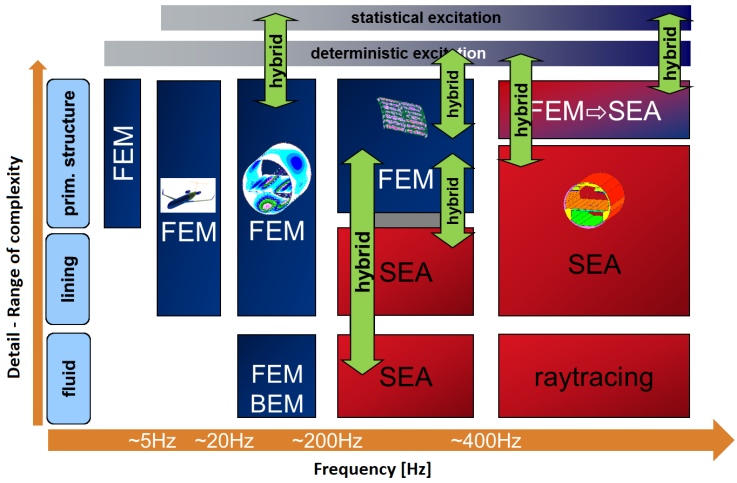

Figure 2.4: Numerical modelling techniques mainly used in aerospace systems (figure of [Peiffer 2016])

3 Hybrid FEM/SEA Method

In this chapter the hybrid FEM/SEA method is explained in detail with the derivation of the reverberant power balance which defines the algebraic system of linear equations for the solution of the statistical subsystems. The derivation was exposed by [Shorter and Langley 2005b] as a generic method, without any reference to the hybrid FEM/SEA. The method is introduced with a description of the junctions and the subsystems, and the assumptions with which they are classified (section 3.1). Then, the Diffuse Field Reciprocity Relationship is derived (section 3.2) in order to correctly write the power transmission at the junctions (section 3.3). Defining a cartesian coordinate system $\left(\hat{i},\hat{j},\hat{k}\right)$, with coordinates $\mathbf{x}$=$[x,y,z]$, the set of displacements and rotations can be written as $\mathbf{y}$=$\left[u_x\hat{i},u_y\hat{j},u_z\hat{k},\theta_x\hat{i},\theta_y\hat{j},\theta_z\hat{k}\right]^{\mathrm{T}}$. It is necessary to make the assumption that the time dependence of the displacements has a harmonic behaviour, so that the set of displacement components can be written as a summation of harmonic contribution, for example through a Fourier Series Decomposition. The single contribution of the set of harmonic displacements $\mathbf{y}(t,\mathbf{x})$ is then related to the velocity $\dot{\mathbf{y}}(t,\mathbf{x})$ as follows:

$$\mathbf{y}(t,\mathbf{x}) = \mathbf{Y}(\mathbf{x})\exp^{\mathrm{i}\omega t} \qquad \dot{\mathbf{y}}(t,\mathbf{x}) = \mathbf{V}(\mathbf{x})\exp^{\mathrm{i}\omega t} = \mathrm{i}\omega\mathbf{Y}(\mathbf{x})\exp^{\mathrm{i}\omega t} = \mathrm{i}\omega\mathbf{y}(t,\mathbf{x}) \tag{3.1}$$

In this chapter the displacements are considered transformed in a discrete set of N_q generalized coordinates $\mathbf{q}(t)$=$\mathbf{q}\exp^{\mathrm{i}\omega t}$, $\mathbf{q}$=$[q_1,q_2,...q_{N_q}]^{\mathrm{T}}$ which give the physical coordinates through N_q basis functions $\psi_{i,k}$, k=1...N_q, for each i-th displacement component. Basis functions can be mode shapes (then giving $\mathbf{q}$ in modal coordinates) or whatever valid basis functions set, capable to represent the results (examples of basis functions as modes or *sinc* function are expounded in subsection 4.3.3 and subsection 4.3.4). Considering a generic displacement

component $u_i(t,\mathbf{x})$, this transformation can be written as

$$\begin{aligned} u_i(t,\mathbf{x}) &= \sum_{k}^{N_q} \psi_{i,k}(\mathbf{x}) q_k(t) \\ \dot{u}_i(t,\mathbf{x}) &= \mathrm{i}\omega \sum_{k}^{N_q} \psi_{i,k}(\mathbf{x}) q_k(t) \end{aligned} \tag{3.2}$$

using as $\left[\psi_{i,1}, \psi_{i,2} ... \psi_{i,N_q}\right]$ the basis functions of the i-th displacement component. Because of next use, is useful to write the conjugate of the velocity as

$$\dot{\mathbf{q}}(t)^* = -\mathrm{i}\omega \mathbf{q}(t)^* \tag{3.3}$$

3.1 Subsystems, Boundaries and Hybrid Junctions

A hybrid or complex system is an ensemble of components whose properties are not known to a sufficient level of precision to justify an approach that is completely deterministic. As explained in section 2.2, the uncertainty of properties of a component is mainly due to a big variance in the response at high frequency excitation, and to the very high precision required by the system to be solved deterministically.
In section 2.4, the need of the hybrid FEM/SEA method is manly attributed to the possible coexistence of deterministic and statistical subsystems because of a mid-frequency range of excitation frequency. Actually, the hybrid modelling is also used in the high-frequency problem, at wavelength values that lies in the statistical case. In fact, even if the very high frequency level leads to choose the only SEA approach, when a junction presents a complex shape which is not traceable as a simple point, line or area, a deterministic description must be adopted, otherwise the SEA CLFs will refer to a different case. Beside, if deterministic boundary conditions are located within a few wavelengths of the connection, its local impedance is largely influenced, and so are the CLFs and the energy flow. For these reasons a deterministic description on some details of the system must be done, and this is allowed by the method presented in what follows.

A **subsystem** of a hybrid model can be "deterministic" or "statistical", see Figure 3.1. The classification of the type of a subsystem can be done by confronting the maximum wavenumber of its vibration with the relative characteristic length, as already done in section 2.4 though the parameter z. The deterministic subsystems are the ones that requires a deterministic approach (low z), and the statistical subsystems are the ones that require a statistical

approach (large z). The response is studied as a random variable as in SEA because of the presence of statistical subsystems. The ensemble average power flow between the statistical subsystems is computed taking into account the influence of the deterministic details, that is the deterministic stiffness. The hybrid algebraic system of equations derives from the power balance over the statistical subsystems, and it is in a similar form to the SEA equations.
A generic statistical subsystem of a hybrid model is characterized by high wavenumbers and strong uncertainty of properties and it is exactly like a SEA subsystem, with the addition of the possibility to possess deterministic details on its boundary.

The subsystems in a generic hybrid model are connected to each other though three possible types of junction, see Figure 3.1

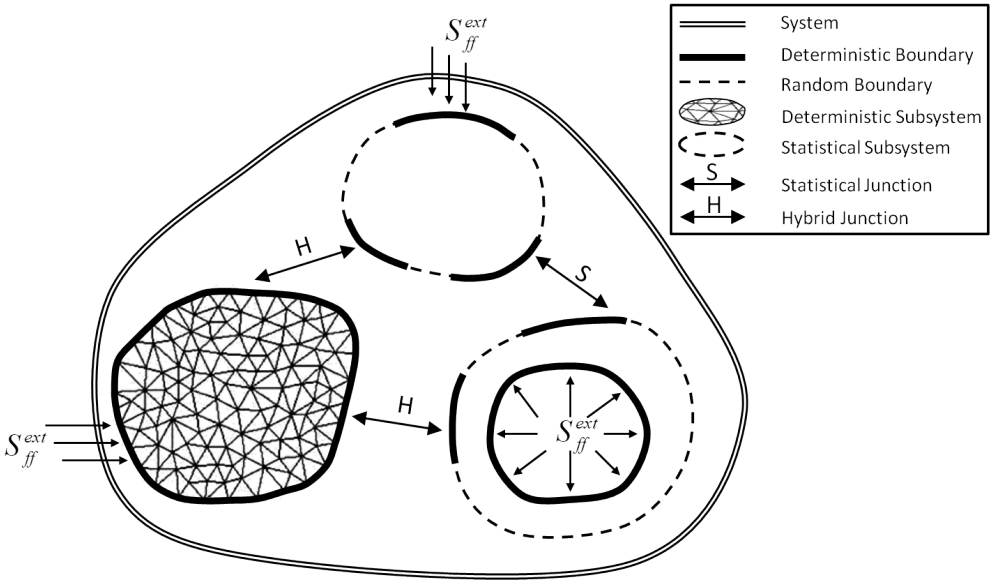

Figure 3.1: Hybrid system composed by generic deterministic and statistical subsystems connected through junctions at their deterministic and random boundaries. Deterministic junctions can be omitted and viewed as part of the connected deterministic subsystems.

1. **deterministic junction**: is the connection between deterministic components and, as such, there is not need of particular discussions since it is sufficient to impose the equality between the connected degrees of freedom or the forces of the two boundaries, in a way which depends on the type of joint

2. **"statistical junction"**: is the connection between two directly coupled statistical subsystems which exchange energy as described by the SEA CLFs in subsection 2.3.4. The SEA approach provides CLFs formulation only for point line and area junctions, then if a "statistical junction" is defined, such a connection can only be modelled as if it represented one of these simple cases. (Using the nomenclature "statistical junction"

can be object of discussion, indeed in order to define the SEA CLFs, one must know how the statistical subsystems are connected, which means that the connection is not completely uncertain. For this reason, this definition is only referred to the fact that there are no deterministic subsystems between the statistical ones and assumptions on the junction geometry are made so that the SEA CLFs can be used).

3. **hybrid junction**: is the connection between two statistical subsystems which are connected through a deterministic subsystem, or directly connected through a deterministically defined junction. Referring to what said regarding the "statistical junction", if the junction geometry does not correspond to one of the simple cases provided by SEA formulas for the CLFs, the connection can be defined deterministically as a hybrid junction.

Considering a group of statistical subsystems, the presence of deterministic subsystems and hybrid junctions requires a new derivation of the power balance defined in subsection 2.3.1. Studying a hybrid junction means to compute the power flow between the connected statistical subsystems, that means compute the **hybrid CLFs**. It will be explained how the properties of the hybrid junction only depend on the well known deterministic impedance and on the impedance of the statistical subsystem defined only in the proximity of the connection. In conclusion, the hybrid model includes statistical subsystems and deterministic details which consist in hybrid junctions. A generic statistical subsystem with uncertain properties and high wavenumber possesses in this model also deterministic details, which are hybrid junction themselves or deterministic boundary conditions, therefore a part of boundary that is deterministic. The part of boundary of a statistical subsystem which is connected through a hybrid junction, is called "**deterministic boundary**". The remaining part of the statistical boundary is called "**random boundary**". Therefore the deterministic boundary must coincide with the connection region with the deterministic subsystems, or with deterministic boundary conditions. In general, it can be stated that a random boundary is the boundary of a statistical subsystem whose dimensions are very large with respect to the wavelengths, so that it is likely that such dimensions will not be know with sufficient precision to be included in a deterministic description.

One particular case of statistical subsystems is represented by a component with large dimensions compared to the wavelengths, and so considered as statistical, which has deterministic connection region all over its boundary. An example can be a thin flat plate with a big area for which a statistical approach is well suited, surrounded at its boundaries by very stiff beams, for which a deterministic description is more opportune (the reasons of this classification lie in the wavenumbers and are discussed in a more detailed way in chapter 4).

Even if the plate has only deterministic boundaries, it must be considered as a statistical subsystem, and a series of hypothetical internal random boundary can be imagined to model the existing random scattering within the plate's domain.

Another detail that is fair to mention is the interaction between multiple deterministic connections in the same statistical subsystem. Considering a statistical subsystem with two or more deterministic connections at its boundary, like for example the statistical subsystems in Figure 3.1. If the two connections of a subsystem are relatively close enough to be in a few wavelengths of each other, then they exhibit coherent interaction with each other and they are said to be "coherently coupled". If the two connections present a distance big enough with respect to the wavelengths, then the interaction is sensitive to perturbations and the connections are said to be "incoherently coupled".

3.2 Diffuse Field Reciprocity Relationship

In this section, the statistical behaviour of the forces on the deterministic boundary of a statistical (hybrid) subsystem are analysed through the derivation of the diffuse field reciprocity relationship, referring to [Shorter and Langley 2005a].

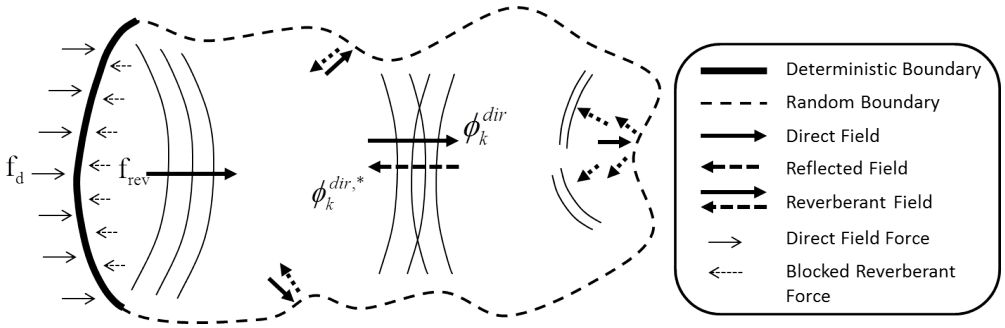

Figure 3.2: Direct and Reverberant Fields in a statistical subsystem connected with a junction at its deterministic boundary.

Looking at Figure 3.2, a statistical subsystem possesses a deterministic boundary because of the connection to a hybrid junction or a deterministic boundary condition. Considering an excitation on the deterministic boundary, a radiation field in the direction of the random boundaries of the statistical subsystem is generated. This field is called "direct field". The direct field radiates the domain until reaching the random boundary, where it gets partially transmitted to other eventual subsystem or dissipated, and partially reflected. The field generated by the reflection of the direct field at the random boundaries is called "reverberant

field". The diffuse field reciprocity relationship discussed in this section shows how, if under some assumptions the reverberant field is a "diffuse field", in a statistical subsystem the loading on the deterministic boundaries due to the reverberant field is statistically zero, and its cross-spectrum is statistically related to the behaviour of the direct field, proportional to the resistive part of its stiffness. In order to derive these results, it is necessary to write the analytical form of the forces related to the direct and the reverberant fields, which requires to define natural coordinates (subsection 3.2.2) and the statistics of boundary conditions at the random boundaries (subsection 3.2.3).

3.2.1 Free Field Radiation Stiffness of Statistical Subsystems

Distinguishing loads and displacement on the two different types of boundaries, $\mathbf{q}_d$, $\mathbf{f}_d$ for the deterministic ones and $\mathbf{q}_r$, $\mathbf{f}_r$ for the random ones, the stiffness problem can be written as $\mathbf{Hq} = \mathbf{Gf}$, writing $\mathbf{q} = \begin{bmatrix}\mathbf{q}_d^{\mathrm{T}} & \mathbf{q}_r^{\mathrm{T}}\end{bmatrix}^{\mathrm{T}}$ and $\mathbf{f} = \begin{bmatrix}\mathbf{f}_d^{\mathrm{T}} & \mathbf{f}_r^{\mathrm{T}}\end{bmatrix}^{\mathrm{T}}$.
Supposing to use a direct boundary element approach as described by [Brebbia and Dominquez 1992] over a boundary which is partitioned into a deterministic part and a random part (Figure 3.2), the relation between loads and generalized displacements becomes:

$$\begin{bmatrix}\mathbf{H}_{dd} & \mathbf{H}_{dr} \\ \mathbf{H}_{rd} & \mathbf{H}_{rr}\end{bmatrix}\begin{pmatrix}\mathbf{q}_d \\ \mathbf{q}_r\end{pmatrix} = \begin{bmatrix}\mathbf{G}_{dd} & \mathbf{G}_{dr} \\ \mathbf{G}_{rd} & \mathbf{G}_{rr}\end{bmatrix}\begin{pmatrix}\mathbf{f}_d \\ \mathbf{f}_r\end{pmatrix} \tag{3.4}$$

In order to calculate only the deterministic displacement which are related to well-known properties of the respective boundary, the system of equation can be reduced to the deterministic variables:

$$\mathbf{f}_d + \mathbf{f}_{rev} = \mathbf{D}_{dir}\mathbf{q}_d \tag{3.5}$$

$\mathbf{D}_{dir}$ is called "direct field dynamic stiffness matrix", or "free field radiation stiffness matrix", and can be expressed as

$$\mathbf{D}_{dir} = \mathbf{G}_{dd}^{-1}\mathbf{H}_{dd} \tag{3.6}$$

The direct field dynamic stiffness of a statistical subsystem is the stiffness that the subsystem presents when excited by the direct field at one of its deterministic boundaries. It can be typically derived from a boundary element method, but for simple cases like point, line and area junction under certain assumptions can be computed analytically, as it will be discussed in section 4.3. If real or imaginary valued basis functions are used to express the generalized

coordinates of the discretization, then Ddir is a complex and symmetric matrix. If the basis functions are complex valued and the functional used to describe the radiation is also complex, then Ddir loses its symmetry, while it is still symmetric its absolute value. This is the case of the application of this thesis (subsection 4.3.3 and subsection 4.3.4).

Looking at Equation 3.5, it is evident how the influence of the random boundary can be totally represented by the so called "blocked reverberant" force $\mathbf{f}_{rev}$ that excites the deterministic boundary. This force can be seen as the effect of the reverberant field reaching the deterministic boundary, behaving like an intrinsic excitation of the subsystem. $\mathbf{f}_{rev}$ can be interpreted as the force that needs to be applied to the deterministic boundary degrees of freedom in order to keep them blocked when the random boundaries are moved by a prescribed displacement boundary condition. The blocked reverberant force can be derived from Equation 3.4 imposing a boundary condition on the random boundary. The derivation of $\mathbf{f}_{rev}$ for clamped and free random boundaries is developed in section A.1, and the results are:

$$\begin{cases} \mathbf{f}_{rev} = -\left(\mathbf{G}_{dd}^{-1}\mathbf{G}_{dr}\mathbf{G}_{rr}^{-1}\mathbf{G}_{rd}\right)\mathbf{f}_d + \left(\mathbf{G}_{dd}^{-1}\mathbf{G}_{dr}\mathbf{G}_{rr}^{-1}\mathbf{H}_{rd}\right)\mathbf{q}_d & , \mathbf{q}_r \text{ clamped} \\ \mathbf{f}_{rev} = -\left(\mathbf{G}_{dd}^{-1}\mathbf{H}_{dr}\mathbf{H}_{rr}^{-1}\mathbf{G}_{rd}\right)\mathbf{f}_d + \left(\mathbf{G}_{dd}^{-1}\mathbf{H}_{dr}\mathbf{H}_{rr}^{-1}\mathbf{H}_{rd}\right)\mathbf{q}_d & , \mathbf{q}_r \text{ free} \end{cases} \tag{3.7}$$

Any random boundary produces a blocked reverberant force which is completely coherent with the direct field that generates it. This means that the reflection of the direct field at the random boundary does not change the phase of the wave at a given frequency.
Since the random boundary is defined as a boundary whose properties are uncertain like over the statistical subsystem, it is opportune to study such a subsystem with a statistical approach, computing the expected value of the cross-spectral response. The cross-spectrum of two signals evolving in space and time domains x and y is indicated with S_{xy}, and it can be computed by multiplying the first signal by the hermitian transpose of the second signal, since the cross-spectrum is the Fourier Transform of the respective convolution (assuming to be in time-frequency domain). The operation generates the cross-spectral matrix

$$\mathbf{S}_{xy} = \mathbf{x}\mathbf{y}^{\mathrm{H}} \tag{3.8}$$

In order to compute the cross-spectrum of the response signals on the deterministic boundary $\mathbf{S}_{q_d q_d}$, Equation 3.5 must be inverted:

$$\mathbf{q}_d = \mathbf{D}_{dir}^{-1}\left(\mathbf{f}_d + \mathbf{f}_{rev}\right) \tag{3.9}$$

The cross-spectrum of the deterministic generalized displacements results in:

$$\mathbf{S}_{q_d q_d} = \mathbf{q}_d \mathbf{q}_d^{\mathrm{H}} = \mathbf{D}_{dir}^{-1} \left(\mathbf{f}_d \mathbf{f}_d^{\mathrm{H}} + \mathbf{f}_d \mathbf{f}_{rev}^{\mathrm{H}} + \mathbf{f}_{rev} \mathbf{f}_d^{\mathrm{H}} + \mathbf{f}_{rev} \mathbf{f}_{rev}^{\mathrm{H}} \right) \mathbf{D}_{dir}^{-\mathrm{H}} \tag{3.10}$$

The term $\mathbf{f}_d \mathbf{f}_d^{\mathrm{H}}$ is the cross-spectrum of all the loadings applied on the deterministic boundary as a result of external excitations or of junction excitation due to a deterministic subsystem. The term $\mathbf{f}_{rev} \mathbf{f}_{rev}^{\mathrm{H}}$ is the cross-spectrum of the blocked reverberant forces applied on the deterministic boundary by the reverberant field, generated by the reflection of the direct field at the random boundary. The mixed factors $\mathbf{f}_d \mathbf{f}_{rev}^{\mathrm{H}}$ and $\mathbf{f}_{rev} \mathbf{f}_d^{\mathrm{H}}$ are the cross-spectra of the loadings on the deterministic boundary due to external forces and reverberant fields. Following the stochastic approach, the expected value $\langle ... \rangle$ of the cross-spectrum can be evaluated:

$$\langle \mathbf{S}_{q_d q_d} \rangle = \langle \mathbf{q}_d \mathbf{q}_d^{\mathrm{H}} \rangle = \mathbf{D}_{dir}^{-1} \left(\mathbf{f}_d \mathbf{f}_d^{\mathrm{H}} + \mathbf{f}_d \langle \mathbf{f}_{rev}^{\mathrm{H}} \rangle + \langle \mathbf{f}_{rev} \rangle \mathbf{f}_d^{\mathrm{H}} + \langle \mathbf{f}_{rev} \mathbf{f}_{rev}^{\mathrm{H}} \rangle \right) \mathbf{D}_{dir}^{-\mathrm{H}} \tag{3.11}$$

where the expected value operator is omitted for the external loading at the deterministic boundary, assuming this load to be known deterministically, so with a single possible value. With the intention of deriving the Diffuse Field Reciprocity Relationship, it is appropriate to define the natural coordinates for the radiating fields which contribute to the vibration of the statistical subsystems.

3.2.2 Natural Coordinates for Direct and Reverberant Fields

Since the direct field is the radiation generated by the deterministic boundary without any interaction with the reflected field, it can be studied by neglecting the random boundaries and so the reverberant field. Regarding the direct field, a set of natural coordinates $\mathbf{q}$ can be defined on the deterministic boundary to describe in the easiest way the power radiating into the subsystem. To find them, one can write the radiated power from the deterministic boundary considering Equation 2.2, 3.1 and 3.3, and recalling that for a complex quantity X is valid $\mathrm{Re}\left[\mathrm{i}X\right] = -\mathrm{Im}\left[X\right]$:

$$P_{dir} = -\frac{\mathrm{i}\omega}{2} \mathrm{Re}\left[\mathbf{q}^{\mathrm{H}} \mathbf{f}\right] = \frac{\omega}{2} \mathrm{Im}\left[\mathbf{q}^{\mathrm{H}} \mathbf{D}_{dir} \mathbf{q}\right] \tag{3.12}$$

This set of natural coordinates is the one for which the imaginary (resistive) part of the radiation stiffness matrix is diagonal, so it comes from the associated eigenvalue problem:

$$\operatorname{Im}\mathbf{D}_{dir}\mathbf{V} = \mathbf{V}\boldsymbol{\lambda} \tag{3.13}$$

Being $\mathbf{V}$ the real orthogonal eigenvectors matrix and $\boldsymbol{\lambda}$ the diagonal eigenvalues matrix. The eigenvectors are conveniently normalized to obtain $\mathbf{V}^{\mathrm{H}}\mathbf{V} = \mathbf{I}$.
The direct field amplitudes $\mathbf{a}$ in the natural coordinates $\mathbf{q}$ can be obtained with the transformation:

$$\mathbf{a} = \mathbf{V}^{\mathrm{T}}\mathbf{q} \tag{3.14}$$

and considering the relation between the physical coordinates and the generalized ones in Equation 3.2, it is possible to relate the displacement component $\mathbf{u}_i$ due to the direct field with the amplitudes $\mathbf{a}$ using the new basis functions $\Phi_k^{dir}(\mathbf{x})$, which are related to the k-th direct field radiation component:

$$u_i^{dir}(t,\mathbf{x}) = \sum_k \Phi_k^{dir}(\mathbf{x}) a_k(t) \tag{3.15}$$

Using this natural coordinates the imaginary part of the radiation stiffness matrix becomes diagonal $\mathbf{V}^{\mathrm{H}}\mathbf{D}_{dir}\mathbf{V} = \boldsymbol{\lambda}$ and substituting Equation 3.14 in Equation 3.12, the direct field radiation power can be written as:

$$P_{dir} = \frac{\omega}{2}\operatorname{Im}\left[\mathbf{a}^{\mathrm{H}}\boldsymbol{\lambda}\mathbf{a}\right] = \frac{\omega}{2}\sum_k a_k^* \lambda_k a_k = \frac{\omega}{2}\sum_k \lambda_k \left|a_k^2\right| \tag{3.16}$$

A certain k-th radiation component with its associated non-zero eigenvalue $\lambda_k \neq 0$ represents a radiation mode of the deterministic boundary which radiates power into the statistical subsystem. A null eigenvalue represent a deterministic boundary mode whose displacement does not introduce energy in the statistical domain. If $\mathbf{D}_{dir}$ is positive semi-definite, then all the eigenvalues are greater or equal to zero.
Considering now the reverberant field, its natural coordinates will be different from the ones used for the direct field, since the reverberant waves are generated from the interaction between the reflected waves and the incident direct field waves at the random boundary. Nevertheless, this fact can be exploited to choose shape functions for the reverberant field as they were generated from the shape functions of the direct field, trying to reply the reflection and the interaction on their formulation.
A reflected wave can therefore be modelled as a time reversal of the incident wave, so the shape functions associated to the reflected waves are the time reversal of the direct field

shape functions. This time reversal can be obtained by conjugating the direct field shape functions[1]. The interaction with the incident waves of the direct field can be modelled with the same philosophy, subtracting the direct field shape functions from the reflected wave shape functions. The shape functions of the reverberant field can therefore be expressed as:

$$\Phi_k^{rev}(\mathbf{x}) = \Phi_k^{dir,*}(\mathbf{x}) - \Phi_k^{dir}(\mathbf{x}) = -2\mathrm{i}\,\mathrm{Im}\left[\Phi_k^{dir}(\mathbf{x})\right] \tag{3.17}$$

Naming $\mathbf{b}$ the deterministic boundary amplitude vector in natural coordinates for the reverberant field, the i-th displacement component due to the reverberant field results in:

$$u_i^{rev}(t,\mathbf{x}) = \sum_k \Phi_k^{rev}(\mathbf{x}) b_k(t) \tag{3.18}$$

Thanks to the definition of these two sets of basis functions, it is now possible to derive an analytical expression for the force at the deterministic boundary related to the direct field, and the blocked reverberant force viewed as a superposition. Substituting Equation 3.14 in Equation 3.5 the free field radiation component of the force at the deterministic boundary is:

$$\mathbf{f}_d = \mathbf{D}_{dir}\mathbf{V}\mathbf{a} \tag{3.19}$$

and considering Equation 3.17, the reverberant force is the superposition

$$\mathbf{f}_{rev} = \left[(\mathbf{D}_{dir}\mathbf{V})^* - \mathbf{D}_{dir}\mathbf{V}\right]\mathbf{b} = \left(\mathbf{D}_{dir}^* - \mathbf{D}_{dir}\right)\mathbf{V}\mathbf{b} = -\mathrm{i}2\,\mathrm{Im}\left[\mathbf{D}_{dir}\right]\mathbf{V}\mathbf{b} \tag{3.20}$$

Substituting Equation 3.13, the blocked reverberant force and its cross-spectrum can be derived as functions of the radiating eigenvalues and eigenvectors of the direct field, and the natural coordinates of the reverberant field:

$$\mathbf{f}_{rev} = -\mathrm{i}2\mathbf{V}\boldsymbol{\lambda}\mathbf{b} \tag{3.21}$$

$$\mathbf{S}_{ff}^{rev} = \mathbf{f}_{rev}\mathbf{f}_{rev}^{\mathrm{H}} = 4\mathbf{V}\boldsymbol{\lambda}\mathbf{b}\mathbf{b}^{\mathrm{H}}\boldsymbol{\lambda}\mathbf{V}^{\mathrm{T}} \tag{3.22}$$

[1]For a given direct wave described as a complex function propagating in the direction of a wall, the respective reflected wave propagating in the opposite direction can be obtained by a phase conjugation, that means changing the sign of the imaginary part of the complex function, maintaining the same amplitude and phase absolute values.

For the derivation of the reciprocity relationship, the amplitudes $\mathbf{a}$ and $\mathbf{b}$ must be made explicit by defining boundary conditions at the random boundary.

3.2.3 Maximum Entropy at Random Boundary: the Diffuse Field

The amplitudes of the direct and the reverberant fields are constrained to satisfy the boundary conditions at the random boundary.
A generic form of the combination between the natural coordinates is $\mathbf{C}_1\mathbf{a}+\mathbf{C}_2\mathbf{b}=0$, where C_1 and C_2 are calculable with a Galerkin method. The reverberant field response is expressed as a function of the direct field, as done in Equation 3.17:

$$\mathbf{b}=\mathbf{T}_0\mathbf{a} \qquad \mathbf{T}_0=-\mathbf{C}_2^{-1}\mathbf{C}_1 \tag{3.23}$$

$\mathbf{T}_0$ is s complex scattering matrix of the direct field at the random boundary. A simple substitution can be done to change the natural coordinates in order to have unitary power in Equation 3.16

$$c_k=a_k\sqrt{\lambda_k} \qquad d_k=b_k\sqrt{\lambda_k} \tag{3.24}$$

The constraint relation becomes then:

$$\mathbf{d}=\mathbf{T}\mathbf{c} \qquad \mathbf{T}=-\boldsymbol{\lambda}^{-1/2}\mathbf{C}_2^{-1}\mathbf{C}_1\boldsymbol{\lambda}^{-1/2} \tag{3.25}$$

There $\mathbf{T}$ is the scattering matrix in the new coordinates. For a single well-known boundary curve, the interaction between direct fields and reverberant fields normalized components is coherent. If there is uncertainty in the the location and definition of the boundary conditions at the random boundary, $\mathbf{T}$ becomes a random variable, and the coherence is perturbed. The interaction between direct and reverberant fields is then related to the statistics of $\mathbf{T}$, which is analysed in what follows.
One could choose whatever definition of the boundary conditions at the random boundary to define $\mathbf{T}$, but if the uncertainty is very strong it is opportune to choose the definition providing the minimum amount of information. This is the case of *maximum entropy* at the boundary, for which none precise statements can be made about the boundary conditions.
The shape function definition can be modified in order to study the behaviour of the random variable $\mathbf{T}$. Supposing to use new generic shape functions defined transforming $\mathbf{c}$ and $\mathbf{d}$:

$$\hat{\mathbf{c}}=\mathbf{R}_1\mathbf{c} \qquad \hat{\mathbf{d}}=\mathbf{R}_2\mathbf{d} \qquad \hat{\mathbf{T}}=\mathbf{R}_2\mathbf{T}\mathbf{R}_1^{\mathrm{H}} \tag{3.26}$$

The first order statistic of the scattering matrix expressed using the new basis functions is:

$$\langle \hat{\mathbf{T}} \rangle = \mathbf{R}_2 \langle \mathbf{T} \rangle \mathbf{R}_1^{\mathrm{H}} \tag{3.27}$$

Equation 3.27 expresses a dependency of the expected value of the scattering matrix upon the shape functions used to define the natural amplitudes. This is an absurd statement, because it means that the statistics of the scattering depends on the mathematics adopted and not on the physics of the wave field deviation. The only mean value of the scattering for which this result can be true is zero.

$$\langle \mathbf{T} \rangle = 0 \tag{3.28}$$

The second order statistics of the scattering can be written as the expected value of the cross-spectrum using Equation 3.27:

$$\langle \hat{T}_{jk} \hat{T}^*_{rs} \rangle = \sum_{m,n,p,q} \langle T_{mn} T^*_{pq} \rangle R_{2,jm} R^*_{2,rp} R_{1,sq} R^*_{1,kn} \tag{3.29}$$

Considering the transformation matrices hermitian to conserve the overall power in the direct field and the overall energy in the reverberant field: $\mathbf{R}^{\mathrm{H}}\mathbf{R} = \mathbf{I}$, the term $\langle T_{mn} T^*_{pq} \rangle$ is written

$$\langle T_{mn} T^*_{pq} \rangle = C' \delta_{mp} \delta_{nq} \tag{3.30}$$

and C' is a constant, which means that $\langle \mathbf{T}\mathbf{T}^{\mathrm{H}} \rangle$ is a diagonal matrix with C' in each element of the diagonal. This guarantees that the second order statistics is invariant to a change of basis functions.
Equation 3.28 and 3.30 show that when the entropy of the definition of the random boundary is maximum, then the first order statistics of the scattering matrix is null, and the second order is constant and invariant to a change of basis functions. Substituting these two equations in Equation 3.25 and considering then the substitution made in Equation 3.24:

$$\langle b_m b^*_n \rangle = \frac{C}{\lambda_m} \delta_{mn}, \quad \langle a_m b^*_n \rangle = 0, \quad \langle b_m \rangle = 0 \tag{3.31}$$

C is a constant dependent on the direct field power incident to the random boundary. The final results shows how the reverberant field produces a power amplitude $\mathbf{b}$ which is **incoherent** with itself and with the direct field power amplitude $\mathbf{a}$. Such statistics are characteristic of a reverberant field that is named "diffuse field".

In conclusion, if there is an extreme uncertainty on the random boundary properties, the reverberant field which it is generated is the **Incoherent Diffuse Field**: the blocked reverberant force presents a null expected value and a cross-spectrum which is proportional to the imaginary part of the radiation stiffness matrix, that corresponds to the resistive impedance of the direct field. This is the definition of the Diffuse Field Reciprocity Relationship and it can be seen substituting Equation 3.31 into Equation 3.21 and 3.22:

$$\langle \mathbf{f}_{rev} \rangle = -2\mathrm{i}\mathbf{V}\boldsymbol{\lambda}\langle \mathbf{b} \rangle = 0 \tag{3.32}$$

$$\langle \mathbf{S}_{ff}^{rev} \rangle = \langle \mathbf{f}_{rev}\mathbf{f}_{rev}^{\mathrm{H}} \rangle = 4\mathbf{V}\boldsymbol{\lambda}\langle \mathbf{b}\mathbf{b}^{\mathrm{H}} \rangle \boldsymbol{\lambda}\mathbf{V}^{\mathrm{T}} = 4C\mathbf{V}\boldsymbol{\lambda}\mathbf{V}^{\mathrm{T}} = 4C\,\mathrm{Im}\left[\mathbf{D}_{dir}\right] \tag{3.33}$$

3.2.4 Cross Spectrum of the Blocked Reverberant Force

In order to use the results of the reciprocity, it is necessary to derive the constant of proportionality of Equation 3.33 ($\alpha = 4C$) in a suitable way for the SEA approach to the statistical subsystems, which means using the ensemble energy and the modal density of the component.

The reverberant field wave components are derived from the direct field modes (Equation 3.17), that means they are orthogonal and can be studied separately. The energy of a reverberant field component can be therefore found as a superposition of energies of two direct field mode waves: one incident to the random boundary and one reflected. Assuming to study the energy condition in an area which is far from the deterministic boundary which generates the waves, the so called "farfield", it is possible to define an imaginary surface R aligned with the local intensity field (Figure 3.3). R is crossed by the incident and the reflected mode waves which must have the same energy so that the total reverberant energy along any possible boundary R is equal to zero. It is now possible to define a group velocity for the k-th component as the ratio of the power incident on R and the energy density of R carried by the component (each waves carries the half of the total reverberant energy):

$$c_{g,k} = \frac{P_{incident,k}}{\frac{1}{2}e_{tot,k}} \tag{3.34}$$

$P_{incident,k}$ is the same for each component because of the independence of the scattering matrix by the basis functions, as can be seen comparing Equation 3.31 and 3.16:

$$P_{incident,k} = \frac{\omega}{2}C \tag{3.35}$$

From the two previous equation, C can be derived as a function of the energy density and the group velocity:

$$C = \frac{e_{tot,k} c_{g,k}}{\omega} \tag{3.36}$$

The term $e_{tot,k}$ represents the energy contained in a unit strip in a direction normal to the R surface due to the k-th component. Considering the modal density of this unit strip being $n_{k,unit} = 1/(\pi c_{g,k})$ (Table 2.1), the total reverberant energy of the unit strip is

$$E_{tot,unit} = \sum_k e_{tot,k} = \sum_k \frac{\omega C}{c_{g,k}} = \pi\omega C \sum_k n_{k,unit} = \pi\omega C n_{tot,unit} \tag{3.37}$$

Since the energy and the modal density can be computed as in Equation 3.37 for any strip and linearly summed, C can be expressed as a function of the total energy of the subsystem due to the reverberant field and its total modal density:

$$C = \frac{E_{tot}}{\pi\omega n_{tot}} \tag{3.38}$$

The expected cross-spectrum of the blocked reverberant force from Equation 3.33 can be finally written as

$$\langle \mathbf{S}_{ff}^{rev} \rangle = \langle \mathbf{f}_{rev} \mathbf{f}_{rev}^{\mathrm{H}} \rangle = \frac{4E_{tot}}{\pi\omega n_{tot}} \operatorname{Im}[\mathbf{D}_{dir}] \tag{3.39}$$

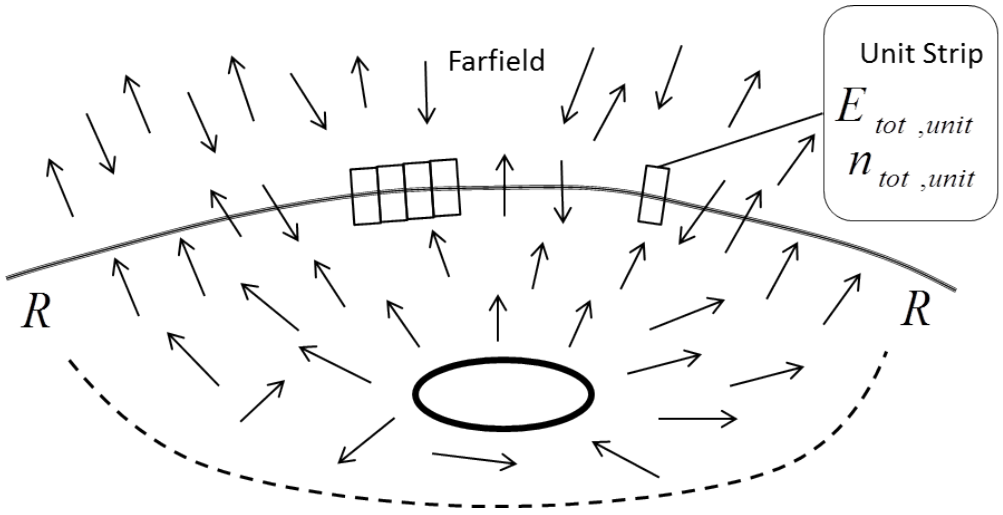

Figure 3.3: Energy flow at the imaginary surface R in the farfield of a statistical subsystem. The unit strip is a portion of unitary volume.

3.3 Hybrid Equations and Coupling Loss Factors

From the previous results regarding the the diffuse field reciprocity, one can understand how in a statistical subsystem connected to a deterministic one makes sense to place nodes only over the deterministic boundary, since the behaviour of such a subsystem under the assumption of diffuse field is statistically defined by the only forces acting on the deterministic boundary Equation 3.5. A typical example of nodes distribution for a hybrid model is given in Figure 3.4, where the two statistical plates do not possess any node within their domains. In this case, nodes are also placed over the line connection between the SEA subsystems, this is linked to what has been said regarding the "statistical junctions" in section 3.1. These junctions can be studied either with the SEA CLFs, or with nodes used to define the geometry of the interface with 1D or 2D elements, despite there are no deterministic components. Naming $\mathbf{q}_1$ the degrees of freedom of the deterministic subsystems, and $\mathbf{q}_2$ the eventual degrees of freedom at the statistical junctions, the column vector of the deterministically calculable generalized displacements is $\mathbf{q} = \begin{bmatrix}\mathbf{q}_1^{\mathrm{T}} & \mathbf{q}_2^{\mathrm{T}}\end{bmatrix}^{\mathrm{T}}$. Being $\mathbf{D}_d^{(i)}$ the dynamic stiffness matrix of the i-th deterministic subsystem which relates the deterministic forces $\mathbf{f}_d$ to the deterministic displacements $\mathbf{q}$, the overall deterministic forces are computed using $\mathbf{D}_d$ which is the assembling of the deterministic matrices $\mathbf{D}_d^{(i)}$ $(i = 1...N_d)$. Such a stiffness can be computed with classical finite element or boundary element methods.

$$\mathbf{f}_d = \mathbf{D}_d\mathbf{q} \qquad\qquad \mathbf{f}_d^{(i)} = \mathbf{D}_d^{(i)}\mathbf{q}^{(i)} \tag{3.40}$$

The behaviour of the statistical subsystems which possess a part of boundary that is deterministic, is the one described in section 3.2. The deterministic boundary of the statistical subsystem constitutes the interface of the hybrid junction. Considering the subset of degrees

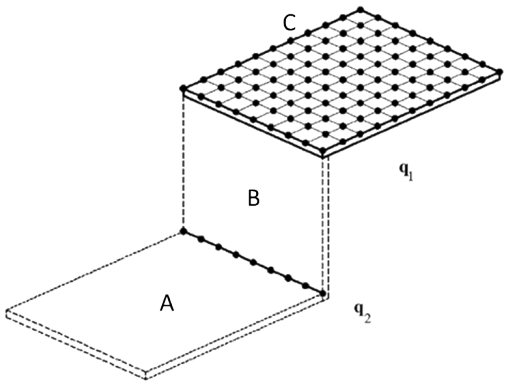

Figure 3.4: Hybrid System example: two statistical plate subsystems (A and B) are connected through a line junction, and the deterministic plate subsystem is connected to the plate B through a hybrid line junction (figure of [Shorter and Langley 2005b])

of freedom laying on the deterministic boundary $\mathbf{q}_{junc} : \mathbf{q}_{junc} \subseteq \mathbf{q}$ (in Figure 3.4 the nodes on the two connections), and recalling subsection 3.2.1 where is explained how the response of a statistical subsystem can be represented by the superposition between a direct and a reverberant field, the force at the boundary $\mathbf{f}_{junc}$ is (Equation 3.5)

$$\mathbf{f}_{junc} = \mathbf{f}_{dir} + \mathbf{f}_{rev} = \mathbf{D}_{dir}\mathbf{q}_{junc} \qquad \mathbf{f}^{(i)}_{junc} = \mathbf{f}^{(i)}_{dir} + \mathbf{f}^{(i)}_{rev} = \mathbf{D}^{(i)}_{dir}\mathbf{q}^{(i)}_{junc} \tag{3.41}$$

where $\mathbf{D}^{(i)}_{dir}$ is the direct field dynamic stiffness matrix of the i-th statistical subsystem connected with a hybrid junction, and $\mathbf{D}_{dir}$ the assembling of all the $\mathbf{D}^{(i)}_{dir}$ over all the hybrid junctions; $\mathbf{f}^{(i)}_{dir}$ and $\mathbf{f}^{(i)}_{rev}$ are the direct and blocked reverberant loads on the deterministic boundary of the i-th statistical subsystem.
Assembling the equation of motion for the statistical and deterministic subsystems, the total dynamic stiffness matrix is obtained: $\mathbf{D}_{tot}$, which is the sum of the deterministic matrix $\mathbf{D}_d$ and the direct field dynamic matrices over N_s statistical subsystems $\sum_i^{N_s} \mathbf{D}^{(i)}_{dir}$. The total stiffness represents the relation between the generalized displacements $\mathbf{q}$ and the assembling of the loads $\mathbf{f}$. The load assembling is a vector containing all the forces applied on the deterministic nodes and on the deterministic boundaries, plus the summation of the blocked reverberant forces over the deterministic boundaries of the i statistical subsystems:

$$\mathbf{f} = \begin{bmatrix} \mathbf{f}_d^{\mathrm{T}} & \sum_i^{N_s} \mathbf{f}^{(i),\mathrm{T}}_{dir} \end{bmatrix}^{\mathrm{T}} + \sum_i^{N_s} \mathbf{f}^{(i)}_{rev} = \mathbf{f}_{ext} + \sum_i^{N_s} \mathbf{f}^{(i)}_{rev} \tag{3.42}$$

$$\mathbf{f}_{ext} + \sum_i^{N_s} \mathbf{f}^{(i)}_{rev} = \mathbf{D}_{tot}\mathbf{q} \tag{3.43}$$

$$\mathbf{D}_{tot} = \mathbf{D}_d + \sum_i^{N_s} \mathbf{D}^{(i)}_{dir} \tag{3.44}$$

$$\mathbf{q} = \mathbf{D}^{-1}_{tot} \left(\mathbf{f}_{ext} + \sum_i^{N_s} \mathbf{f}^{(i)}_{rev} \right) \tag{3.45}$$

Studying forces and displacements as stochastic variables, the expected cross spectrum of the force $\mathbf{f} = \mathbf{f}_{ext} + \sum_i^{N_s} \mathbf{f}^{(i)}_{rev}$ acting on the complex system is

$$\langle \mathbf{S}_{ff} \rangle = \langle \mathbf{f}\mathbf{f}^{\mathrm{H}} \rangle = \mathbf{S}^{ext}_{ff} + \langle \mathbf{S}^{ext,rev}_{ff} \rangle + \langle \mathbf{S}^{rev,ext}_{ff} \rangle + \langle \mathbf{S}^{rev}_{ff} \rangle \tag{3.46}$$

This equation reflects Equation 3.11 considering any amount of subsystems. The first term is the cross spectrum of the external forces which is know deterministically, so it has constant probability and the expected value is omitted. The three remaining terms are respectively

the cross-correlations between external and blocked reverberant force (and vice versa), and the cross-correlation of the single $\mathbf{f}_{rev}$:

$$\mathbf{S}_{ff}^{ext} = \mathbf{f}_{ext}\mathbf{f}_{ext}^{\mathrm{H}} \tag{3.47}$$

$$\langle \mathbf{S}_{ff}^{ext,rev} \rangle + \langle \mathbf{S}_{ff}^{rev,ext} \rangle = \sum_{i}^{N_s} \left(\mathbf{f}_{ext} \langle \mathbf{f}_{rev}^{(i),\mathrm{H}} \rangle + \langle \mathbf{f}_{rev}^{(i)} \rangle \mathbf{f}_{ext}^{\mathrm{H}} \right) \tag{3.48}$$

$$\langle \mathbf{S}_{ff}^{rev} \rangle = \sum_{i}^{N_s} \mathbf{S}_{ff}^{rev(i)} = \sum_{i}^{N_s} \sum_{j}^{N_s} \langle \mathbf{f}_{rev}^{(i)} \mathbf{f}_{rev}^{(j),\mathrm{H}} \rangle \tag{3.49}$$

The results of the diffuse field reciprocity relationship (Equation 3.32, 3.39) can now be taken in account to simplify the equations. It can be stated that if the properties of the random boundaries of the statistical subsystems are extremely uncertain so that the maximum entropy is reached in their definition, the reverberant fields are diffusive and they are incoherent with each other and with all the direct fields, which means:

$$\langle \mathbf{S}_{ff}^{ext,rev} \rangle = \langle \mathbf{S}_{ff}^{rev,ext} \rangle = 0 \tag{3.50}$$

$$\langle \mathbf{S}_{ff}^{rev} \rangle = \sum_{j}^{N_s} \frac{4E_j}{\pi \omega n_j} \operatorname{Im}\left[\mathbf{D}_{dir}^{(j)} \right] \tag{3.51}$$

Being $\mathbf{q}^{\mathrm{H}} = \mathbf{f}^{\mathrm{H}} \mathbf{D}_{tot}^{-\mathrm{H}}$, the power spectrum of the generalized coordinate response is

$$\langle S_{qq} \rangle = \mathbf{D}_{tot}^{-1} \langle S_{ff} \rangle \mathbf{D}_{tot}^{-\mathrm{H}} = \mathbf{D}_{tot}^{-1} \left(\mathbf{S}_{ff}^{ext} + \sum_{j}^{N_s} \frac{4E_j}{\pi \omega n_j} \operatorname{Im}\left[\mathbf{D}_{dir}^{(j)} \right] \right) \mathbf{D}_{tot}^{-\mathrm{H}} \tag{3.52}$$

Recalling Equation 3.12, the time and ensemble average input power to the direct field of the i-th statistical subsystem through its deterministic boundary can be written, using l,m as node indices for a total number of N_{tot} nodes in the system:

$$P_{in,dir}^{(i)} = \frac{\omega}{2} \operatorname{Im}\left[\mathbf{q}_{junc}^{\mathrm{H}} \mathbf{f}_{junc} \right] = \frac{\omega}{2} \sum_{l}^{N_{tot}} \operatorname{Im}\left[\mathbf{q}_{junc,l}^{*} \mathbf{f}_{junc,l} \right] \tag{3.53}$$

Writing the generalized forces for the hybrid connection of the i-th statistical subsystem as in Equation 3.41 and considering its cross-spectrum, the input power results in:

$$\begin{aligned} P_{in,dir}^{(i)} = \frac{\omega}{2} \operatorname{Im}\left[\mathbf{q}_{junc}^{\mathrm{H}} \mathbf{D}_{dir}^{(i)} \mathbf{q}_{junc}\right] = \frac{\omega}{2} \sum_{l}^{N_{tot}} \operatorname{Im}\left[\mathbf{q}_{junc,l}^{*} \left(\sum_{m}^{N_{tot}} \mathbf{D}_{dir,lm}^{(i)} \mathbf{q}_{junc,m}\right)\right] = \\ = \frac{\omega}{2} \sum_{l,m}^{N_{tot}} \operatorname{Im}\left[\mathbf{D}_{dir,lm}^{(i)} \langle \mathbf{S}_{qq,lm} \rangle\right] \end{aligned} \tag{3.54}$$

Since $\langle \mathbf{S}_{qq,lm} \rangle$ is real, it can be set outside the imaginary part operator of the multiplication. Under the assumption of extremely uncertainty on the property of the random boundaries, the response cross-spectrum can be written usgin Equation 3.52, and the input power to the direct field of i results in a final form

$$P_{in,dir}^{(i)} = \frac{\omega}{2} \sum_{l,m}^{N_{tot}} \operatorname{Im}\left[\mathbf{D}_{dir,lm}^{(i)}\right] \left\{ \mathbf{D}_{tot}^{-1} \left(\mathbf{S}_{ff}^{ext} + \sum_{j}^{N_s} \frac{4E_j}{\pi \omega n_j} \operatorname{Im}\left[\mathbf{D}_{dir}^{(j)}\right] \right) \mathbf{D}_{tot}^{-\mathrm{H}} \right\}_{lm} \tag{3.55}$$

This formula results simplified thanks to the assumptions of the direct field reciprocity relationship. If the random boundary cannot be studied as extremely uncertain, then the reverberant field is not a diffuse field and it is coherent to the direct field. If a correlation between the results and the shape of the boundary is wanted or cannot be neglected, then it cannot be found under the assumption of diffuse field and the matrix $\mathbf{D}_{dir}$ must be computed considering the reverberant field. In that case, also the complete formulation of the force cross-spectrum must be used (Equation 3.46).

The input power to the direct field of the i-th statistical subsystem can be divided in two contributions, one due to the external loading $\left(P_{in,ext}^{(i)}\right)$ and one due to the reverberant loading associated with its reverberant field and the reverberant fields of any other statistical subsystem $\left(P_{in,rev}^{(i)}\right)$

$$P_{in,dir}^{(i)} = \left(P_{in,ext}^{(i)}\right) + \left(P_{in,rev}^{(i)}\right) \tag{3.56}$$

$$P_{in,ext}^{(i)} = \frac{\omega}{2} \sum_{l,m}^{N_{tot}} \operatorname{Im}\left[\mathbf{D}_{dir,lm}^{(i)}\right] \left\{ \mathbf{D}_{tot}^{-1} \mathbf{S}_{ff}^{ext} \mathbf{D}_{tot}^{-\mathrm{H}} \right\}_{lm} \tag{3.57}$$

$$P_{in,rev}^{(i)} = \sum_{j}^{N_s} \frac{2E_j}{\pi n_j} \sum_{l,m}^{N_{tot}} \operatorname{Im}\left[\mathbf{D}_{dir,lm}^{(i)}\right] \left\{ \mathbf{D}_{tot}^{-1} \operatorname{Im}\left[\mathbf{D}_{dir}^{(j)}\right] \mathbf{D}_{tot}^{-\mathrm{H}} \right\}_{lm} = \sum_{j}^{N_s} \omega_j E_j \eta_{ji} \tag{3.58}$$

$\left(P_{in,rev}^{(i)}\right)$ is the net power input in the i-th subsystem as effect of the reverberant fields of all the statistical subsystems. In Equation 3.58, this power can therefore be seen as the sum of

the gross incoming power flows, by analogy with the transmitted power of the SEA equations (term $P_{j\to i}$ of Equation 2.5). Therefore, using the same form of SEA equations, it is possible to write the average transmitted power of the reverberant field as a sum of the reverberant energies, modal densities and coupling loss factors between statistical subsystems.
From Equation 3.58, the **Hybrid Coupling Loss Factor** which identifies the average transmission of power from the reverberant field of the statistical subsystem i to the one of the statistical subsystem j is:

$$\eta_{ij} = \frac{2}{\pi\omega n_i} \sum_{l,m}^{N_{tot}} \mathrm{Im}\left[\mathbf{D}^{(j)}_{dir,lm}\right] \left\{\mathbf{D}^{-1}_{tot}\, \mathrm{Im}\left[\mathbf{D}^{(i)}_{dir}\right] \mathbf{D}^{-\mathrm{H}}_{tot}\right\}_{lm} \tag{3.59}$$

It follows that the energy exchange properties between very uncertain subsystems is totally determined by the deterministic behaviour of the hybrid junction. This method for the derivation of the coupling loss factors is totally general in terms of the junction type. It can be indistinctly used for point, line or area junctions. It can be noticed that if there are not deterministic subsystems, for a point junction the coupling loss factor reflects perfectly the SEA formulation in Equation 2.40 and 2.43.
Since the total stiffness matrix can be obtained in a symmetric form by using real valued shape functions, also the hybrid coupling loss factor can be written in a symmetric form called "ensemble average power transfer coefficient", which is useful for handling the matrices:

$$h_{ij} = \omega n_i \eta_{ij} \quad , \quad h_{ij} = \frac{2}{\pi} \sum_{l,m,r,s}^{N_{tot}} \mathrm{Im}\left[\mathbf{D}^{(i)}_{dir}\right]_{lm} \mathrm{Im}\left[\mathbf{D}^{(j)}_{dir}\right]_{rs} \left(\mathbf{D}^{-1}_{tot}\right)_{lr} \left(\mathbf{D}^{-\mathrm{H}}_{tot}\right)_{ms} = h_{ji} \tag{3.60}$$

The coefficients h_{ij} describes the average energy flow in a reverberant field of a system per number of modes (so it is still assumed that the modal energy is constant).
Figure 3.5 shows the ensemble average energy flows in the reverberant field of the i-th statistical subsystem. The input power presented in Equation 3.56 gets lost because of dissipation within the reverberant field $P^{(i)}_{diss}$ and because of the work done by the blocked reverberant force on the deterministic boundaries $P^{(i)}_{out,rev}$. Therefore, the power balance for the reverberant field of the statistical subsystem can be written:

$$P^{(i)}_{in,dir} = P^{(i)}_{out,rev} + P^{(i)}_{diss} \tag{3.61}$$

The power lost because of the reverberant force depends on the cross-spectrum of the displacement due to the single action of the reverberant field (second term of Equation 3.52), which involves the total set of degrees of freedom. Using the same procedure of Equation 3.54:

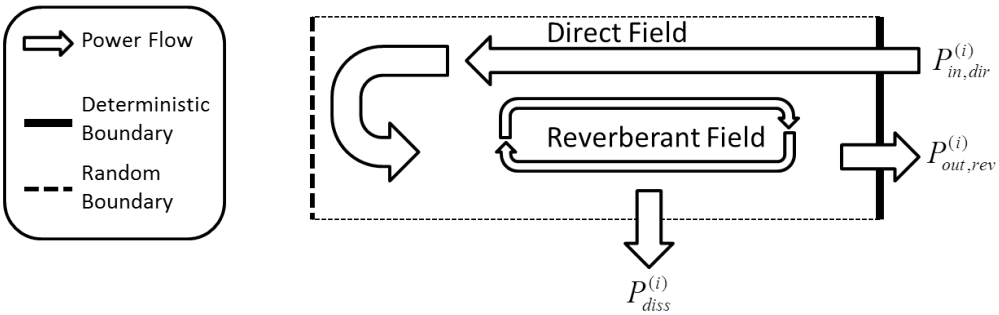

Figure 3.5: Power balance in a statistical subsystem excited by external and reverberant loadings $P_{in,dir}$.

$$P^{(i)}_{out,rev} = \frac{\omega}{2} \sum_{lm}^{N_{tot}} \mathbf{S}^{(i),rev}_{qq,lm} \operatorname{Im}\left[\mathbf{D}_{tot}\right]_{lm} = \frac{E_i}{n_i} h_{tot,i} \tag{3.62}$$

where in the last equation is used a power loss coefficient for this power flow, which describes the energy leaving the i-th statistical subsystem per its unit modal energy density, and can be defined by multiplying the power by the modal density and dividing by the energy of the subsystem:

$$h_{tot,i} = \frac{2}{\pi} \sum_{lm}^{N_{tot}} \operatorname{Im}\left[\mathbf{D}_{tot}\right]_{lm} \left(\mathbf{D}^{-1}_{tot} \operatorname{Im}\left[\mathbf{D}^{(i)}_{dir}\right] \mathbf{D}^{-\mathrm{H}}_{tot}\right)_{lm} \tag{3.63}$$

This work rate of the blocked reverberant force is a power transmitted to other subsystems. Therefore, the loss of this power flow can be seen as the result of two contribution: the dissipation by the damping of the deterministic subsystems (that depends only on the deterministic stiffness), and the transmission to reverberant fields of other subsystems (that is described by the coupling loss factors, and so by $\sum h_{ij}$). Considering Equation 3.44, the total stiffness matrix which identifies this power loss can be divided in the deterministic part and free field radiation part $\operatorname{Im}\left[\mathbf{D}_{tot}\right] = \operatorname{Im}\left[\mathbf{D}_{d}\right] + \sum_{j}^{N_s} \operatorname{Im}\left[\mathbf{D}^{(j)}_{dir}\right]$. By naming h^{α}_{i} the transmission coefficient relative to the dissipation in the damped deterministic subsystems due to the reverberant power leaving the i-th statistical subsystem, the total power loss due to the blocked reverberant force is:

$$P^{(i)}_{out,rev} = \frac{\omega}{2} \sum_{lm}^{N_{tot}} \mathbf{S}^{(i),rev}_{qq,lm} \left(\operatorname{Im}\left[\mathbf{D}_{d}\right]_{lm} + \sum_{j}^{N_s} \operatorname{Im}\left[\mathbf{D}^{(i)}_{dir}\right]_{lm} \right) = \frac{E_i}{n_i} \left(h^{\alpha}_{i} + \sum_{j}^{N_s} h_{ij} \right) \tag{3.64}$$

$$h_{tot,i} = \left(h^{\alpha}_{i} + \sum_{j}^{N_s} h_{ij} \right) \tag{3.65}$$

Considering the already stated formulation of h_{ji} from Equation 3.59, and substituting the reverberant term of Equation 3.52 in Equation 3.64:

$$h_i^{\alpha} = \frac{2}{\pi} \sum_{lm}^{N_{tot}} \mathrm{Im}\left[\mathbf{D}_d\right]_{lm} \left(\mathbf{D}_{tot}^{-1} \mathrm{Im}\left[\mathbf{D}_{dir}^{(i)}\right] \mathbf{D}_{tot}^{-\mathrm{H}}\right)_{lm} \tag{3.66}$$

If the deterministic subsystems are undamped, the imaginary part of the deterministic stiffness is null and h_i^{α}=0.
The dissipated power in the reverberant field $P_{diss}^{(i)}$ can be written as in Equation 2.4 using the damping loss factor, and also transformed as a function of the modal energy so that can be compatible with the previous transmission coefficients h:

$$P_{diss}^{(i)} = \omega \eta_i E_i = M_i \frac{E_i}{n_i} \tag{3.67}$$

$$M_i = \omega n_i \eta_i \tag{3.68}$$

The transmission loss coefficient for this dissipated power M_i is the half power bandwidth[2] modal overlap[3] of the i-th reverberant field.
Substituting in Equation 3.61 the three power flow expressions (Equation 3.56, 3.62 and 3.67), the final form of the power balance can be obtained, with the relative matrix formulation:

$$P_{in,ext}^{(i)} = \left(M_i + h_{tot,i}\right) \frac{E_i}{n_i} - \sum_{j}^{N_s} h_{ji} \frac{E_j}{n_j} \tag{3.69}$$

$$\begin{pmatrix} P_{in,ext}^{(1)} \\ \vdots \\ P_{in,ext}^{i} \end{pmatrix} = \begin{bmatrix} M_1 + h_{tot,1} - h_{11} & \dots & -h_{i1} \\ & \ddots & \\ symm. & & M_i + h_{tot,i} - h_{ii} \end{bmatrix} \begin{pmatrix} \frac{E_1}{n_1} \\ \vdots \\ \frac{E_i}{n_i} \end{pmatrix} \tag{3.70}$$

If the power dissipated in the work done by the reverberant field $P_{out,rev}$ is written in the form of Equation 3.64 distinguishing the dissipation in the deterministic subsystems and the

[2]The "half power" or "-3dB" bandwidth of a resonant frequency is the range of frequencies for which the response amplitude is larger than the amplitude corresponding to the half of the power of the resonant peak. The half power amplitude is located at -3dB from the maximum amplitude.
[3]The modal overlap factor can be interpreted as the number of resonances within the half power bandwidth of a certain resonance frequency.

transmission to other reverberant fields, the power balance equation becomes:

$$P_{in,ext}^{(i)} = \left(M_i + h_i^{\alpha} + \sum_j h_{ij} \right) \frac{E_i}{n_i} - \sum_j^{N_s} h_{ji} \frac{E_j}{n_j} \tag{3.71}$$

$$\begin{pmatrix} P_{in,ext}^{(1)} \\ \vdots \\ P_{in,ext}^{i} \end{pmatrix} = \begin{bmatrix} M_1 + h_1^{\alpha} + \sum\limits_{j \neq 1} h_{1j} & \dots & -h_{i1} \\ & \ddots & \\ symm. & & M_i + h_i^{\alpha} + \sum\limits_{j \neq 1} h_{ij} \end{bmatrix} \begin{pmatrix} \frac{E_1}{n_1} \\ \vdots \\ \frac{E_i}{n_i} \end{pmatrix} \tag{3.72}$$

If the deterministic subsystem is undamped and so $h_i^{\alpha} = 0$, Equation 3.72 corresponds to the symmetric form of the SEA equations in Equation 2.14 derived in a different form, that is considering the power balance of subsystems with random boundaries.

From the power balance of the reverberant field, it is possible to derive the ensemble average modal energy density of the reverberant field of each statistical subsystem. Using these energies is then possible to compute the cross-spectral response using Equation 3.52. The total energy of a statistical subsystem can be derived by summing the energy of the reverberant field with the energy of the direct field.

In conclusion, a hybrid system can be viewed as an assembly of statistical subsystems connected trough deterministic subsystems, that constitute the hybrid junctions and contribute to the power flow with the damping dissipation. Everything stated in the procedure exposed by [Shorter and Langley 2005b] is an analytically exact statistic, under the assumption of diffuse field. Because of such an assumption, defining the deterministic domains, the deterministic boundaries and the direct field dynamic stiffness of the statistical subsystems, implicitly defines the hybrid equations. Eventual approximations may occur in defining the free field radiation stiffness.

It must be noticed that if a detail is considered uncertain in this analysis, the results will be generated by the condition of maximum entropy on the definition of such a detail. This means that a certain detail can only be modelled as totally deterministic, or as totally random. The assumption of random detail produces results which are not linked to a particular condition of the statistical subsystem, like its overall dimension, but only on its characterising properties for the definition of the direct field radiation stiffness, like the element type (beam, bar, plate, etc.).

The big advantage of this method is that it allows to consider an arbitrary amount of deterministic details to be included in the analysis, and provides a totally generic approach and systematic procedure for predicting the response of complex systems which require both

statistical and deterministic treating, differently from SEA. Equation 3.59 is a generic formulation for computing the coupling loss factors between statistical subsystems, and it can be used in a very fast way to perform a parametric study of the noise transmission between components, varying the subsystems properties like the damping, or the junction's features. A similar study is presented in chapter 5.

In conclusion, the method explained is totally generic and does not depend on the geometry of the junctions and components. The type of junction only influences the formulation of the direct field dynamic stiffness.

As done in [Peiffer et al 2009], modal coordinates and mode shapes can be used to express the displacements. Considering M modes, the i-th component of displacement is:

$$u^{(i)}(t,\mathbf{x}) = \sum_{k}^{M} \Phi_k^{(i)}(\mathbf{x}) q_k(t) \tag{3.73}$$

$\mathbf{q} = [q_1, q_2 ... q_M]$ is the displacement vector in modal coordinates and $\Phi_1^{(i)}(\mathbf{x}), \Phi_2^{(i)}(\mathbf{x}) ... \Phi_M^{(i)}(\mathbf{x})$ are the mass-normalized mode shapes of the system of the i-th component of displacement. Using the modal expansion, a generic stiffness matrix $\mathbf{D}$ can be expressed in modal coordinates using the modal matrix $\boldsymbol{\mathcal{M}}$, which is composed by the column vectors of mode shapes assembled considering all the displacement components. Indicating with $\boldsymbol{\Phi}_k(\mathbf{x})$ the mass-normalized mode shape column vector of the k-th mode mapped on N points, for a set of three displacements $\mathbf{u}_x, \mathbf{u}_y, \mathbf{u}_z$ the mode vector is composed by the three displacement components of mode as follows:

$$\boldsymbol{\Phi}_k(\mathbf{x}) = \left[\Phi_{k,1}^{\mathbf{u}_x}, \Phi_{k,1}^{\mathbf{u}_y}, \Phi_{k,1}^{\mathbf{u}_z}, \Phi_{k,2}^{\mathbf{u}_x}, \Phi_{k,2}^{\mathbf{u}_y}, \Phi_{k,2}^{\mathbf{u}_z} ... \Phi_{k,N}^{\mathbf{u}_x}, \Phi_{k,N}^{\mathbf{u}_y}, \Phi_{k,N}^{\mathbf{u}_z}\right]^{\mathrm{T}} \tag{3.74}$$

the modal matrix and a generic stiffness matrix result in:

$$\boldsymbol{\mathcal{M}} = [\boldsymbol{\Phi}_1(\mathbf{x}), \boldsymbol{\Phi}_2(\mathbf{x}) ... \boldsymbol{\Phi}_k(\mathbf{x}) ... \boldsymbol{\Phi}_M(\mathbf{x})] \tag{3.75}$$

$$\mathbf{D}^{mod} = \boldsymbol{\mathcal{M}}^{\mathrm{H}} \mathbf{D} \boldsymbol{\mathcal{M}} \tag{3.76}$$

If $\mathbf{D}$ is a deterministic stiffness matrix te modes are mapped over the relative deterministic subsystem, if $\mathbf{D}$ is a direct field dynamic stiffness matrix then the modes are mapped over the deterministic boundary of the relative statistical subsystem.

4 Hybrid Line Junction

As shown in chapter 3, when a statistical subsystem presents deterministic details on its boundary and the remaining part of the boundary is defined with the condition of maximum entropy, the power balance Equation 3.69 (or in the form of Equation 3.71) which allows to compute the ensemble average response of the statistical subsystems depends on: frequency, modal density, damping loss factor, deterministic dynamic stiffness matrix and direct field dynamic stiffness matrix. Since the deterministic matrix can be computed with a finite element or boundary element method, the damping loss factor depends on the material, and the modal density depends on the type of component, the only parameters that must be defined is the radiation stiffness matrix of the boundary.
In this chapter, the radiation stiffness matrix for a plate-beam-plate line junction is derived, so that the hybrid coupling loss factors can be computed.

4.1 Plate - Beam - Plate System

The system presented in Figure 4.1a is composed by two plates and one beam in aluminium (Table B.1) connected along one edge under an angle of 120°. Referring to Figure 4.1b, the plates A and B are flat rectangular statistical subsystems with one deterministic edge each in correspondence of the connection, the beam is a straight C-type cross section and is modelled deterministically. According to the hybrid theory, this system contains one hybrid junction which is constituted by the beam and the two connected edges of plates. Since the beam is modelled with 1-dimensional elements using FEM, the hybrid junction is a simple straight line of nodes in which the beam and the two deterministic edges are overlapped, that means all the deterministic degrees of freedom are on the line junction and the deterministic matrix coincides with the beam matrix:

$$\mathbf{q}_{junc} \equiv \mathbf{q} \qquad \mathbf{D}_d \equiv \mathbf{D}_{beam} \tag{4.1}$$

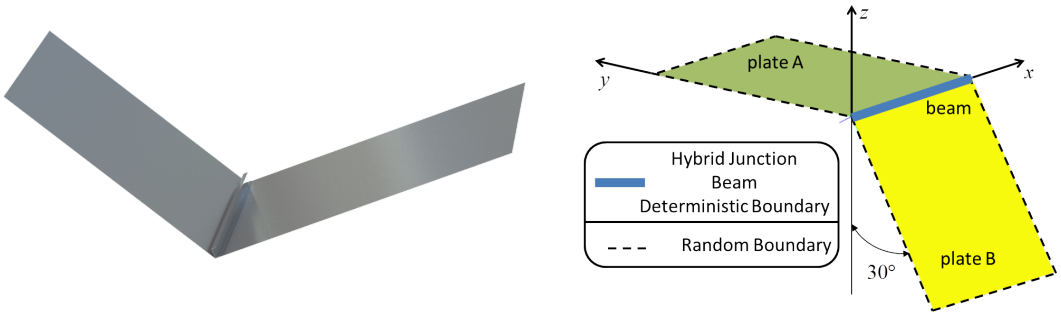

(a) Plate - Beam - Plate system **(b)** Global coordinate system of the model

Figure 4.1: Hybrid System

In Figure 4.1b, the global cartesian coordinate system is chosen in a way that the hybrid junction lays on the x-axis.
In chapter 5 the results are presented on two different model set-ups: one shorter and one longer dimension in the x direction. For these two configurations the geometry of the subsystems is reported in Table B.2 and Table B.3.
The simulated frequency range is the interval 100Hz $\sim$ 2000Hz. In figure 5.1b it can be seen how, over such a frequency range, the plates show wavelengths short enough to be studied as statistical subsystems.

4.2 Assumptions

The principal assumption of the model regards the classification of the subsystems. As already introduced, the plates are considered as statistical subsystems while the beam is deterministic. The reason lies in the wavelengths within the frequency range of simulation, which are short compared to the length of the two plates in the direction of the propagation of the direct field (perpendicular to the junction) see Figure 5.1b. The wavelength of the bending motion is indeed very short with respect to the plate dimension which is 1.2 m for plate A and 1 m for plate B. At 2000Hz the parameter z introduced in section 2.2 is around $12 \sim 15$ for the two plates, which is a value generically associated to SEA components in Table 2.2. Looking at the wavenumbers of the in-plane motion of the plate, they are considerable smaller than the bending one. This is due to the higher stiffness of the component to the shear and longitudinal displacements. Such a difference in the wavelengths allows to separate the out-of-plane and the in-plane motions, if they are decoupled, and to study only the flexural one in the statistical subsystem, while the in-plane motions could be considered deterministically. However, it must be noticed that such a distinction is much more

difficult to be done in more complex geometries, then usually all the motions of a certain subsystem are classified in the same way, as it is done in this report. Regarding the beam, it can be stated that since the bending stiffness is strongly greater than the plate's one, the wavenumbers which can be computed with Equation 2.25 using the modal density formulas in subsection 2.3.3, lead to wavelengths which are higher in magnitude order with respect to the beam length over the simulated frequency range. For this reason, the beam is considered as a deterministic subsystem.

Another important assumption comes from the hypothesis of diffuse reverberant field, which allows to use the equations presented in section 3.3. As already explained, under this assumption the reverberant field is incoherent, and the power balance depends only on the direct field. To study only the direct field of vibration corresponds to neglect all the random boundaries, and model the vibration coming from the deterministic ones as if there were no interactions with other fields or discontinuities in the domain. In the case of the plate subsystem, the direct field can be studied considering the only deterministic boundary, which means modelling the plate as a semi-infinite space. This result presents a big advantage since the solution for the semi-infinite and infinite spaces are typically analytic, and simpler respect to a general component with boundaries. An example for infinite plate solution can be seen in [Cremer et al 2010] and in subsection 4.3.2, where the response depends only on the distance from the application point of the loading.

The considered motions of the plate are produced by the bending, shear and longitudinal forces in the direction perpendicular to the junction. They can be expressed in the semi-infinite space by the three displacements and the rotation in the direction of the junction. The local coordinate system used to describe the semi-infinite plate can be seen in Figure 4.2. The displacements along x,y,z are respectively $\mathbf{u}$,$\mathbf{v}$,$\mathbf{w}$, the forces per unit length are $\mathbf{T}$,$\mathbf{N}$,$\mathbf{F}$. The rotation of the edge in the x-axes is $\boldsymbol{\theta}$ and the moment per unit length is $\mathbf{M}$.
The plate is considered to be isotropic and thin, and the in-plane and out-of-plate motions are supposed to be decoupled for the Kirchhoff-Love theory, so that the behaviour is the summation of the bending theory of plates and the membrane theory of shells. The constitutive equations can be derived from the stress-resultants and the Hooke's law [Timošenko and Woinowsky-Krieger 1996]. The boundary equations required to describe the motion of

the boundary are [Ventsel and Krauthammer 2001]:

$$T = -S\left(\frac{\partial u}{\partial y} + \frac{\partial v}{\partial x}\right) \tag{4.2}$$

$$N = -C\left(\frac{\partial v}{\partial y} + \nu\frac{\partial u}{\partial x}\right) \tag{4.3}$$

$$F = -B\left(\frac{\partial^3 w}{\partial y^3} + (2-\nu)\frac{\partial^3 w}{\partial x^2 \partial y}\right) \tag{4.4}$$

$$M = -B\left(\frac{\partial^2 w}{\partial y^2} + \nu\frac{\partial^2 w}{\partial x^2}\right) \tag{4.5}$$

Where the negative signs of the in-plane forces are due to the correspondence between the coordinate system and the positive direction of the loads (a positive N generates a compression of the plate in y). B, C and S are respectively the bending stiffness, in-plane longitudinal stiffness and in-plane shear stiffness of a thin plate of thickness h:

$$B = \frac{Eh^3}{12\,(1-\nu^2)} \tag{4.6}$$

$$C = \frac{Eh}{1-\nu^2} \tag{4.7}$$

$$S = \frac{Eh}{2\,(1+\nu)} \tag{4.8}$$

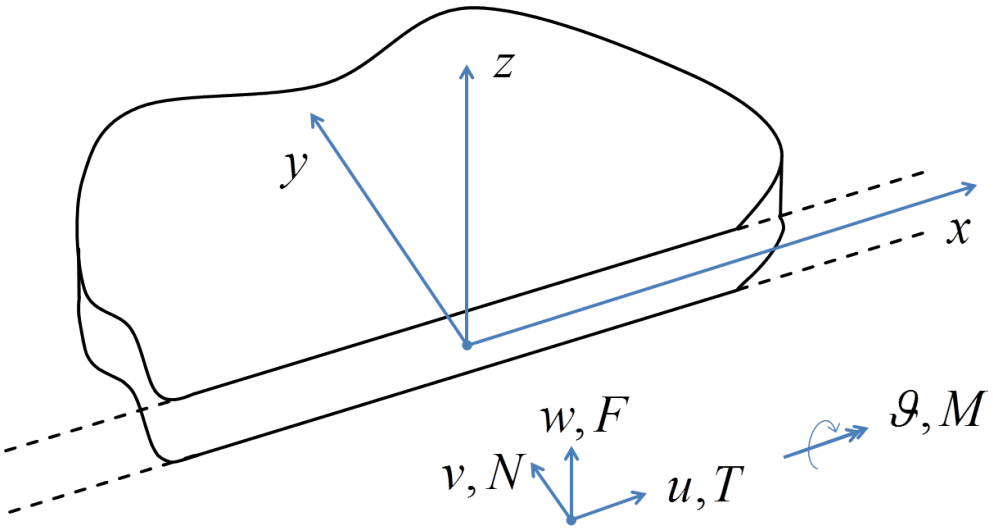

Figure 4.2: Local coordinate system for a semi-infinite plate.

Another assumption is made regarding the coordinates in which the stiffness matrices of the plates and the beam will be presented. A modal-based approach is used to derive the stiffness of the system, so that the deterministic matrices can be found to be diagonal under the assumption of proportional damping, and the direct field stiffness of the plates is expressed in modal coordinates using the modal expansion. The modal analysis is performed with a finite element method.

Under the previous assumptions, the direct field dynamic stiffness matrix for the plates can be computed considering these statistical components to be semi-infinite.

4.3 Direct Field Dynamic Stiffness Matrix

In this subsection, the governing equations for the vibration of thin plates are presented. The solution of the vibration must lead to the semi-infinite plate free field radiation stiffness matrix. In what follows the damping η is neglected to simplify the equations, but it can be easily considered under the assumption of hysteretic damping, by multiplying the elastic constants with $(1 + \mathrm{i}\eta)$ as explained in subsection 2.3.2, and so the bending, shear and longitudinal stiffness since they are proportional to the Young's modulus (for example $B \rightarrow B\,(1 + \mathrm{i}\eta)$).

4.3.1 Governing equations for the Direct Field

Writing the dynamic equilibrium of an infinitesimal thin volume with density ρ loaded by a force per unit area $\mathbf{p} = \{p_x,p_y,p_z\}$, the governing differential equations for plates can be derived for the deflection and the in-plane motion [Ventsel and Krauthammer 2001].
The deflection dynamic is given by:

$$B\nabla^4 w\,(x,y,z,t) + \rho h \frac{\partial^2 w\,(x,y,z,t)}{\partial t^2} = p_z\,(x,y,z,t) \tag{4.9}$$

where ∇^4 is the biharmonic operator[1]. Considering the bending wavenumber of the plate k_B, the differential equation can be rewritten from the time domain to the wavenumber domain

[1] $\nabla^4 = \nabla^2\,(\nabla^2) = \frac{\partial^4}{\partial x^4} + 2\frac{\partial^4}{\partial x^2 \partial y^2} + \frac{\partial^4}{\partial y^4}$

assuming the harmonic time dependency with time frequency ω:

$$k_B = \sqrt[4]{\frac{\rho h \omega^2}{B}} \tag{4.10}$$

$$B\left(\nabla^4 - k_B^4\right) w\left(x,y,z\right) = p\left(x,y,z\right) \tag{4.11}$$

The in-plane dynamic is given by:

$$\begin{cases} C\dfrac{\partial^2 u}{\partial x^2} + S\dfrac{\partial^2 u}{\partial y^2} + S\left(1-\nu^2\right)\dfrac{\partial^2 v}{\partial x \partial y} - \rho h \dfrac{\partial^2 u}{\partial t^2} = p_x & (4.12) \\ C\dfrac{\partial^2 v}{\partial y^2} + S\dfrac{\partial^2 v}{\partial x^2} + S\left(1-\nu^2\right)\dfrac{\partial^2 u}{\partial x \partial y} - \rho h \dfrac{\partial^2 v}{\partial t^2} = p_y & (4.13) \end{cases}$$

As done for the out-of-plane equation, considering the longitudinal and shear wavenumbers k_L, k_S and assuming the harmonic time dependency, the differential equation can be rewritten in wavenumber domain:

$$k_L = \omega\sqrt{\frac{\rho h}{C}} \tag{4.14}$$

$$k_S = \omega\sqrt{\frac{\rho h}{S}} \tag{4.15}$$

$$\begin{cases} C\dfrac{\partial^2 u}{\partial x^2} + S\dfrac{\partial^2 u}{\partial y^2} + S\left(1-\nu^2\right)\dfrac{\partial^2 v}{\partial x \partial y} + Ck_L^2 u = p_x & (4.16) \\ C\dfrac{\partial^2 v}{\partial y^2} + S\dfrac{\partial^2 v}{\partial x^2} + S\left(1-\nu^2\right)\dfrac{\partial^2 u}{\partial x \partial y} + Sk_S^2 v = p_y & (4.17) \end{cases}$$

It must be noticed that the last coefficients are equal $Ck_L^2 = Sk_S^2$, so they can be inverted between the two equations.

4.3.2 Green's Function Method

The Green's Functions for the semi-infinite plate can be used to solve the differential equations. Once the Green's function G is defined, the displacements of the plate boundary can be expressed in one point directly as a function of a unit harmonic point force:

$$q_j = G\left(\mathbf{r}_i,\mathbf{r}_j\right) f_i \qquad \left(\mathbf{D}_{dir}\right)_{ji} = \frac{1}{G\left(\mathbf{r}_i,\mathbf{r}_j\right)} \tag{4.18}$$

where $\mathbf{r}_i$,$\mathbf{r}_j$ are the coordinate of two points, i for the force and j for the response. In [Gunda et al 1998], a general method for the derivation of the harmonic Green's Function in wavenumber domain for the bending of a semi-infinite plate is presented. The derivation comes from the Green's function of an infinite plate, using the superposition principle with the boundary conditions. The solution takes into account the only normal force acting on the plate as a unit harmonic point force at the boundary, and is developed in wavenumber domain as an improper integral over all the possible wavenumbers. The function is derived using the zero order Hankel function of the first kind in polar coordinates, and transformed in cartesian coordinates in order to have a suitable form to apply boundary conditions from a straight edge. From the derivation reported in section A.2, the Green's function of equation Equation 4.11 for an infinite plate in cartesian coordinates results in:

$$G_\infty\left(\mathbf{r}_i,\mathbf{r}_j,k_B\right) = \frac{2c}{\pi}\int_0^{+\infty} \cos\left[k_x\left(x_j - x_i\right)\right]\left[\frac{e^{\mathrm{i}\sqrt{k_B^2-k_x^2}}\left|y_j - y_i\right|}{\sqrt{k_B^2-k_x^2}} + \mathrm{i}\frac{e^{-\sqrt{k_B^2+k_x^2}}\left|y_j - y_i\right|}{\sqrt{k_B^2+k_x^2}}\right]\mathrm{d}k_x \tag{4.19}$$

Where $c = \mathrm{i}/8k_B^2B$ ad k_x is the wavenumber in the x direction. The integrand function is a sum of an even and an odd functions, so that the odd part can be deleted and the even part can be doubled and integrated only over a half interval $[0;+\infty)$. Such an integral is convergent and the solution obtained with the adaptive quadrature "integral" function in MATLAB matches with the theoretical point impedance of the infinite plate in [Cremer et al 2010]:

$$Z_\infty = -\frac{1}{\mathrm{i}\omega G_\infty\left(\mathbf{r}_i,\mathbf{r}_i,k_B\right)} = 8\sqrt{\rho h B} \tag{4.20}$$

For an infinite plate of thickness $h = 3$ mm and same material of Table B.1 excited by a unit force at 1000 Hz, the point impedance results to be 0,305 N/(mm s) for both the formulas. As reported in section A.2, using the method of images as shown in [Gunda et al 1995], it is possible to find the Green's functions of the semi-infinite plate for a simply supported edge and roller supported edge. Then, the superposition of the boundary displacements can be used to reproduce clamped and free boundary conditions. A resume of the Green's functions for the normal loading of the semi-infinite plate can be found in [Cuenca 2009, Section 4.3.2]. In this context, only the Green's function for the free edge is reported in order to underline the problem of this method. Since excitation and response are of interest only on the semi-infinite plate edge, is advantageous to use the free boundary formula derived from the simply supported case (Equation A.18), since the Green's function of the simply supported plate in

Equation A.11 at the edge is zero, and referring to Figure 4.2:

$$G_{/\infty,f_s}|_{y_i=y_j=0} = \\ = \frac{\mathrm{i}8ck_B^4}{\pi} \int_0^{+\infty} \frac{\cos\left[k_x\left(x_j - x_i\right)\right]}{\sqrt{k_B^2 + k_x^2}\left(k_B^2 - (1-\nu)\,k_x^2\right)^2 + \mathrm{i}\sqrt{k_B^2 - k_x^2}\left(k_B^2 + (1-\nu)\,k_x^2\right)^2} \mathrm{d}k_x \tag{4.21}$$

As it can be seen from the denominator, the integrand function presents a discontinuity of the second type (essential discontinuity) which is not easy to be solved. Simple adaptive quadrature is not suitable for this function, even if very small tolerances are imposed. In [Gunda et al 1998] an integration technique is proposed using the Clenshaw-Curtis integration with the Čebyšëv polynomial of the first kind.
Looking at the line junction and the assumption made about the degrees of freedom, the bending deflection is not sufficient to describe the semi-infinite plate behaviour. Regarding the out of plane motion, one way to represent the Green's function for the moment excitation $\mathbf{M}$ is shown in [Filippi 2008] as the derivative of the deflection Green's function in the direction of the moment, which complicates even more the formulas. Regarding the in-plane motion, similar procedure for the derivation of the longitudinal and shear waves Green's function could be adopted, actually not easily available in literature.

Despite the possibility to find an approximate solution for the Green's function and so to derive the radiation stiffness matrix for a given set of nodes on the edge, this method is not easy to implement because of the complexity of the integration and the very high sensitivity of the result to the tolerance adopted for the approximation. In the next subsections, two better suitable methods are presented for the derivation of the direct field stiffness.

4.3.3 Wavenumber Direct Modal Transformation Method

Instead of deriving the Green's functions, the equations of motion for the out-of-plane and in-plane vibration of the semi-infinite plate can be obtained directly from the stress resultant relations (Equation 4.2, 4.3, 4.4, 4.5) under the assumption of harmonic response in time and space propagation. The following derivation is also done in [Langley and Heron 1990] and corrected in [Johansson and Comnell 2010], in this thesis some more clarifications are made as explained in section A.3.
Referring to the coordinate system in Figure 4.2, a generic component p_i of the direct wave field generated from the boundary is supposed to have a harmonic space and time dependency

written as:

$$p_i(x,y,t) \sim e^{-(\mathrm{i}k_x x+\mathrm{i}k_y y)+\mathrm{i}\omega t} \tag{4.22}$$

where k_x and k_y are the wavenumber components in the plate. The displacements associated to this wave will have the same time/space dependency expressed by a superposition of amplitudes and wavenumbers which is governed by the differential equations of motion. Indeed, if the harmonic behaviour is substituted in the homogeneous equations of the out-of-plane and in-plane motions, the eigenvalues of the resulting eigeproblems will be the bending, shear and longitudinal wavenumbers needed to describe the motion of the plate.
While the dependency $e^{-\mathrm{i}k_x x+\mathrm{i}\omega t}$ is given in all the plate by the compatibility at the junction because of the space and time frequency excitations k_x, ω, the y dependency is given by the plate equations of motion. Wanting to derive the shape of the y dependency as $e^{\mu_B y}$, the response can be written as:

$$p_i(x,y,t) \sim e^{-\mathrm{i}k_x x+\mu_B y+\mathrm{i}\omega t} \tag{4.23}$$

Considering in first instance the out-of-plane motion. From Equation 4.11, the homogeneous equation in wavenumber domain and the corresponding eigenproblem deriving form the harmonic dependency are:

$$B\left(\nabla^4 - k_B^4\right)\mathrm{w}\,(x,y,z) = 0 \tag{4.24}$$

$$\left(\nabla^4 - k_B^4\right)e^{-\mathrm{i}k_x x+\mu_B y+\mathrm{i}\omega t} = 0 \tag{4.25}$$

Developing Equation 4.25 leads to:

$$\left(k_x^2 + \mu_B^2\right)^2 = k_B^4 \tag{4.26}$$

Four possible solutions for the y component of the wavenumber can be found. Two are positive (one imaginary and one real) and two are negative (one imaginary and one real). Since the plate is semi-infinite, the response must tend to zero at y values which are far from the boundary. This can only be obtained if μ_B is negative (Equation 4.22), so the two negative roots are considered and are called μ_{B1} and μ_{B2} for specify the bending case:

$$\mu_{B1} = -\sqrt{k_x^2 + k_B^2} \qquad\qquad \mu_{B2} = -\sqrt{k_x^2 - k_B^2} \tag{4.27}$$

μ_{B2} is imaginary for $|k_x| < |k_B|$. Using these two wavenumbers, the out-of-plane response can be written as:

$$\mathrm{w} = \sum_{n=1}^{2} \alpha_{Bn} e^{-\mathrm{i}k_x x + \mu_{Bn} y + \mathrm{i}\omega t} \tag{4.28}$$

$$\theta = \frac{\partial w}{\partial y} = \sum_{n=1}^{2} \mu_{Bn} \alpha_{Bn} e^{-\mathrm{i}k_x x + \mu_{Bn} y + \mathrm{i}\omega t} \tag{4.29}$$

where α_{Bn} are the amplitudes of the two waves. Substituting these displacements in the stress resultant relations for the deflection (Equation 4.4, 4.5), the relation between the edge forces $\mathrm{F}_e, \mathrm{M}_e$ and displacements w_e, θ_e both defined in wavenumber domain can be found imposing $y = 0$. The formulas are reported in section A.3, and the final result contains the direct field dynamic stiffness matrix for the out-of-plane motion in wavenumber domain $\mathbf{D}^{\mathrm{wn}}_{dir,out}$:

$$\begin{aligned} \begin{pmatrix} \mathrm{F}_e(k_x) \\ \mathrm{M}_e(k_x) \end{pmatrix} &= \mathbf{D}^{\mathrm{wn}}_{dir,out} \begin{pmatrix} \mathrm{w}_e(k_x) \\ \theta_e(k_x) \end{pmatrix} = \\ &= B \begin{bmatrix} \mu_{B1}^2 \mu_{B2} + \mu_{B1} \mu_{B2}^2 & -\mu_{B1}\mu_{B2} - \nu k_x^2 \\ \mu_{B1}\mu_{B2} + \nu k_x^2 & -\mu_{B1} - \mu_{B2} \end{bmatrix} \begin{pmatrix} \mathrm{w}_e(k_x) \\ \theta_e(k_x) \end{pmatrix} \end{aligned} \tag{4.30}$$

which is antisymmetric. Since μ_{B2} participates in all the coefficients of Equation 4.30, the out-of-plane radiation stiffness matrix is complex valued for $|k_x| < |k_B|$. Repeating the same procedure for the in-plane case in Equation 4.16 and 4.17, the solutions for the y dependency are:

$$\mu_S = -\sqrt{k_x^2 - k_S^2} \tag{4.31}$$

$$\mu_L = -\sqrt{k_x^2 - k_L^2} \tag{4.32}$$

and the consequent in-plane displacements:

$$\mathrm{u} = \left[\alpha_L k_x e^{\mu_L y} + \mathrm{i}\alpha_S \mu_S e^{\mu_S y}\right] e^{-\mathrm{i}k_x x + \mathrm{i}\omega t} \tag{4.33}$$

$$\mathrm{v} = \left[\mathrm{i}\alpha_L \mu_L e^{\mu_L y} - \alpha_S k_x e^{\mu_S y}\right] e^{-\mathrm{i}k_x x + \mathrm{i}\omega t} \tag{4.34}$$

The in-plane motion equations can be derived with the same approach, and the matrix $\mathbf{D}^{\mathrm{wn}}_{dir,in}$ is written as:

$$\begin{aligned}\begin{pmatrix}\mathrm{T}_e\left(k_x\right)\\ \mathrm{N}_e\left(k_x\right)\end{pmatrix} &= \mathbf{D}^{\mathrm{wn}}_{dir,in}\begin{pmatrix}\mathrm{u}_e\left(k_x\right)\\ \mathrm{v}_e\left(k_x\right)\end{pmatrix} = \\ &= \frac{S}{k_x^2-\mu_L\mu_S}\begin{bmatrix}-\mu_L k_S^2 & -\mathrm{i}k_x\left(2\mu_L\mu_s+k_S^2-2k_x^2\right)\\ \mathrm{i}k_x\left(2\mu_L\mu_s+k_S^2-2k_x^2\right) & -\mu_S k_S^2\end{bmatrix}\begin{pmatrix}\mathrm{u}_e\left(k_x\right)\\ \mathrm{v}_e\left(k_x\right)\end{pmatrix}\end{aligned} \tag{4.35}$$

Also the in-plane matrix is antisymmetric and is complex valued for $|k_x|<|k_L|$ in the terms containing μ_L and for $|k_x|<|k_S|$ in the terms containing μ_S. The complete radiation stiffness matrix in wavenumber domain for the semi-infinite plate is then antisymmetric:

$$\begin{pmatrix}\mathrm{T}_e\left(k_x\right)\\ \mathrm{N}_e\left(k_x\right)\\ \mathrm{F}_e\left(k_x\right)\\ \mathrm{M}_e\left(k_x\right)\end{pmatrix} = \mathbf{D}^{\mathrm{wn}}_{dir}\left(k_x\right)\begin{pmatrix}\mathrm{u}_e\left(k_x\right)\\ \mathrm{v}_e\left(k_x\right)\\ \mathrm{w}_e\left(k_x\right)\\ \theta_e\left(k_x\right)\end{pmatrix} \qquad \mathbf{D}^{\mathrm{wn}}_{dir}\left(k_x\right) = \begin{bmatrix}\mathbf{D}^{\mathrm{wn}}_{dir,in}\left(k_x\right) & \mathbf{0}\\ \mathbf{0} & \mathbf{D}^{\mathrm{wn}}_{dir,out}\left(k_x\right)\end{bmatrix} \tag{4.36}$$

$$\mathbf{D}^{\mathrm{wn}}_{dir}\left(k_x\right) = \begin{bmatrix}D11\left(k_x\right) & D12\left(k_x\right) & 0 & 0\\ D21=-D12 & D22\left(k_x\right) & 0 & 0\\ 0 & 0 & D33\left(k_x\right) & D34\left(k_x\right)\\ 0 & 0 & D43=-D34 & D44\left(k_x\right)\end{bmatrix} \tag{4.37}$$

As introduced in section 4.2, the matrices for the calculation of the coupling loss factors are considered in modal coordinates, so it is necessary to apply a modal transformation to the system in Equation 4.36. In this case, the modal transformation is done directly in wavenumber domain using a wavenumber integral.

Considering the stress resultants, the force-displacements relation in space domain can be written as a differential equation where the force functions $\mathbf{f}^{\mathrm{space}}\left(x,y,z\right) = \left[\mathrm{T,N,F,M}\right]^{\mathrm{T}}$ can be written through the differential operator matrix $\boldsymbol{\mathcal{Q}}$ operating on the space displacements

vector $\mathbf{u}^{\text{space}}(x,y,z) = [\text{u,v,w,}\theta]^{\text{T}}$:

$$\mathbf{f}^{\text{space}} = \boldsymbol{\mathcal{Q}}\mathbf{u}^{\text{space}} \tag{4.38}$$

$$\boldsymbol{\mathcal{Q}} = \begin{bmatrix} \mathcal{Q}_{11} & \mathcal{Q}_{12} & 0 & 0 \\ \mathcal{Q}_{21} & \mathcal{Q}_{22} & 0 & 0 \\ 0 & 0 & \mathcal{Q}_{33} & \mathcal{Q}_{34} \\ 0 & 0 & \mathcal{Q}_{43} & \mathcal{Q}_{44} \end{bmatrix} \tag{4.39}$$

For the modal transformation, the displacements are written as a summation of mode shapes of the plate edge $\boldsymbol{\Phi}_i(x)$ in space domain, multiplied by the modal displacements q_i:

$$\mathbf{u}^{\text{space}} = \sum_i \boldsymbol{\Phi}_i(x) q_i \tag{4.40}$$

$$\boldsymbol{\Phi}_i(x) = \left[\Phi_i^{\text{u}}(x), \Phi_i^{\text{v}}(x), \Phi_i^{\text{w}}(x), \Phi_i^{\theta}(x)\right]^{\text{T}} \tag{4.41}$$

A generic mode shape presents four components, one for each type of displacements considered are the edge. The differential equations can be then written substituting the modal transformation, and integrating the residual over the plate edge with the pre-multiplication of the transposed mode shapes:

$$\mathbf{f}^{\text{space}} = \boldsymbol{\mathcal{Q}} \sum_i \boldsymbol{\Phi}_i(x) q_i \tag{4.42}$$

$$\int_L \boldsymbol{\Phi}_j^{*^{\text{T}}}(x) \mathbf{f}^{\text{space}} \text{d}x = \sum_i q_i \int_L \boldsymbol{\Phi}_j^{*^{\text{T}}}(x) \boldsymbol{\mathcal{Q}} \boldsymbol{\Phi}_i(x) \text{d}x \tag{4.43}$$

The mode shapes must be transposed in the pre-multiplication in order to obtain the modal transformation. Equation 4.43 represents the force displacements relation in modal coordinates, where the modal force on the j-th coordinate is the left part of the equation and is given by the direct field dynamic stiffness matrix in modal coordinates $\mathbf{D}_{dir}^{mod}$ multiplied by the modal displacements:

$$\mathbf{f}_j^{\text{mod}} = \int_L \boldsymbol{\Phi}_j^{*^{\text{T}}}(x) \mathbf{f}^{\text{space}} \text{d}x = \sum_i D_{dir,ji}^{mod} q_i \tag{4.44}$$

$$D_{dir,ji}^{mod} = \int_L \boldsymbol{\Phi}_j^{*^{\text{T}}}(x) \boldsymbol{\mathcal{Q}} \boldsymbol{\Phi}_i(x) \text{d}x \tag{4.45}$$

Considering Equation 4.42, the term $\boldsymbol{\mathcal{Q}}\boldsymbol{\Phi}_i(x)$ can be seen as the i-th contribution of the summation for the force vector function in space domain $\mathbf{f}_i^{\text{space}}$, normalized with the i-th

modal displacement q_i:

$$\frac{\mathbf{f}_i^{\text{space}}}{q_i} = \boldsymbol{\mathcal{Q}}\boldsymbol{\Phi}_i(x) \tag{4.46}$$

$$D_{dir,ji}^{mod} = \int_L \boldsymbol{\Phi}_j^{*\mathrm{T}}(x)\frac{\mathbf{f}_i^{\text{space}}}{q_i}\mathrm{d}x \tag{4.47}$$

The modal free field radiation stiffness matrix can then be derived from the contribution of force in space domain due to the i-th mode shape. Such contribution can be written in wavenumber domain using $\mathbf{D}_{dir}^{\text{wn}}$ considering that the modal displacements are the same as in space domain. The wavenumber Fourier Transform of the mode shapes is:

$$\boldsymbol{\Phi}_i(k_x) = \int_{-\infty}^{+\infty} \boldsymbol{\Phi}_i(x)e^{-\mathrm{i}k_x x}\mathrm{d}x = \left[\Phi_i^{\mathrm{u}}(k_x), \Phi_i^{\mathrm{v}}(k_x), \Phi_i^{\mathrm{w}}(k_x), \Phi_i^{\theta}(k_x)\right]^{\mathrm{T}} \tag{4.48}$$

$$\mathbf{U}^{\text{wn}} = \sum_i \boldsymbol{\Phi}_i(k_x)q_i \tag{4.49}$$

where $\mathbf{U}^{\text{wn}}$ is the wavenumber transform of the space displacements obtained transforming Equation 4.40. The i-th force contribution derives from the substitution of Equation 4.49 in Equation 4.36:

$$\frac{\mathbf{F}_i^{\text{wn}}}{q_i} = \mathbf{D}_{dir}^{\text{wn}}\boldsymbol{\Phi}_i(k_x) \tag{4.50}$$

where $\mathbf{F}_i^{\text{wn}}$ is the force per unit length vector in wavenumber domain. The inverse Fourier Transform of Equation 4.50 must lead to the same force written in Equation 4.46, and is:

$$\frac{\mathbf{f}_i^{\text{space}}}{q_i} = \frac{1}{2\pi}\int_{-\infty}^{+\infty} \mathbf{D}_{dir}^{\text{wn}}\boldsymbol{\Phi}_i(k_x)e^{\mathrm{i}k_x x}\mathrm{d}k_x \tag{4.51}$$

Substituting Equation 4.51 in Equation 4.47:

$$D_{dir,ji}^{mod} = \frac{1}{2\pi}\int_{-\infty}^{+\infty}\left(\int_L \boldsymbol{\Phi}_j^{*\mathrm{T}}(x)e^{\mathrm{i}k_x x}\mathrm{d}x\right)\mathbf{D}_{dir}^{\text{wn}}\boldsymbol{\Phi}_i(k_x)\mathrm{d}k_x \tag{4.52}$$

Inverting the integration order of the line integral, the term in the parenthesis corresponds to the waveunmber transform of the j-th transposed conjugated mode shape, so the modal

radiation stiffness matrix can be finally written as a wavenumber integral:

$$D^{mod}_{dir,ji} = \frac{1}{2\pi}\int_{-\infty}^{+\infty} \mathbf{\Phi}_j^{*^{\mathrm{T}}}(k_x)\mathbf{D}^{\mathrm{wn}}_{dir}\mathbf{\Phi}_i(k_x)\mathrm{d}k_x \tag{4.53}$$

$\mathbf{D}^{mod}_{dir}$ is in modal coordinates, so it has $M \times M$ elements with M number of modes considered, and $D^{mod}_{dir,ji}$ is a single element which is function of the time-frequency excitation ω. Indicating the ij element of $\mathbf{D}^{\mathrm{wn}}_{dir}$ as D^{wn}_{ij}, the modal stiffness can be written as:

$$\begin{aligned} D^{mod}_{dir,ji} =& \frac{1}{2\pi}\int_{-\infty}^{+\infty} \Big[\Phi^u_j(k_x)\left(D^{\mathrm{wn}}_{11}\Phi^u_i(k_x) + D^{\mathrm{wn}}_{12}\Phi^v_i(k_x)\right) + \Phi^v_j(k_x)\left(D^{\mathrm{wn}}_{21}\Phi^u_i(k_x) + D^{\mathrm{wn}}_{22}\Phi^v_i(k_x)\right) + \\ &+\Phi^w_j(k_x)\left(D^{\mathrm{wn}}_{33}\Phi^w_i(k_x) + D^{\mathrm{wn}}_{34}\Phi^\theta_i(k_x)\right) + \Phi^\theta_j(k_x)\left(D^{\mathrm{wn}}_{43}\Phi^w_i(k_x) + D^{\mathrm{wn}}_{44}\Phi^\theta_i(k_x)\right)\Big]\,\mathrm{d}k_x \end{aligned} \tag{4.54}$$

The improper integral should be evaluated over all the possible infinite wavenumber values. In the context of a simulation, there must be a maximum wavenumber calculable, given by the Shannon theorem[2] for the sampling of mode shapes. Since the modes are taken from a FE model, their maximum wavelength is related to the FE grid of nodes used to discretize the junction.
Assuming an equispaced grid to be used with a spacing of ΔL between each node. The sampling space-frequency is $f_s = 1/\Delta L$, consequently there will not be mode shapes with wavelength components smaller than $2\Delta L$, and so the corresponding maximum wavenumber is $k_{max} = \pi/\Delta L$. The integration in Equation 4.54 can then be computed only over the range defined by the maximum wavenumber. One possible way to compute the ij entry of the radiation stiffness is reported in Appendix D.

$$\begin{aligned} D^{mod}_{dir,ji} =& \frac{1}{2\pi}\int_{-f_s\pi}^{+f_s\pi} \Big[\Phi^u_j(k_x)\left(D^{\mathrm{wn}}_{11}\Phi^u_i(k_x) + D^{\mathrm{wn}}_{12}\Phi^v_i(k_x)\right) + \Phi^v_j(k_x)\left(D^{\mathrm{wn}}_{21}\Phi^u_i(k_x) + D^{\mathrm{wn}}_{22}\Phi^v_i(k_x)\right) + \\ &+\Phi^w_j(k_x)\left(D^{\mathrm{wn}}_{33}\Phi^w_i(k_x) + D^{\mathrm{wn}}_{34}\Phi^\theta_i(k_x)\right) + \Phi^\theta_j(k_x)\left(D^{\mathrm{wn}}_{43}\Phi^w_i(k_x) + D^{\mathrm{wn}}_{44}\Phi^\theta_i(k_x)\right)\Big]\,\mathrm{d}k_x \end{aligned} \tag{4.55}$$

As anticipated in subsection 3.2.1, the mode shapes used in this case are complex valued, since they are the result of a Fourier Transform. The consequence is that the pre-multiplication by the j-th conjugated shape and post-multiplication by the i-th shape of the wavenumber stiffness coefficients is not a complete symmetric operation. Indeed, considering two recipro-

[2] If a sampling frequency f_s is used while sampling a signal containing a certain ensemble of frequency contributions, the maximum frequency that can be sampled is $f_s/2$

cal elements $D^{mod}_{dir,ji}$ and $D^{mod}_{dir,ij}$ only their absolute values are equal, while real and imaginary parts may be different.

Once the radiation stiffness is totally computed for both the statistical subsystems, the coupling loss factors can be obtained by using Equation 3.59. In order to do this, the modal dynamic stiffness of the beam must be computed. Since the mode shapes are needed and usually calculated with a FEM software, this matrix can be directly extracted from the FE model. Otherwise, it can be simply written in modal coordinates using the natural frequencies ω_n, under the assumption of proportional damping which allows the decoupling of the modes, and so the matrix results to be diagonal:

$$D^{mod}_{beam,ii} = \omega^2_{n,i}\left(1 + \mathrm{i}\eta_{beam}\right) - \omega^2 \tag{4.56}$$

The deterministic matrix corresponds to the beam stiffness, and the total matrix is:

$$\mathbf{D}^{mod}_{tot} = \mathbf{D}^{mod}_{beam} + \mathbf{D}^{mod,A}_{dir} + \mathbf{D}^{mod,B}_{dir} \tag{4.57}$$

Considering M as the number of modes taken in account, the coupling loss factors are then computed:

$$h_{AB} = \frac{2}{\pi}\sum_{l,m}^{M} \mathrm{Im}\left[\mathbf{D}^{(B)}_{dir,lm}\right]\left\{\mathbf{D}^{-1}_{tot}\,\mathrm{Im}\left[\mathbf{D}^{(A)}_{dir}\right]\mathbf{D}^{-\mathrm{H}}_{tot}\right\}_{lm} = h_{BA} \tag{4.58}$$

$$\eta_{AB} = \frac{h_{AB}}{\omega n_A} \tag{4.59}$$

$$\eta_{BA} = \frac{h_{BA}}{\omega n_B} \tag{4.60}$$

4.3.4 Wavenumber Cardinal Sine Method

Another approach for developing the differential equation in Equation 4.38 and transforming it in a discrete function formulation, is to use generic shape functions and apply the Galerkin Method to each stress resultant equation in order to obtain forces and displacement in the generic set of generalized coordinates.
Considering a set of shape functions $\boldsymbol{\varphi}_i(x)$ which are bases of the $\mathbf{q}$ set of generalized coordinates, the vector of the four displacements is expressed as:

$$\mathbf{u}^{\mathrm{space}} = \sum_i \boldsymbol{\varphi}_i(x) q_i \tag{4.61}$$

The shape functions and their wavenumber Fourier transforms are written as:

$$\boldsymbol{\varphi}_i(x) = \left[\varphi_i^{\mathrm{u}}(x), \varphi_i^{\mathrm{v}}(x), \varphi_i^{\mathrm{w}}(x), \varphi_i^{\theta}(x)\right]^{\mathrm{T}} \tag{4.62}$$

$$\boldsymbol{\varphi}_i(k_x) = \int_{-\infty}^{+\infty} \boldsymbol{\varphi}_i(x) e^{-\mathrm{i}k_x x} \mathrm{d}x = \left[\varphi_i^{\mathrm{u}}(k_x), \varphi_i^{\mathrm{v}}(k_x), \varphi_i^{\mathrm{w}}(k_x), \varphi_i^{\theta}(k_x)\right]^{\mathrm{T}} \tag{4.63}$$

Applying the Galerkin method to the stress resultant (Equation 4.38), the residual is integrated with the substitution of the displacements in Equation 4.61 and with the pre-multiplication of a set of weight functions which is the chosen to be equal to the set of shape functions:

$$\int_L \boldsymbol{\varphi}_j^*(x) \mathbf{f}^{\mathrm{space}} \mathrm{d}x = \sum_i q_i \int_L \boldsymbol{\varphi}_j^*(x) \boldsymbol{\mathcal{Q}} \boldsymbol{\varphi}_i(x) \mathrm{d}x = \sum_i \mathbf{D}_{dir,\mathbf{q}} q_i \tag{4.64}$$

where $\mathbf{D}_{dir,\mathbf{q}}$ is the direct field dynamic stiffness matrix in the generalized coordinates $\mathbf{q}$. Equation 4.64 is similar to Equation 4.43. The only difference is in the transposition of the pre-multiplied shape function which is adopted for the modal transformation and is not adopted for this generic solution. Proceeding in the same way as in subsection 4.3.3, the ji entry of the free field stiffness matrix is:

$$D_{dir,\mathbf{q},ji}^{mod} = \int_L \boldsymbol{\varphi}_j^*(x) \frac{\mathbf{f}_i^{\mathrm{space}}}{q_i} \mathrm{d}x \tag{4.65}$$

Writing the force vector in wavenumber domain and its inverse Fourier transform as in Equation 4.51:

$$\frac{\mathbf{F}_i^{\mathrm{wn}}}{q_i} = \mathbf{D}_{dir}^{\mathrm{wn}} \boldsymbol{\varphi}_i(k_x) \tag{4.66}$$

$$\frac{\mathbf{f}_i^{\mathrm{space}}}{q_i} = \frac{1}{2\pi} \int_{-\infty}^{+\infty} \mathbf{D}_{dir}^{\mathrm{wn}} \boldsymbol{\varphi}_i(k_x) e^{\mathrm{i}k_x x} \mathrm{d}k_x \tag{4.67}$$

Equation 4.67 can be substituted in Equation 4.65, and inverting the integration order of the L integral, the entry of the direct field dynamic stiffness matrix in generalized coordinates for the j-th generalized vector of four forces on the i-th generalized vector of four displacements is:

$$\left(D_{dir,\mathbf{q}}\right)_j = \frac{1}{2\pi} \int_{-\infty}^{+\infty} \boldsymbol{\varphi}_j^*(k_x) \mathbf{D}_{dir}^{\mathrm{wn}} \boldsymbol{\varphi}_i(k_x) \mathrm{d}k_x \tag{4.68}$$

The ji entry is a submatrix of the same dimension of $\mathbf{D}^{\mathrm{wn}}_{dir}$ (in this case is a 4×4), because the method is applied separately to each stress resultant. The submatrix entry can be written developing Equation 4.68:

$$\left(D_{dir,\mathbf{q}}\right)_{ji} = \frac{1}{2\pi} \int_{-\infty}^{+\infty} \begin{bmatrix} \varphi^{\mathrm{u}}_j D^{\mathrm{wn}}_{11} \varphi^{\mathrm{u}}_i & \varphi^{\mathrm{u}}_j D^{\mathrm{wn}}_{12} \varphi^{\mathrm{v}}_i & 0 & 0 \\ \varphi^{\mathrm{v}}_j D^{\mathrm{wn}}_{21} \varphi^{\mathrm{u}}_i & \varphi^{\mathrm{v}}_j D^{\mathrm{wn}}_{22} \varphi^{\mathrm{v}}_i & 0 & 0 \\ 0 & 0 & \varphi^{\mathrm{w}}_j D^{\mathrm{wn}}_{33} \varphi^{\mathrm{w}}_i & \varphi^{\mathrm{w}}_j D^{\mathrm{wn}}_{34} \varphi^{\theta}_i \\ 0 & 0 & \varphi^{\theta}_j D^{\mathrm{wn}}_{43} \varphi^{\mathrm{w}}_i & \varphi^{\theta}_j D^{\mathrm{wn}}_{4} \varphi^{\theta}_i \end{bmatrix} \mathrm{d}k_x \tag{4.69}$$

where the shape functions are in wavenumber domain $\varphi_i = \varphi_i(k_x)$. The total stiffness is then a $4N \times 4N$ matrix frequency dependent, where N is the number of shape functions adopted to represent the displacements. Such an approach can be used for any kind of valid set of orthogonal shape functions, but the problem of the improper integral must be solved.

It can be seen that for a 1-dimensional problem like the boundary response-excitation relation treated in this chapter, a basis function capable to appropriately reproduce the wave propagation is the cardinal sine $\mathrm{sinc}\,(x)$. In [Langley 2007], the corresponding 2-dimensional function (jinc) is used for the normal displacement of plane structures. In its normalized form, this function can be written as:

$$\mathrm{sinc}\,(x - x_i) = \frac{\sin\left[\pi\,(x - x_i)\right]}{\pi\,(x - x_i)} \tag{4.70}$$

Such a function intersect the x axis in all the integer values of x, apart from $x = x_i$ where $\mathrm{sinc}\,(0) = 1$. An extremely helpful property of this function is represented by its wavenumber transform, which is the rectangular function of height 1 and width 2π (range$[-\pi; \pi]$) in the wavenumber domain. The rectangular is the total real part of the transform only if the sinc is in the origin of the coordinate system, so if $x_i = 0$. Otherwise the wavenumber transform is rectangular only in its absolute value, since is complex valued with harmonic real and imaginary parts but still null out of the rectangular base. If the frequency of the normalized sinc is changed from 1 to a generic sampling frequency value f_s, the Fourier Transform is still rectangular with amplitude f_s and frequency band is $[-f_s\pi; f_s\pi]$. In conclusion, if sinc shape functions are adopted in space domain, their wavenumber transforms are all zero for $|k| > f_s\pi$, which means that the integral in Equation 4.69 is computed only over the bandwidth $[-f_s\pi; f_s\pi]$. Beside, the same sinc functions φ_i can be adopted to describe all the four displacements of the plate's edge, so that $\varphi_i = \varphi^{\mathrm{u}}_i = \varphi^{\mathrm{v}}_i = \varphi^{\mathrm{w}}_i = \varphi^{\theta}_i$.
The sinc shape functions can be chosen in a particular way so that the formulas get simplified. The target is to obtain a shape function matrix in space domain which is the identity matrix, that means no coordinate transformation is needed between the nodal coordinates and the

"sinc" coordinates. The number of shape functions corresponds to the number of nodes: in order to form the identity matrix, each sinc function must correspond to one node and the shape function related to the i-th node must have unitary amplitude in correspondence of that node and null amplitude in correspondence of all the other $j \neq i$ nodes.
If the nodes grid is equispaced and the spacing is ΔL, indicating the sampling space-frequency as $f_s = 1/\Delta L$ the i-th shape function and its wavenumber transform are:

$$\varphi_i(x) = \varphi_i^{\mathrm{u}}(x) = \varphi_i^{\mathrm{v}}(x) = \varphi_i^{\mathrm{w}}(x) = \varphi_i^{\theta}(x) = \mathrm{sinc}\left[f_s\left(x - x_i\right)\right] = \frac{\sin\left[f_s\pi\left(x - x_i\right)\right]}{f_s\pi\left(x - x_i\right)} \tag{4.71}$$

$$\varphi_i(k_x) = \varphi_i^{\mathrm{u}}(k_x) = \varphi_i^{\mathrm{v}}(k_x) = \varphi_i^{\mathrm{w}}(k_x) = \varphi_i^{\theta}(k_x) = \begin{cases} \Delta L e^{-\mathrm{i}k_x x_i} & |k_x| \leq \pi f_s \\ 0 & |k_x| > \pi f_s \end{cases} \tag{4.72}$$

Using as shape functions these sinc functions with frequency f_s, the wavenumber is simplified in:

$$\left(D_{dir,\mathbf{q}}\right)_{ji} = \frac{1}{2\pi}\int_{-f_s\pi}^{+f_s\pi} \begin{bmatrix} \varphi_j D_{11}^{\mathrm{wn}}\varphi_i & \varphi_j D_{12}^{\mathrm{wn}}\varphi_i & 0 & 0 \\ \varphi_j D_{21}^{\mathrm{wn}}\varphi_i & \varphi_j D_{22}^{\mathrm{wn}}\varphi_i & 0 & 0 \\ 0 & 0 & \varphi_j D_{33}^{\mathrm{wn}}\varphi_i & \varphi_j D_{34}^{\mathrm{wn}}\varphi_i \\ 0 & 0 & \varphi_j D_{43}^{\mathrm{wn}}\varphi_i & \varphi_j D_4^{\mathrm{wn}}\varphi_i \end{bmatrix} \mathrm{d}k_x \tag{4.73}$$

where the shape functions are in wavenumber domain $\varphi_i = \varphi_i(k_x)$. In Figure 4.3, the sinc function in Equation 4.71 is represented together with the sinc at the origin.
In Figure 4.4 two generic wavenumber transforms of the sinc are represented in the absolute value. The effect of the translation from the origin of a distance x_i is the multiplication of the exponential term in wavenumber domain, which is a harmonic function of k_x and does not affect the absolute value.
Once the free field radiation stiffness matrix is expressed in sinc coordinates it is automatically represented in space domain in nodal coordinates, since the transformation from the general coordinates of the sinc functions to the nodal coordinates is the identity matrix. The stiffness matrix can then be expressed in modal coordinates using the modal transformation. Indicating with $\boldsymbol{\mathcal{M}}$ the modal matrix of the line edge as in Equation 3.75:

$$\mathbf{D}_{dir} = \boldsymbol{\mathcal{M}}^{\mathrm{H}}\mathbf{D}_{dir,\mathbf{q}}\boldsymbol{\mathcal{M}} \tag{4.74}$$

Finally, the coupling loss factors can be computed in modal coordinates as in Equation 4.58, 4.59 and 4.60.
One possible way to compute the ij entry of the radiation stiffness with this method is

reported in Appendix D.

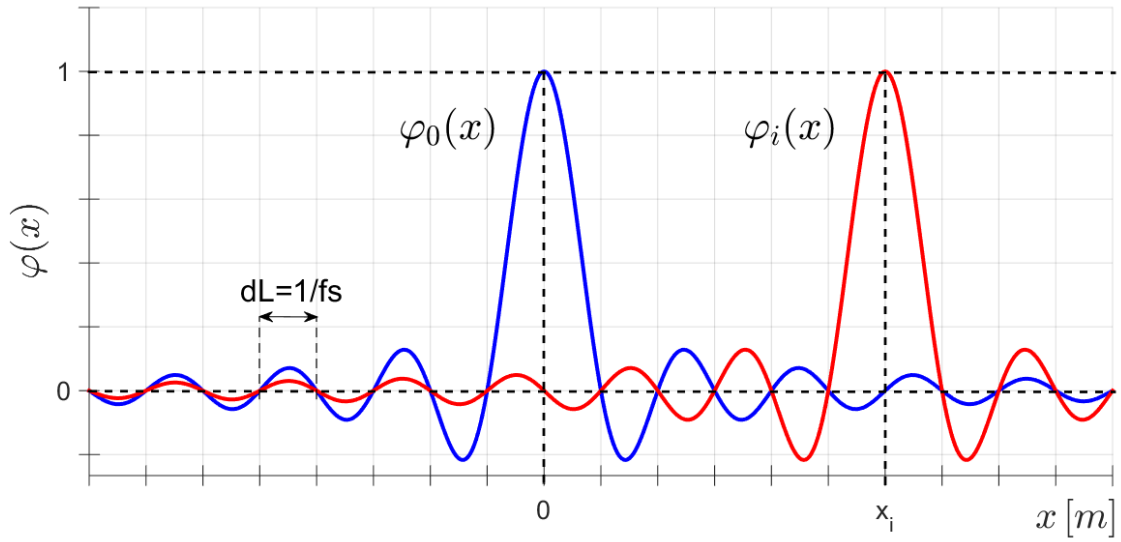

Figure 4.3: sinc Shape Functions in the origin $\varphi_0(x)$ and in a generic node $\varphi_i(x)$

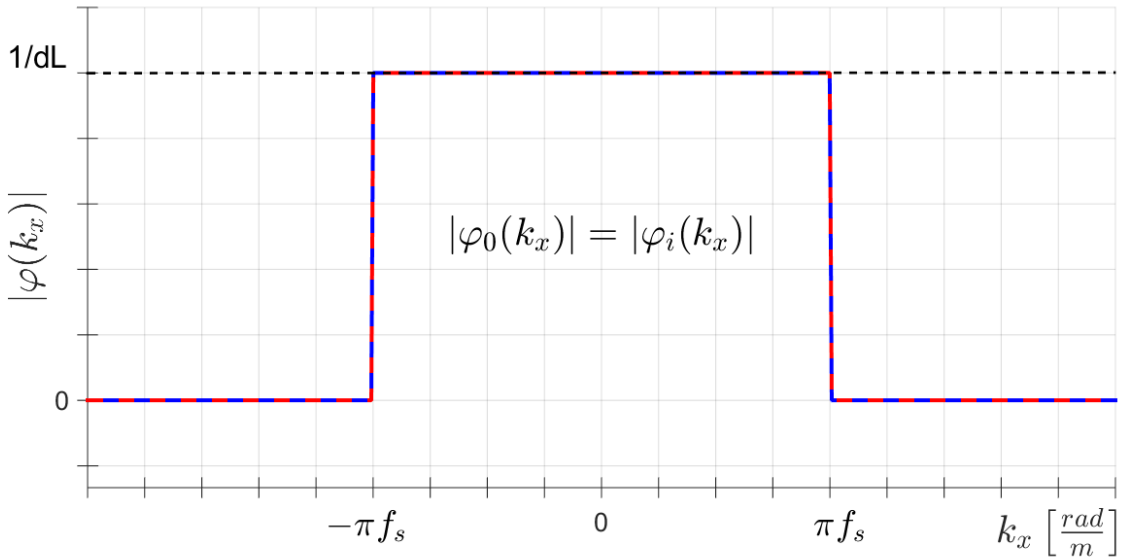

Figure 4.4: sinc Fourier Transform $\varphi_0(k_x)$, $\varphi_i(k_x)$: the absolute values of the shape functions in wavenumber domain are equals for all the generalized coordinates and differ from zero only within a certain frequency range

4.4 Procedure for the Coupling Loss Factors and Power Balance

In what follow, the procedure for the calculation of the coupling loss factors of the hybrid junction adopted for this model is resumed. Given a certain system excited over a certain range of frequencies:

1. The system is subdivided in a set of coupled subsystems (plate A, plate B, beam) connected among them through regions on the boundaries that have to be defined (two edges of the plates and the beam).

2. The deterministic boundaries of all the subsystems are defined, and so the subsystems are classified as statistical (the two plates) or deterministic (the beam). The classification is made estimating the minimum wavelength of vibration in each subsystem and choosing a wavelength threshold below which the subsystem is defined as deterministic. Using simple formulas like in subsection 2.3.3 it is possible to compute the wavenumber of simple components, so that more complex domains can be approximated in order to get the magnitude of the wavelength. In section 2.4 general thresholds are proposed.

3. The hybrid junctions are then defined in correspondence of deterministic boundaries of statistical subsystems.

4. Degrees of freedom are defined by placing nodes over the deterministic subsystems and over the "statistical junctions" which directly connect two statistical subsystems through a deterministic boundary.

5. The excitation applied to the system is defined as a cross-spectral matrix function of the excitation frequency $\mathbf{S}_{ff}^{ext}(\omega)$.

6. The dynamic stiffness matrix of the deterministic subsystem is computed. Deterministic methods like FEM and BEM can be adopted. In this case, the matrices are derived in modal base, so a preliminary modal analysis of the system is done in order to obtain natural frequencies and modes over the deterministic region. The beam matrix is then a diagonal defined by the natural frequencies of the system over the simulated frequency range.

7. The direct field dynamic stiffness matrix is computed for each statistical subsystem in modal coordinates, mapping the modes over the deterministic boundaries in their local

coordinate systems. In this thesis two methods are presented with the derivation from the stiffness of a semi-infinite plate in wavenumber domain $\mathbf{D}_{dir}^{\mathrm{wn}}$:

a) If the direct modal transformation is used (subsection 4.3.3), the mode shapes are transformed in the wavenumber domain and used in the wavenumber integral of Equation 4.54 which gives the direct field stiffness.

b) If a Galerkin method is used with generalized coordinates, the displacements are described by a set of shape functions which must be transformed in wavenumber domain. The direct field stiffness is computed in the generalized coordinates as well as the modal transformation. If sinc functions are used, the wavenumber integral results simplified because the Fourier transform of the shape functions are zero out of a certain interval of wavenumbers, and the generalized coordinates coincide with the nodal coordinates, so that the modal transformation can be done using the modal matrix in nodal coordinates coming from the modal analysis.

8. The total modal dynamic stiffness matrix $\mathbf{D}_{tot}$ is assembled like in Equation 3.44.

9. Once the modal density of each statistical subsystem is known the coupling loss factor's are computed for all the ij combinations of energy exchanges between statistical subsystems Equation 3.59.

10. The total power transfer coefficients are computed Equation 3.63.

11. The modal overlap factors are computed Equation 3.68.

12. The system of linear equations in Equation 3.70 is solved and the ensemble average modal energy densities are computed for each statistical subsystem. The input power are computed from the cross-spectral excitation (Equation 3.57).

13. The modal energy densities are inserted in Equation 3.52 in order to compute the cross-spectral response $\langle S_{qq} \rangle$ of each statistical subsystem as a contribution of external and reverberant loading.

5 Results

In order to implement the method for the calculation of the coupling loss factor's of the model presented in section 4.1, the stiffness matrices are computed in modal coordinate. For this purpose, a preliminary modal analysis with finite element method is performed on the entire system. The software used to compute the mode shapes and the natural frequencies is MSC NASTRAN™. The extraction of the FEM results and the definition of the subsystems is done with the library "NV_MATLAB_lib". All the subsequent operations are done in MATLAB® and implemented in the library. The commercial software VAOne is adopted for a comparison of the results. For software citations see Appendix C.

5.1 Wavenumbers and Mode Shapes

The simulation is performed on two models, which differ in the length in the x dimension. This is done for testing that the magnitude and the shape of the resulting CLFs do not present big differences when compared in the two models, and so for proving that the method is length-independent and can be applied to any line junction. As reported in Table B.3, the shortest model present a x length of 0.9 meters and the longest 2.2 meters. The FE model for the modal analysis is the discretization of the system were the beam is modelled with 45 elements (46 nodes) in the shortest version and with 110 elements (111 nodes) in the longest version. These elements are 1-dimensional CBEAM type with property PBEAML. The plates are modelled with shell elements of type CQUAD4 with property PSHELL, and are 2699 for the plate A and 2249 for the plate B. All the nodes are equispaced, so the length of each CBEAM element is 20 mm in both the two versions.

In Table 5.1 the structural properties related to the plates of the model of x length 0.9 meters are reported. It can be seen in 5.1a and 5.1b how the bending wavenumber of the smallest plate (B) is larger than the beam bending wavenumber[1]. The comparison

[1] $k_{beam} = \sqrt{\omega}\sqrt[4]{\frac{\rho A_{beam}}{EI}}$. A_{beam}: cross section area. I: inertia of the section to the bending moment.

Plate	A [m^2]	h [mm]	B [N/m]	C [N/m]	S [N/m]	$n(\omega)$
A	1.08	1.4	18.2	1.115e+08	3.73e+07	0.0391
B	0.9	1.2	11.5	9.56e+07	3.20e+07	0.0381

Table 5.1: Area, Thickness, Bending Stiffness, Longitudinal Stiffness, Shear Stiffness and Modal Density for the two plates in the version with junction length 0.9 m.

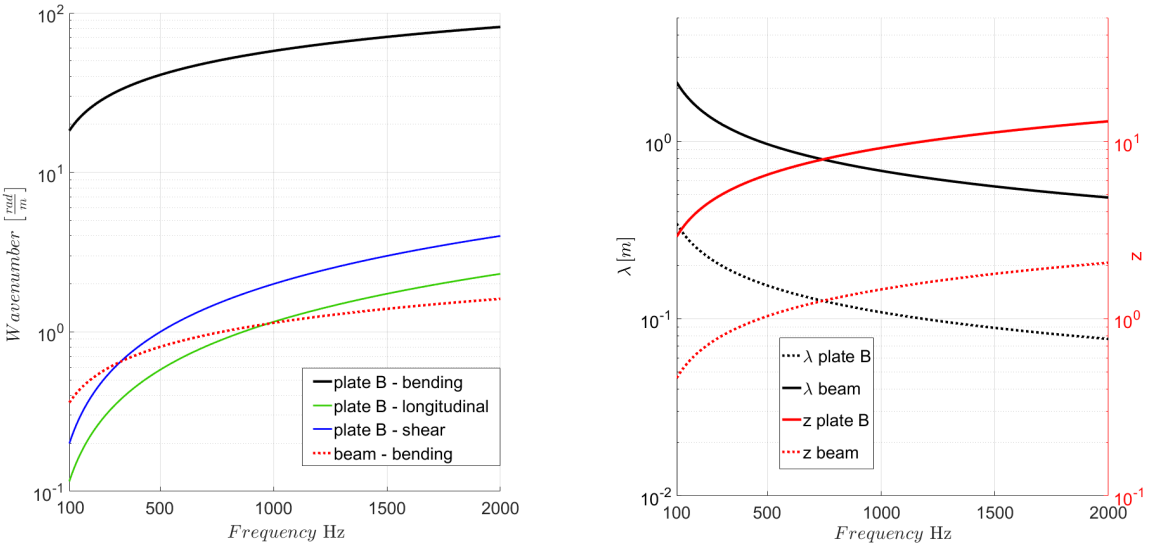

(a) Wavenumbers of the plate B for the bending, longitudinal and shear waves, and of the beam for the bending waves.

(b) Wavelengths and factor z for the bending waves of the beam and the plate B.

Figure 5.1: Wavenumbers and Wavelengths

is made considering the smallest plate because the wavelength of a vibration is shorter if the component presents a bigger stiffness to that motion. Since the smallest plate has the smallest stiffness, its wavelengths will be for sure the longest. This is the reason why the plates are modelled as statistical subsystems, and the beam as deterministic. The torsional and shear wavenumbers of the beam are not considered in the comparison since they are much smaller than the bending one. It must be noticed that the in-plane wavenumbers of the plate are of the same magnitude of the beam bending wavenumber, but they are included in the statistical subsystem as explained in section 4.2.

Over the frequency range $100 - 2000$ Hz the modal analysis gives 62 modes for the model with junction length 0.9 m and 149 modes for the longest junction. The mode shapes are extracted from the FEM results and mapped over the junction, and subsequently projected into the local coordinates of the two deterministic edges of the plates. This is done in order to express the direct field stiffness in the local coordinates, using the same equations reported

in subsection 4.3.3 and 4.3.4, and performing the modal transformation without the need for a coordinate system rotation. The minimum number of points that have to be used in the mapping must be large enough to guarantee a correct Fourier Transform for the wavenumber modal transformation method, that means at least larger than the number of nodes of the junctions used to compute the mode shapes. But also, there must be enough points to represent the stiffness in wavenumber domain in Equation 4.36. An example mode is shown in Figure 5.2, projected in the local coordinate system of the plate A. The Fourier Transform of the mode shapes used in the direct modal transformation method is done by the FFT function in MATLAB. An example use of the function is reported in section D.1, and a mode shape in space and wavenumber domains is shown in Figure 5.3. Using 64 interpolating point for the junction of 0.9 m, the sampling space frequency is $f_s = (N_{point} - 1)/L = 70\ 1/m$, and the limits of the FFT domain are $k_{x,s} = \pm\pi f_s = 219.9\ rad/m$.

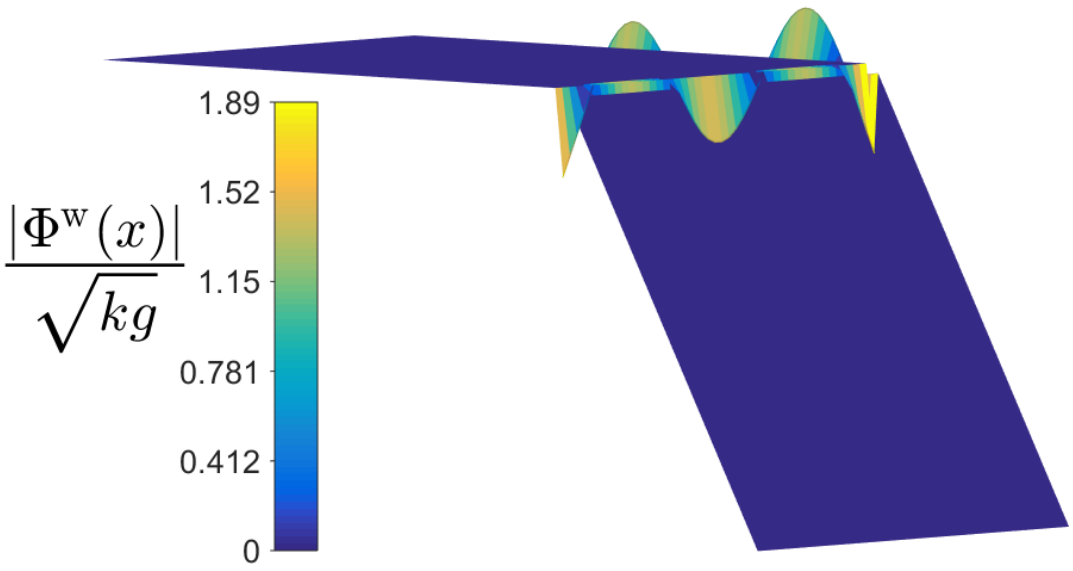

Figure 5.2: Component $w - z$ of the resonant mass-normalized mode in space domain with natural frequency of 2143 Hz, projected in the coordinate system of the edge of plate A, in the model with the shortest junction length 0.9 m.

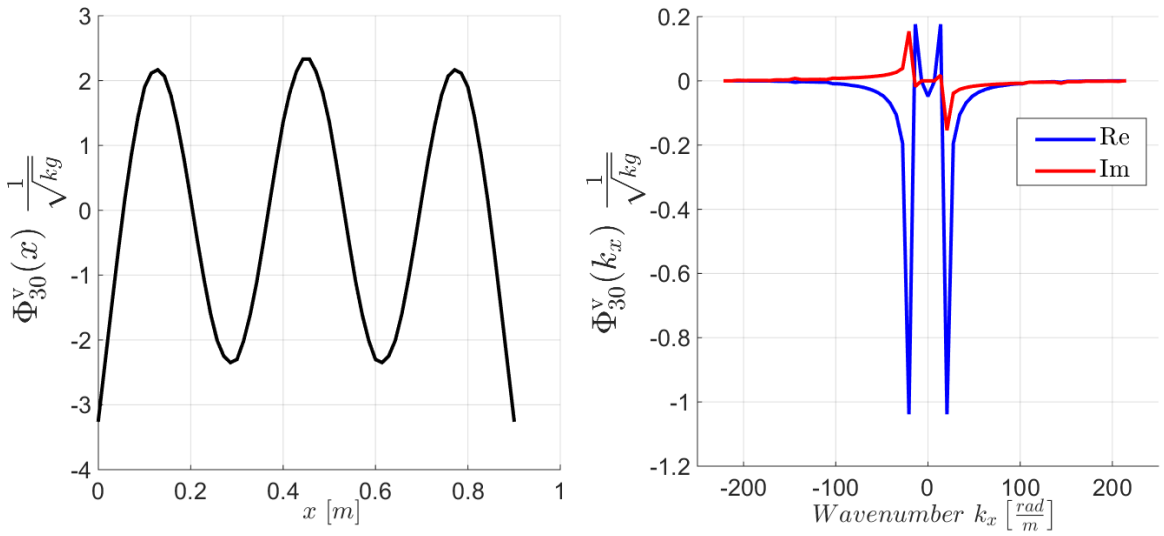

Figure 5.3: Component v − y of the 30-th mode (1754.4 Hz) projected in the edge coordinate of plate A in space domain $\Phi^{v}_{30}(x)$, and its discrete wavenumber Fourier transform $\Phi^{v}_{30}(k_x)$ real and imaginary parts.

It can be stated that, generally, the Fourier Transform of a generic mode shape is not very uniform over the wavenumber domain. This means that in a discrete form it is not easy to reproduce appropriately, with consequences on the final results as shown in section 5.3, where the wavenumber transform results very sharp. Zero padding[2] can help to obtain a better approximation of the transform.

5.2 Wavenumber Domain Direct Field Stiffness

The direct field dynamic stiffness matrix in wavenumber domain is a function of the wavenumber component in the direction of the edge k_x. The shape of these functions must be considered when the number of point is chosen, in order to have a good interpolation. Thankfully, all the eight functions of the stiffness can be well represented by a number of point equal to the nodes on the junction of the FE model. As an example, in Figure 5.4a and 5.4b is reported the stiffness element which identifies the contribution of the edge rotation to the edge moment in its real and imaginary part, that is the element D_{44} of Equation 4.37. This means that the shape of the stiffness elements does not have much influence on the choice of the number of interpolating points, which can be totally based on the space frequency of

[2]The Zero Padding consists in extend the signal in the starting domain with a certain number of elements whose values are all zero. Such an extension does not modify the Fourier Transform resulting in a more dense interpolation.

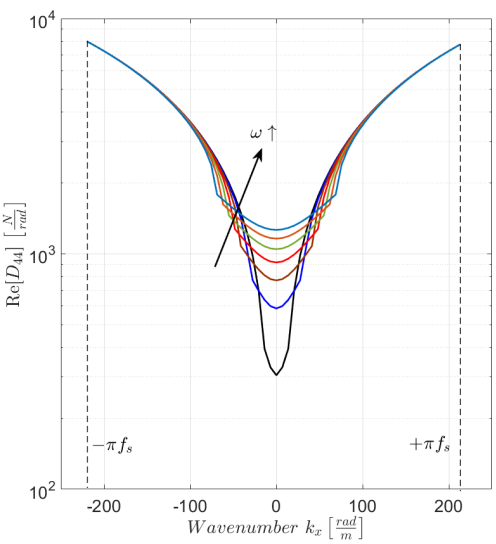

(a) Real part of the wavenumber stiffness element $D44$ for the plate A, with a damping loss factor $\eta = 0.01$.

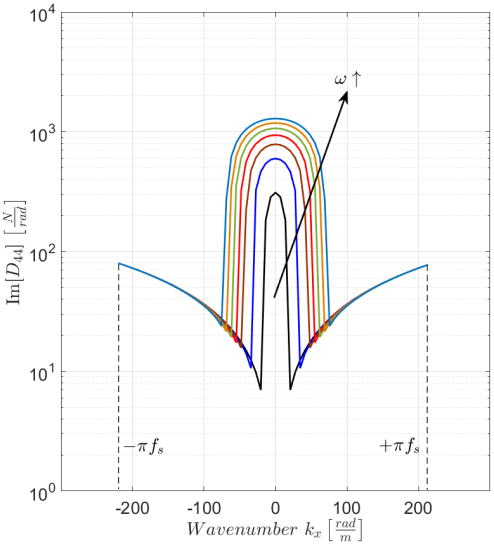

(b) Immaginary part of the wavenumber stiffness element $D44$ for the plate A, with a damping loss factor $\eta = 0.01$.

Figure 5.4: Wavenumber Stiffness $D44$

the modes. It must be noticed that if the plates are undamped, the imaginary part of the roots μ_{B2}, μ_L and μ_S differs from zero only within the absolute value of the corresponding wavenumbers k_B, k_L and k_S. If damping is present, then the imaginary part is potentially always present.
The free field dynamic stiffness is then computed in modal coordinates using the direct modal transformation in wavenumber domain and the sinc shape function methods Equation 4.54, 4.69.

5.3 Power Transmission Coefficients and Coupling Loss Factors

The power transmission coefficients are computed with the two methods proposed. The result with the direct wavenumber modal transform is reported in Figure 5.5 referring to the model with the shortest junction. The symmetry of the power transmission is perfectly respected since the curves of the coefficients h_{ij} and h_{ji} coincide. It can be seen how the resonances arise at high frequencies in several visible humps of the curves. This can be a natural behaviour because of the resonant modes but also a numerical error due to the fast Fourier transform used for the mode shapes which is not analytic. The symmetry in the

power flow gets lost when expressed with the coupling loss factors since they depends on the modal density of the plates, that are slightly different in this case. The plates with the smallest modal density will present the largest CLF.
Results for the CLFs of the model with shortest junction are shown again in Figure 5.6, where also a zero padding is performed in order to reduce the error in the approximation of the wavenumber transform, and compared to the results obtained with the simulation in VAOne.

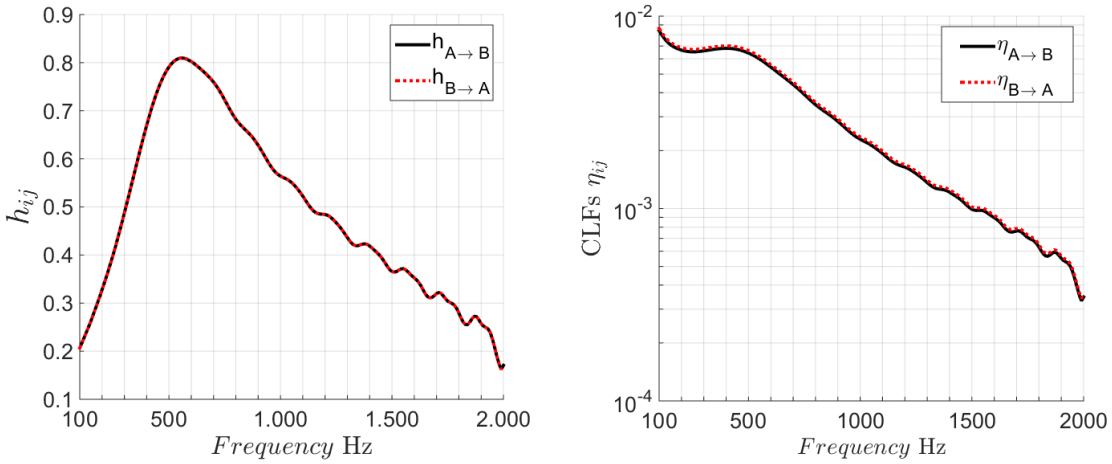

Figure 5.5: Power Transmission Coefficients and Coupling Loss Factors computed with the wavenumber modal transformation method for the model with junction length $L_j = 0.9$ m using 64 point for the interpolation of the functions along the junction and no zero padding.

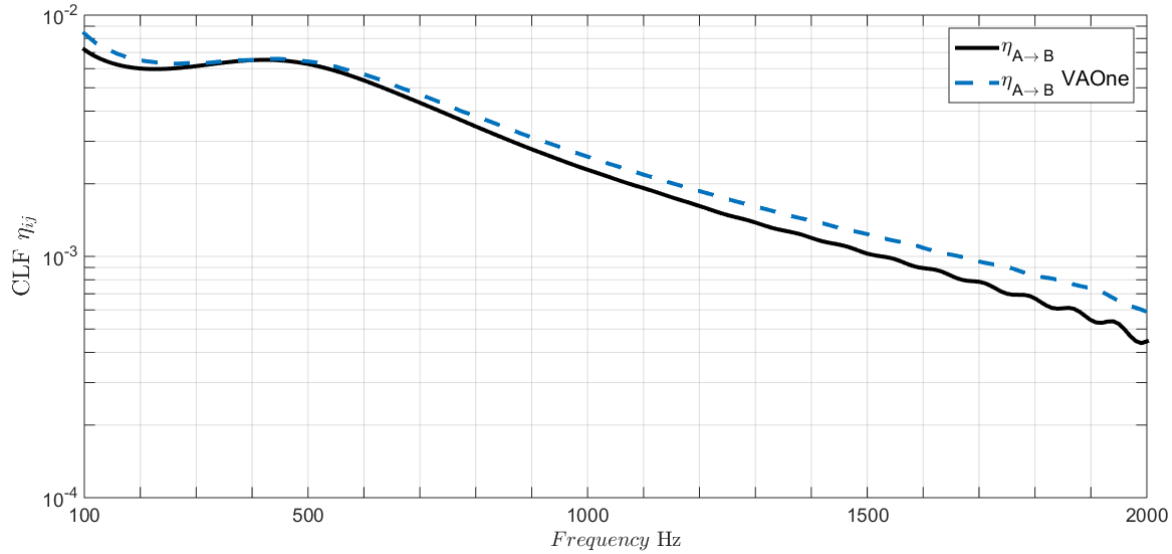

Figure 5.6: Coupling Loss Factor computed with the wavenumber modal transformation method for the model with junction length $L_j = 0.9$ m using 64 point for the interpolation of the functions along the junction, and 64 points of zero padding.

Only $\eta_{A\to B}$ is reported for better legibility. A visible result on the humps is given by the zero padding, which makes them arise with a smoother shape. The mitigation of the sharpening due to the FFT shows oscillations which are better attributable totally to the resonances. Although the results of the commercial software must be taken with a large margin of error since the exact method which it refers to for the computation of the $\mathbf{D}_{dir}$ is not known, the comparison gives a correspondence in the magnitude and a good fitting of the shape.
The validation of the second method (sinc shape functions) could be done again in the model with the shortest junction, which presents results very similar to the ones already presented. However, it is more interesting comparing the two methods in the calculation of the model with the longest junction where the weaknesses of the wavenumber modal transformation is more evident: in Figure 5.7, the CLF η_{AB} presents a shape which is similar to the previous results when the "sinc" method is used, while it presents a strong discontinuity in the slope at high frequencies when computed using the modal wavenumber transformation. Such a discontinuity has no reason to exist in nature, indeed it can be addressed to numerical errors, like in Figure 5.5. Using a large zero padding the slope of this curve tends to be more uniform as shown in Figure 5.8.

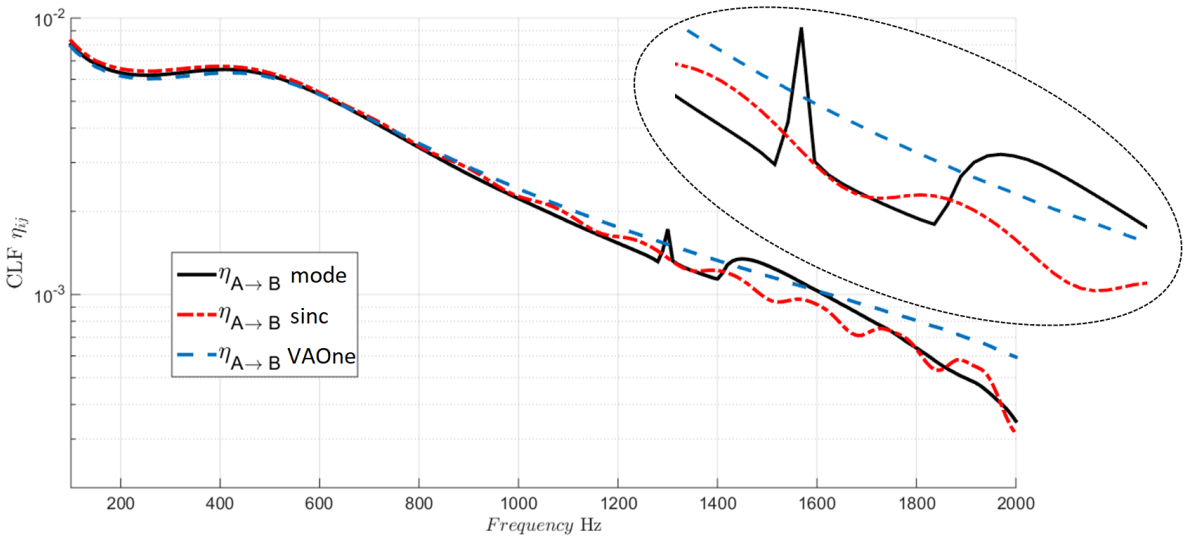

Figure 5.7: Coupling Loss Factor $A \to B$ computed with the wavenumber modal transformation method and sinc method for the model with junction length $L_j = 2.2$ m using 64 point for the interpolation of the functions along the junction, and no zero padding.

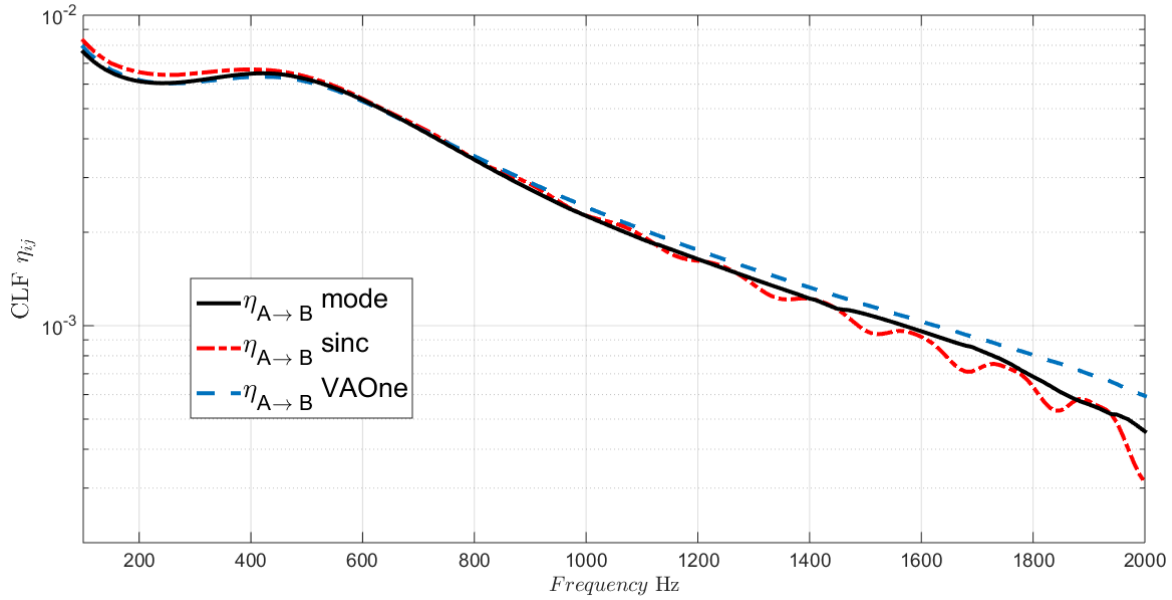

Figure 5.8: Coupling Loss Factor computed with 64 interpolating points and 64 points of zero padding in the wavenumber modal transformation.

There is not a big difference in the results of the two methods, which are not the same because of the different choice of generalized coordinates.
The slope discontinuity of the CLF in the longest junction may be generated by modes which are more difficult to transform in a discrete form without making a not negligible error, with respect to the shortest junction. The Fourier transform is only performed in the direct modal transformation method, and this reveals a big advantage of the "sinc" method, which does not require the use of FFT since the Fourier transform is know analytically. On the contrary, the wavenumber modal transformation is advantageous in terms of computational time, indeed referring to the results obtained in Figure 5.8 the time spent to build the only direct field dynamic stiffness matrix of one plate is shorter, see Table 5.2. The simulation with the wavenumber modal transform are very fast even if a large number of points for the interpolation and for the zero padding is used. For example using 1024 points on the

Method	Interpolating Points	Zero Padding	Time [s]
Wavenumber Mode Shapes	64	0	0.5
Wavenumber Mode Shapes (padding)	64	128	2.1
sinc Shape Functions	64	-	14.5

Table 5.2: Time spent in the computation of the $\mathbf{D}_{dir}$ with the two methods.

junctions plus 512 points for the zero padding the computation takes 8 seconds, while using even only 512 points in for the sinc method, it takes around 13 minutes. This results suggest that for bigger and more complex models where it can be necessary to compute the CLFs of many junctions the wavenumber modal transform may be preferred, but attention must be paid to the minimum number of point and the minimum zero padding.
In figure Figure 5.9 the sensitivity of the CLFs to a change of the damping loss factor of the deterministic beam is finally shown. With the aim of reducing the power flow between the two statistical subsystems, is easier and more efficient to increase the damping of the only deterministic subsystem which constitutes the hybrid junction, indeed when the damping loss factor of the beam increases, the transmission coefficient decreases. In this case, the increasing damping of the beam tends to level the resonant peaks, that means they are mostly due to the beam frequency response function, and not to the modes of the plates. It follows that the CLFs are mainly governed by the most stiff subsystems, which are typically modelled as deterministic because of their low wavenumbers.

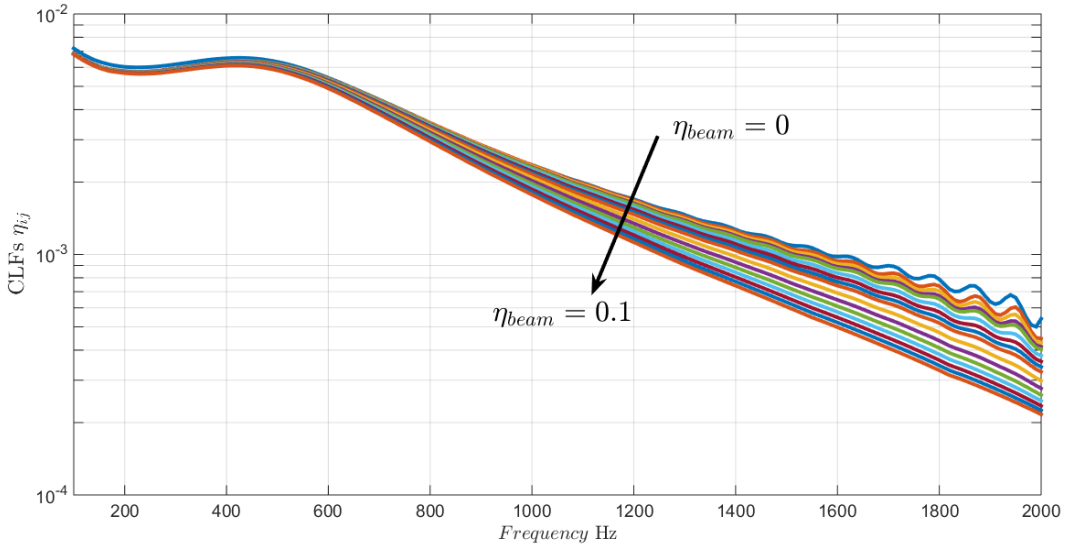

Figure 5.9: Effect of the damping of the beam on the CLFs for the model with the shortest junction.

6 Conclusions

For the line junction studied in this thesis, three methods are proposed for the derivation of the direct field stiffness. The Green's Function method can be applied with the known Green's Functions of the semi-infinite plate for the normal displacements with a complicated integration technique, while the Green's functions for the in-plane motion have to be derived. Starting from the stress resultant in wavenumber domain, the direct field stiffness can be derived with a direct wavenumber modal transformation or with appropriate shape functions for the Galerkin method, in this case sinc functions are selected.

From the results of the coupling loss factors it can be seen how the direct wavenumber modal transform is much faster but requires high precision in the definition of the nodes grid and in the number of point for the zero padding of the mode shapes, since it involves the wavenumber Fourier transform which must be done in the discrete form. The sinc shape functions method is much slower in the computation but the Fourier transform of its shape functions is known analytically, so that errors on the transformation are avoided. If correctly treated, both the methods lead to similar results, representing a valid option for the implementation of the calculation of CLFS for hybrid junctions. The results are also in good comparison with the output of commercial software.

Another results is carried out by the influence of the damping loss factor on the power transmission coefficients. The CLFs are mainly governed by the damping loss factor of the deterministic subsystem which constitutes the hybrid junction. It is shown in Figure 5.9 how an increase in the damping of the beam can lower the coupling loss factors between the two plates.

The total error of these methods is the results of the residual due to the discretization in the modal analysis, the residual due to the discretization in the generalised coordinates of the Galerkin Method, the error of approximation in the numerical integration and the overall numerical error in the computation. Another aspect which is not a proper error but that must be taken in account when considering the results, is the statistical approach and its

consequences on the impossibility to define a correlation between the results and an exact configuration of the system.

The great advantages of the hybrid method presented are the possibility to model a very large range of frequencies and the definition of vibration in the statistical subsystems as if they were semi-infinite components, identified only by the geometry of the hybrid junction. The incoherence of the reverberant field allows to describe the property of a junction independently on the geometry of the statistical subsystem far from the junction. This means that if a complex component needs to be modelled statistically with a point, line or surface connection, the definition of the junction can be reduced to a simplified case where the component is modelled as semi-infinite beam, semi-infinite plate or semi-infinite 3D solid defining the direct field dynamic stiffness matrix as in one of this simple cases.
Such an advantage fits very well the early design stage simulation, when the exact geometry of the components is not known exactly but an approximation of the dynamic properties of the system is required for the subsequent dimensioning.

It must be noticed that the free field which defines the properties of a junction does not only depend on the junction dimension (1D, 2D or 3D), but on the overall effect of the geometry on the wave propagation in the proximity of the junction. This means that the semi-infinite plate connection discussed in this thesis can be used as an approximation of line connection between flat subsystem, at least in the proximity of the junction. If a subsystem presents a certain curvature at the connection, then the direct field is influenced and the stiffness must be modelled taking into account this geometrical feature.

A Derivations

A.1 Blocked Reverberant Force

The system in Equation 3.4 is reduced to the deterministic variables by pre-multiplying the first equation with $\mathbf{G}_{dd}^{-1}$:

$$\mathbf{G}_{dd}^{-1}\mathbf{H}_{dd}\mathbf{q}_d = \mathbf{f}_d + \mathbf{G}_{dd}^{-1}\left(\mathbf{G}_{dr}\mathbf{f}_r - \mathbf{H}_{dr}\mathbf{q}_r\right) \qquad \mathbf{D}_{dir}\mathbf{q}_d = \mathbf{f}_d + \mathbf{f}_{rev} \tag{A.1}$$

which gives the expressions for the stiffness and the blocked reverberant force:

$$\mathbf{D}_{dir} = \mathbf{G}_{dd}^{-1}\mathbf{H}_{dd} \tag{A.2}$$

$$\mathbf{f}_{rev} = \mathbf{G}_{dd}^{-1}\left(\mathbf{G}_{dr}\mathbf{f}_r - \mathbf{H}_{dr}\mathbf{q}_r\right) \tag{A.3}$$

For a clamped boundary condition at the random boundary, $\mathbf{q}_r$ must be zero. Substituting this condition in the second equation of Equation 3.4, the force at the random boundary and so the blocked reverberant force result in:

$$\mathbf{f}_r\left(\mathbf{q}_r = 0\right) = \mathbf{G}_{rr}^{-1}\mathbf{H}_{rd}\mathbf{q}_d - \mathbf{G}_{rr}^{-1}\mathbf{G}_{rd}\mathbf{f}_d \tag{A.4}$$

$$\mathbf{f}_{rev}\left(\mathbf{q}_r = 0\right) = -\left(\mathbf{G}_{dd}^{-1}\mathbf{G}_{dr}\mathbf{G}_{rr}^{-1}\mathbf{G}_{rd}\right)\mathbf{f}_d + \left(\mathbf{G}_{dd}^{-1}\mathbf{G}_{dr}\mathbf{G}_{rr}^{-1}\mathbf{H}_{rd}\right)\mathbf{q}_d \tag{A.5}$$

For a free boundary condition at the random boundary, $\mathbf{f}_r$ must be zero. Substituting this condition in the second equation of Equation 3.4, the displacement at the random boundary and so the blocked reverberant force result in:

$$\mathbf{q}_r\left(\mathbf{f}_r = 0\right) = \mathbf{H}_{rr}^{-1}\mathbf{G}_{rd}\mathbf{f}_d - \mathbf{H}_{rr}^{-1}\mathbf{H}_{rd}\mathbf{q}_d \tag{A.6}$$

$$\mathbf{f}_{rev}\left(\mathbf{f}_r = 0\right) = -\left(\mathbf{G}_{dd}^{-1}\mathbf{H}_{dr}\mathbf{H}_{rr}^{-1}\mathbf{G}_{rd}\right)\mathbf{f}_d + \left(\mathbf{G}_{dd}^{-1}\mathbf{H}_{dr}\mathbf{H}_{rr}^{-1}\mathbf{H}_{rd}\right)\mathbf{q}_d \tag{A.7}$$

A.2 Green's Function derivation for the deflection of plates

The Green's function of the biharmonic deflection equation (Equation 4.11) can be derived for infinite plate in wavenumber domain as showed in [Gunda et al 1998]. The Green's function for the infinite plate in polar coordinate can be expressed as a function of the only bending wavenumber k_B (and so the frequency ω) and the distance between the excitation point $\mathbf{r}_i$ and the point where the response is observed $\mathbf{r}_j$, using the zero order Hankel function of the first kind H_0^1:

$$G_\infty\left(\mathbf{r}_i,\mathbf{r}_j,k_B\right) = c\left[H_0^1\left(k_B\left|\mathbf{r}_i-\mathbf{r}_j\right|\right) - H_0^1\left(\mathrm{i}k_B\left|\mathbf{r}_i-\mathbf{r}_j\right|\right)\right] \tag{A.8}$$

The derivation of the Green's function for the semi-infinite plate requires the application of boundary conditions, which is not convenient in polar coordinates. For this reason, Equation A.8 must be written in cartesian coordinetes by decomposing the Henkel function.
This can be done comparing the different expressions for the solution U of the 2D Helmotz equation in frequency domain with a unit harmonic point source. Using the notation $r = |\mathbf{r}_i - \mathbf{r}_j|$:

$$\nabla^2 U + k_B^2 U = \delta(\mathbf{r}) \tag{A.9}$$

Using the wavenumber decomposition $k_B^2 = k_x^2 + k_y^2$, the resulting Hankel function in cartesian coordinates is:

$$H_0^1\left(k,r\right) = \frac{1}{\pi}\int_{-\infty}^{+\infty}\frac{e^{\mathrm{i}k_x x}e^{ik_y|y|}}{k_y}\mathrm{d}k_x = \frac{1}{\pi}\int_{0}^{+\infty}\cos\left(\mathrm{i}k_x x\right)\frac{e^{ik_y|y|}}{k_y}\mathrm{d}k_x \tag{A.10}$$

Substituting Equation A.10 in Equation A.8, the Green's function for the infinite plate deflection in cartesian coordinates is Equation 4.19.
Considering four possible boundary conditions at the edge of the semi-infinite plate:

- simply supported (s): $w = 0$ and $M\left(w\right) = 0$ on the edge
- roller supported (r): $\frac{\partial w}{\partial y} = 0$ and $F\left(w\right) = 0$ on the edge
- clamped (c): $w = 0$ and $\frac{\partial w}{\partial y} = 0$ on the edge
- free (f): $F\left(w\right) = 0$ and $M\left(w\right) = 0$ on the edge

The solution for the semi infinite plate with simply supported edge can be found by using the images method [Gunda et al 1995], that means subtracting the infinite plate solution to

its symmetric image:

$$G_{/\infty,s}\left(\mathbf{r}_j,\mathbf{r}_i,k_B\right) = G_{\infty}\left(\mathbf{r}_j,\mathbf{r}_i,k_B\right) - G_{\infty}\left(\mathbf{r}_j,\mathbf{r}_{-i},k_B\right) \tag{A.11}$$

where, considering Figure 4.2, $\mathbf{r}_{-i}$ is the symmetric location of $\mathbf{r}_i$ with respect to the x axis in the edge, so with an opposite sign of the y coordinate. The Green's function for the roller supported case is obtained by summing the images:

$$G_{/\infty,r}\left(\mathbf{r}_j,\mathbf{r}_i,k_B\right) = G_{\infty}\left(\mathbf{r}_j,\mathbf{r}_i,k_B\right) + G_{\infty}\left(\mathbf{r}_j,\mathbf{r}_{-i},k_B\right) \tag{A.12}$$

Being the response to the unitary harmonic point force:

$$w_j = G_{/\infty,r}\left(\mathbf{r}_j,\mathbf{r}_i,k_B\right) \tag{A.13}$$

edge displacements and edge reactions can be computed in both the conditions (simply and roller supported), using Equation 4.4 and Equation 4.5 under the assumption of harmonic motion in time and wavenumber. This force-displacement relation at the boundary can be derived as it is done in subsection 4.3.3, using the Equation 4.28, 4.29 and Equation 4.30. Clamped and free boundary conditions are derived by the superposition of simply or roller supported case, with the edge displacements or reactions.
The clamped edge Green's function can be found by subtracting to the roller supported Green's function the response at the edge of the roller supported plate $w_{edge,c_r}\left(\mathbf{r}_j,\mathbf{r}_i\right)$ due to an edge normal displacement excitation; or also by subtracting to the simply supported Green's function the response at the edge of the simply supported plate $w_{edge,c_s}\left(\mathbf{r}_j,\mathbf{r}_i\right)$ due to an edge slope excitation:

$$G_{/\infty,c_r}\left(\mathbf{r}_j,\mathbf{r}_i,k_B\right) = G_{\infty,r}\left(\mathbf{r}_j,\mathbf{r}_i,k_B\right) - w_{edge,c_r}\left(\mathbf{r}_j,\mathbf{r}_i\right) \tag{A.14}$$

$$G_{/\infty,c_s}\left(\mathbf{r}_j,\mathbf{r}_i,k_B\right) = G_{\infty,s}\left(\mathbf{r}_j,\mathbf{r}_i,k_B\right) - w_{edge,c_s}\left(\mathbf{r}_j,\mathbf{r}_i\right) \tag{A.15}$$

Similarly, the free edge Green's function can be found by subtracting to the roller supported Green's function the response at the edge of the roller supported plate $w_{edge,f_r}\left(\mathbf{r}_j,\mathbf{r}_i\right)$ due to an edge moment excitation; or also by subtracting to the simply supported Green's function the response at the edge of the simply supported plate $w_{edge,f_s}\left(\mathbf{r}_j,\mathbf{r}_i\right)$ due to an edge normal

force excitation:

$$G_{/\infty,f_r}\left(\mathbf{r}_j,\mathbf{r}_i,k_B\right) = G_{\infty,r}\left(\mathbf{r}_j,\mathbf{r}_i,k_B\right) - w_{edge,f_r}\left(\mathbf{r}_j,\mathbf{r}_i\right) \tag{A.16}$$

$$G_{/\infty,f_s}\left(\mathbf{r}_j,\mathbf{r}_i,k_B\right) = G_{\infty,s}\left(\mathbf{r}_j,\mathbf{r}_i,k_B\right) - w_{edge,f_s}\left(\mathbf{r}_j,\mathbf{r}_i\right) \tag{A.17}$$

The case of free edge derived from the simply supported edge is particularly convenient to use since the Green's function of the simply supported edge at the boundary is zero:

$$G_{/\infty,f_s}\left(\mathbf{r}_j,\mathbf{r}_i,k_B\right) = -w_{edge,f_s}\left(\mathbf{r}_j,\mathbf{r}_i\right) \tag{A.18}$$

This form is made explicit in Equation 4.21.

A.3 Wavenumber Domain Free Field Dynamic Stiffness Matrix

The out-of-plane radiation stiffness matrix is obtained substituting the harmonic normal displacement and x rotation of Equation 4.28 and 4.29, in the stress resultant equations of force and moment (Equation 4.4, 4.5), and evaluating the expression at the edge imposing $y = 0$. In order to do this, it is necessary to compute all the second and third order derivatives and mixed derivatives appearing in the stress resultants:

$$w_e = \left(\alpha_{B1} + \alpha_{B2}\right) e^{-\mathrm{i}k_x x + \mathrm{i}\omega t} \tag{A.19}$$

$$\theta_e = \left(\mu_{B1}\alpha_{B1} + \mu_{B2}\alpha_{B2}\right) e^{-\mathrm{i}k_x x + \mathrm{i}\omega t} \tag{A.20}$$

$$\left.\frac{\partial^2 w}{\partial x^2}\right|_{y=0} = -k_x^2 w_e \tag{A.21}$$

$$\left.\frac{\partial^2 w}{\partial y^2}\right|_{y=0} = \left(\alpha_{B1}\mu_{B1}^2 + \alpha_{B2}\mu_{B2}^2\right) e^{-\mathrm{i}k_x x + \mathrm{i}\omega t} = \theta_e\left(\mu_{B1} + \mu_{B2}\right) - w_e \mu_{B1}\mu_{B2} \tag{A.22}$$

$$\left.\frac{\partial^3 w}{\partial y^3}\right|_{y=0} = \left(\alpha_{B1}\mu_{B1}^3 + \alpha_{B2}\mu_{B2}^3\right) e^{-\mathrm{i}k_x x + \mathrm{i}\omega t} \tag{A.23}$$

$$\left.\frac{\partial^3 w}{\partial x^2 \partial y}\right|_{y=0} = -k_x^2 \theta_e \tag{A.24}$$

From the substitution in the stress resultants, the equations at the edge are:

$$\begin{aligned} F_e &= \frac{B}{\mu_{B1}-\mu_{B2}}\left\{w_e\left(\mu_{B1}^3\mu_{B2}-\mu_{B2}^3\mu_{B1}\right)+\right. \\ &\left.+\theta_e\left[\mu_{B2}^2-\mu_{B1}^2+k_x^2\left(2-\nu\right)\left(\mu_{B1}-\mu_{B2}\right)\right]\right\}= \\ &= B\left[w_e\left(\mu_{B1}^2\mu_{B2}+\mu_{B1}\mu_{B2}^2\right)+\theta_e\left(-\mu_{B1}^2-\mu_{B2}^2-\mu_{B1}\mu_{B2}+k_x^2\left(2-\nu\right)\right)\right] \end{aligned} \tag{A.25}$$

$$\begin{aligned} M_e &= -B\left[\left(\alpha_{B1}\mu_{B1}^2+\alpha_{B2}\mu_{B2}^2\right)e^{-\mathrm{i}k_x x+\mathrm{i}\omega t}-\nu k_x^2 w_e\right]= \\ &= B\left[w_e\left(\mu_{B1}\mu_{B2}+\nu k_x^2\right)-\theta_e\left(\mu_{B1}+\mu_{B2}\right)\right] \end{aligned} \tag{A.26}$$

And in matrix form:

$$\begin{aligned} &\begin{pmatrix} F\left(k_x\right) \\ M\left(k_x\right) \end{pmatrix}= \\ &= B\begin{bmatrix} \mu_{B1}^2\mu_{B2}+\mu_{B1}\mu_{B2}^2 & -\mu_{B1}^2-\mu_{B2}^2-\mu_{B1}\mu_{B2}+k_x^2\left(2-\nu\right) \\ \mu_{B1}\mu_{B2}+\nu k_x^2 & -\mu_{B1}-\mu_{B2} \end{bmatrix}\begin{pmatrix} w_e\left(k_x\right) \\ \theta_e\left(k_x\right) \end{pmatrix} \end{aligned} \tag{A.27}$$

Writing all the off-diagonal terms μ_{B1}^2 and μ_{B2}^2 as in Equation 4.27, the out-of-plane matrix results to be antisymmetric as reported in Equation 4.30:

$$\begin{pmatrix} F\left(k_x\right) \\ M\left(k_x\right) \end{pmatrix}= B\begin{bmatrix} \mu_{B1}^2\mu_{B2}+\mu_{B1}\mu_{B2}^2 & -\mu_{B1}\mu_{B2}-\nu k_x^2 \\ \mu_{B1}\mu_{B2}+\nu k_x^2 & -\mu_{B1}-\mu_{B2} \end{bmatrix}\begin{pmatrix} w_e\left(k_x\right) \\ \theta_e\left(k_x\right) \end{pmatrix} \tag{A.28}$$

Using the same procedure for the in-plane motion, the results is:

$$\begin{aligned} &\begin{pmatrix} T\left(k_x\right) \\ N\left(k_x\right) \end{pmatrix}= \\ &= \frac{1}{k_x^2-\mu_L\mu_S}\begin{bmatrix} -S\mu_L\left(k_x^2-\mu_S^2\right) & -\mathrm{i}Sk_x\left(2\mu_L\mu_s+k_S^2-2k_x^2\right) \\ -\mathrm{i}Ck_x\left[\mu_L^2-\nu k_x^2-\mu_L\mu_s\left(1-\nu\right)\right] & -C\mu_S k_L^2 \end{bmatrix}\begin{pmatrix} u_e\left(k_x\right) \\ v_e\left(k_x\right) \end{pmatrix} \end{aligned} \tag{A.29}$$

Writing all the terms μ_S^2 and μ_L^2 like in Equation 4.31 and Equation 4.32, and considering the two following relations coming from Equation 4.7, 4.8 and Equation 4.14, 4.15:

$$C = S\frac{2}{1-\nu} \tag{A.30}$$

$$k_L^2 = k_S^2\frac{1-\nu}{2} \tag{A.31}$$

the in-plane matrix results to be antisymmetric as reported in Equation 4.35:

$$\begin{aligned}&\begin{pmatrix} T\left(k_x\right) \\ N\left(k_x\right) \end{pmatrix} = \\ &= \frac{S}{k_x^2 - \mu_L \mu_S} \begin{bmatrix} -\mu_L k_S^2 & -\mathrm{i}k_x \left(2\mu_L \mu_s + k_S^2 - 2k_x^2\right) \\ \mathrm{i}k_x \left(2\mu_L \mu_s + k_S^2 - 2k_x^2\right) & -\mu_S k_S^2 \end{bmatrix} \begin{pmatrix} u_e\left(k_x\right) \\ v_e\left(k_x\right) \end{pmatrix}\end{aligned} \tag{A.32}$$

In [Langley and Heron 1990] the out of plane relations corresponds to this result, with the only difference in the sign of the moment which is in contradiction with the coordinate system of the figures, while the in-plane relations present some mistakes. In [Johansson and Comnell 2010] the sign of the two moment coefficients are not compatible with the illustrated coordinate system and positive direction of the forces. One of the two must be inverted depending on the x axis direction considered, and the substitution for the symmetric (or antisymmetric) form is missing. Also the in plane stress resultant are referred to a different coordinate system from the one reported in the corresponding figure. In this thesis, the equations are consistent with the directions and the cartesian system in Figure 4.2.

B Model Data

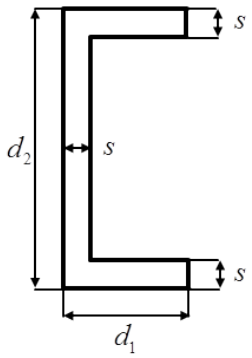

Figure B.1: The beam section presents the same geometry in both the configurations of the length of the junction.

Material	$\rho\,[\mathrm{kg/m^3}]$	$E\,[\mathrm{GPa}]$	ν	$G\,[\mathrm{GPa}]$
Aluminium	2700	71	0.33	27

Table B.1: Generic aluminium mechanical properties used in the simulation

$d_1\,[mm]$	$d_2\,[mm]$	$s\,[mm]$
20	40	2

Table B.2: Beam Cross Section data referred to Figure B.1

$L_{junc}\,[\mathrm{mm}]$	900		2200	
Plate	A	B	A	B
$h\,[\mathrm{mm}]$	1.4	1.2	1.4	1.2
$A\,[\mathrm{mm^2}]$	1.08 e+06	0.9 e+06	2.64 e+06	2.2 e+06

Table B.3: Geometry of the statistical rectangular plates

C Software

NASTRAN of MSC Software ® is one of the most common FEM program. In this these is used to build the FE model of the plate-beam-plate system and to perform the modal analysis. `http://www.mscsoftware.com/`

MATLAB of MathWorks® is a numerical computing environment working with its specific programming language. Is used in this thesis for reading the FEM model and results obtained in NASTRAN, and to perform array operations like multiplications, discrete Fourier transform, discrete integrals. `https://www.mathworks.com/`

"NV_MATLAB_lib" is a tool for vibroacoustics developed by the Airbus Defence and Space dynamics and vibroacoustics department. The code used for the calculation of the CLFs in this thesis is based on this tool, which is mainly used for reading the FEM results, for defining the subsystems and the hybrid junction, and for the mapping of modes over the nodes of interest.

VAOne is a software of ESI Group® which allows to perform vibroacoustic FEM, BEM SEA and Hybrid simulations. In this thesis is used to compute and compare the CLFs of the same model. `https://www.esi-group.com/`

D MATLAB® Code examples

D.1 Fast Fourier Transform

Listing D.1: Example of Fast Fourier Transform of the mode shapes

```
%% Space and wavenumber domains definition
% space data
L = $$$; % Line Junction Length
dL = $$$; % Length increment of nodes in the junction, costant spacing
Npad= $$$; % Number of point for the zero padding
Nnodes=L/dL+1; % Number of nodes on the junction
fs = 1/dL; % Space sampling frequency
% wavenumber data
if mod(Nnodes,2) == 0 % if Nnodes is even
    dF = fs/(Nnodes+Npad); % Wavenumber domain increment [Hz]
    dk = dF*2*pi; % Wavenumber domain increment [rad/s]
    Fdata_shift = 0 : dF : fs; % Wavenumber domain vector to be shifted [Hz]
    kdata_shift = Fdata_shift*2*pi; % Wavenumber domain vector to be shifted [rad
    /s]
    kdata = [-flip(kdata_shift(2:(Nnodes+Npad)/2+1)) , kdata_shift(1:(Nnodes+Npad
    )/2)];
    % Wavenumber domain vector [rad/s]
else % if Nnodes is odd
    dF = fs/(Nnodes+Npad-1);
    dk = dF*2*pi;
    Fdata_shift = 0 : dF : fs;
    kdata_shift = Fdata_shift*2*pi;
    kdata = [-flip(kdata_shift(2:(Nnodes+Npad-1)/2+1)) , kdata_shift(1:(Nnodes+
    Npad+1)/2)];
end
%% Build modal matrix and mode shapes in waveumber domain
```

```
Nmodes = $$$; % Number of modes
uvw = $$$; % Mode shapes displacements in space domain [Nnodes x 3 x Nmodes]
rxryrz = $$$; % Mode shapes retations in space domain [Nnodes x 3 x Nmodes]
for i = 1:Nmodes
% fft of the mode shapes
    UVW(:,:,i) = fftshift((fft(uvw(:,:,i), [Nnodes+Npad], 1)/fs),1);
    % mode shape displacements in wavenumber domain
    RzRyRz(:,:,i) = fftshift((fft(rxryrz(:,:,i), [Nnodes+Npad], 1)/fs),1);
    % mode shape rotations in wavenumber domain
end
```

D.2 Wavenumber Direct Modal Transformation Method

Listing D.2: Example of computation for $\mathbf{D}_{dir}$ with the wavenumber modal transformation

```
D_wn = $$$; % Wavenumber stiffness [4 x 4 x Nnodes+Npad x Nfreq]
Nfreq = $$$; % Number of simulated frequencies
FI = permute([UVW(:,:,:), RxRyRz(:,1,:)], [3 2 1]); % Mode shapes vector
D_integrand = zeros(Nmodes, Nmodes, Nnodes+Npad);
for ifreq = 1:Nfreq
    for ipoint = 1:Nnodes+Npad
        D_integrand(:,:,ipoint) = conj(FI(:,:,ipoint))*...
            (D_wn(:,:,ipoint,ifreq)*FI(:,:,ipoint).');
        % Integrand for the wavenumber integral
    end
    Ddir(:,:,ifreq) = 1/(2*pi)*trapz(D_integrand,3)*dk;
end
```

The variable D_wn is the semi-infinite plate wvenumber stiffness defined in Equation 4.37 as a $[4 \times 4 \times (Nnodes + Npad) \times Nfreq]$ matrix. All the remaining variables are defined as in section D.1.

D.3 Wavenumber Cardinal Sine Method

Listing D.3: Example of computation for $\mathbf{D}_{dir}$ with the sinc shape functions method

```
% Analytical efinition of the sinc transform shape functions
modematrix = $$$; % Modal matrix built with uvw and rx [4*Nnodes x Nmodes]
x_junc = linspace(0,L,Nnodes); % Nodes grid of the junction
sinc_tranform = @(k,xnode) ((heaviside(pi*fs - k) -...
    heaviside(- k - pi*fs))/fs).*exp(-1i.*k.*xnode);
dist = x_junc-x_junc(1); % Distances of nodes from the origin
FI = sinc_tranform(kdata,dist'); % Shape functions in wavenumber domain [Nnodes x
    Nnodes]
D_sinc = zeros(4*Nnodes,4*Nnodes); % Stiffness in the sinc generalized
   coordinates
for ifreq = 1:Nfreq
    % Build the 8 integrand functions
    for inode = 1:Nnodes
    D11_integrand(:,:,inode) = conj(FI(:,inode)).*(D11(ifreq,inode).*FI(:,inode)
    .');
    D12_integrand(:,:,inode) = conj(FI(:,inode)).*(D12(ifreq,inode).*FI(:,inode)
    .');
    D21_integrand(:,:,inode) = conj(FI(:,inode)).*(D21(ifreq,inode).*FI(:,inode)
    .');
    D22_integrand(:,:,inode) = conj(FI(:,inode)).*(D22(ifreq,inode).*FI(:,inode)
    .');
    D33_integrand(:,:,inode) = conj(FI(:,inode)).*(D33(ifreq,inode).*FI(:,inode)
    .');
    D34_integrand(:,:,inode) = conj(FI(:,inode)).*(D34(ifreq,inode).*FI(:,inode)
    .');
    D43_integrand(:,:,inode) = conj(FI(:,inode)).*(D43(ifreq,inode).*FI(:,inode)
    .');
    D44_integrand(:,:,inode) = conj(FI(:,inode)).*(D44(ifreq,inode).*FI(:,inode)
    .');
    end
% Wavenumber integrals
D_sinc(1:4:end-3,1:4:end-3) = 1/(2*pi)*trapz(D11_integrand,3)*dk;
D_sinc(2:4:end-2,2:4:end-2) = 1/(2*pi)*trapz(D22_integrand,3)*dk;
D_sinc(3:4:end-1,3:4:end-1) = 1/(2*pi)*trapz(D33_integrand,3)*dk;
D_sinc(4:4:end,4:4:end)     = 1/(2*pi)*trapz(D44_integrand,3)*dk;
```

```
D_sinc(1:4:end-3,2:4:end-2) = 1/(2*pi)*trapz(D12_integrand,3)*dk;
D_sinc(2:4:end-2,1:4:end-3) = 1/(2*pi)*trapz(D21_integrand,3)*dk;
D_sinc(3:4:end-1,4:4:end)   = 1/(2*pi)*trapz(D34_integrand,3)*dk;
D_sinc(4:4:end,3:4:end-1)   = 1/(2*pi)*trapz(D43_integrand,3)*dk;
% Modal transformation
Ddir(:,:,ifreq)=modematrix'*D_sinc(:,:)*modematrix;
end
```

The shape functions sinc_transform are defined analytically using the rectangular function. The variables D11, D12, D21... are the matrix functions of the wavenumber stiffness defined in Equation 4.37, and are stored for each simulated frequency as $[Nfreq \times Nnodes]$ matrices. The variables D11_integrand, D12_integrand, D22_integrand... are the integrand functions of the wavenumber integral of Equation 4.69, and Dsinc is the stiffness matrix resulting from the integral, which is defined in the generalized coordinate of the sinc shape functions, which coincide with the nodal coordinates. The last operation is the transformation of the stiffness in modal coordinates.

Bibliography

[Banerjee 1994] Banerjee, Prasanta K.: *The boundary element methods in engineering.* McGraw-Hill, 1994

[Brebbia and Dominquez 1992] Brebbia, C. A. ; Dominquez, J: *Boundary elements.* WIT Press, 1992

[Cremer et al 2010] Cremer, L. ; Heckl, M. ; Petersson, B. A. T.: *Structure-borne sound.* Springer, 2010

[Cuenca 2009] Cuenca, J., Université du Maine, Ph.D. thesis, 2009

[von Estorff 2007] Estorff, O. von: Numerical methods in acoustics: facts, fears, future. In: *19th International congress on acoustic, Madrid, 2-7 September 2007* (2007)

[Fahy 2000] Fahy, Frank J.: *Foundations of engineering acoustics.* Academic Press, 2000

[Fasana and Marchesiello 2006] Fasana, A ; Marchesiello, S: *Meccanica delle vibrazioni.* Clut, 2006

[Fasana and Marchesiello 2016] Fasana, A ; Marchesiello, S: Lecture notes in Vibration Mechanics, Politecnico di Torino, 2016

[Filippi 2008] Filippi, P: *Vibrations and acoustic radiation of thin structures.* ISTE, 2008

[Gunda et al 1998] Gunda, R. ; Vijayakar, S. M. ; Singh, R. ; Farstad, J. E.: Harmonic Green's functions of a semi-infinite plate with clamped or free edges. In: *The Journal of the Acoustical Society of America* 103 (1998), Nr. 2, p. 888–899

[Gunda et al 1995] Gunda, R. ; Vijayakar, S.M. ; Singh, R.: Method of images for the harmonic response of beams and rectangular plates. In: *Journal of Sound and Vibration* 185 (1995), Nr. 5, p. 791–808

[Hambric et al 2016] Hambric, S.A. ; Sung, S.H. ; Nefske, D.J.: *Engineering vibroacoustic analysis: Methods and Applications.* Wiley, 2016

[Johansson and Comnell 2010] Johansson, Daniel ; Comnell, Peter: *Statistical Energy Analysis software*, Chalmers University of Technology, Master thesis, 2010

[Langley and Shorter 2003] Langley, R. S. ; Shorter, P. J.: The wave transmission coefficients and coupling loss factors of point connected structures. In: *The Journal of the Acoustical Society of America* 113 (2003), Nr. 4, p. 1947–1964

[Langley 2007] Langley, R.S.: Numerical evaluation of the acoustic radiation from planar structures with general baffle conditions using wavelets. In: *The Journal of the Acoustical Society of America* 121 (2007), Nr. 2, p. 766–777

[Langley and Heron 1990] Langley, R.S. ; Heron, K.H.: Elastic wave transmission through plate/beam junctions. In: *Journal of Sound and Vibration* 143 (1990), Nr. 2, p. 241–253

[Lyon and DeJong 1995] Lyon, R.H. ; DeJong, R.G.: *Theory and application of statistical energy analysis*. Butterworth-Heinemann, 1995

[Peiffer et al 2009] Peiffer, A. ; BrÃ$\frac{1}{4}$hl, S. ; Tewes, S.: Comparison of hybrid modelling tools for interior noise prediction. In: *INTER-NOISE and NOISE-CON Congress and Conference Proceedings* 2009 (2009), Nr. 5, p. 1749–1756

[Peiffer 2016] Peiffer, Alexander: Full frequency vibro-acoustic simulation in the aeronautics industry. In: *Conference Proceedings of ISMA 2016* (2016), 09

[Shorter and Langley 2005a] Shorter, P.J. ; Langley, R.S.: On the reciprocity relationship between direct field radiation and diffuse reverberant loading. In: *The Journal of the Acoustical Society of America* 117 (2005), Nr. 1, p. 85–95

[Shorter and Langley 2005b] Shorter, P.J. ; Langley, R.S.: Vibro-acoustic analysis of complex systems. In: *Journal of Sound and Vibration* 288 (2005), Nr. 3, p. 669–699

[Skeen and Kessissoglou 2007] Skeen, M.B. ; Kessissoglou, N.J.: An investigation of transmission coefficients for finite and semi-infinite coupled plate structures. In: *The Journal of the Acoustical Society of America* 122 (2007), Nr. 2, p. 814–822

[Somà 2016] Somà, A: Lecture notes in Numerical Methods for Product Design, Politecnico di Torino, 2016

[Timošenko and Woinowsky-Krieger 1996] Timošenko, Stepan P. ; Woinowsky-Krieger, S: *Theory of plates and shells*. McGraw-Hill, 1996

[Ventsel and Krauthammer 2001] Ventsel, E. ; Krauthammer, T.: *Thin plates and shells*. Marcel Dekker, 2001